

The physics and chemistry of the Schottky barrier height

Raymond T. Tung

Citation: [Applied Physics Reviews](#) **1**, 011304 (2014); doi: 10.1063/1.4858400

View online: <http://dx.doi.org/10.1063/1.4858400>

View Table of Contents: <http://scitation.aip.org/content/aip/journal/apr2/1/1?ver=pdfcov>

Published by the [AIP Publishing](#)

Articles you may be interested in

[Schottky barrier height and interface chemistry of annealed metal contacts to alpha 6HSiC: Crystal face dependence](#)

[Appl. Phys. Lett. **62**, 2685 \(1993\); 10.1063/1.109257](#)

[Schottky barrier heights and interface chemistry in Ag, In, and Al overlayers on GaP\(110\)](#)

[J. Vac. Sci. Technol. B **8**, 955 \(1990\); 10.1116/1.584949](#)

[Engineered Schottky barrier diodes for the modification and control of Schottky barrier heights](#)

[J. Appl. Phys. **61**, 5159 \(1987\); 10.1063/1.338290](#)

[Influence of S and Se on the Schottkybarrier height and interface chemistry of Au contacts to GaAs](#)

[J. Vac. Sci. Technol. B **3**, 1197 \(1985\); 10.1116/1.583039](#)

[Fluctuations in Schottky barrier heights](#)

[J. Appl. Phys. **55**, 980 \(1984\); 10.1063/1.333153](#)

The logo for AIP Journal of Applied Physics. It features the letters "AIP" in a large, bold, white font on the left, followed by a vertical yellow bar, and the words "Journal of Applied Physics" in a white serif font to the right.

Journal of Applied Physics is pleased to
announce **André Anders** as its new Editor-in-Chief

APPLIED PHYSICS REVIEWS

The physics and chemistry of the Schottky barrier height

Raymond T. Tung (董梓則)^{a)}

*Department of Physics, Brooklyn College, CUNY, 2900 Bedford Avenue, Brooklyn, New York 11210, USA
and Physics Ph.D. Program, The Graduate Center, CUNY, 365 Fifth Avenue, New York 10016, USA*

(Received 20 September 2013; accepted 17 October 2013; published online 13 January 2014)

The formation of the Schottky barrier height (SBH) is a complex problem because of the dependence of the SBH on the atomic structure of the metal-semiconductor (MS) interface. Existing models of the SBH are too simple to realistically treat the chemistry exhibited at MS interfaces. This article points out, through examination of available experimental and theoretical results, that a comprehensive, quantum-mechanics-based picture of SBH formation can already be constructed, although no simple equations can emerge, which are applicable for all MS interfaces. Important concepts and principles in physics and chemistry that govern the formation of the SBH are described in detail, from which the experimental and theoretical results for individual MS interfaces can be understood. Strategies used and results obtained from recent investigations to systematically modify the SBH are also examined from the perspective of the physical and chemical principles of the MS interface. © 2014 AIP Publishing LLC. [<http://dx.doi.org/10.1063/1.4858400>]

TABLE OF CONTENTS

I. INTRODUCTION	1
II. REVIEW OF SBH RESULTS	3
A. SBH formation without chemistry: Schottky-Mott rule	3
B. What makes SBH mysterious: Interface chemistry.....	4
C. Fermi level pinning and simple SBH models	5
D. Epitaxial MS interfaces and theoretical calculations.....	8
E. Inhomogeneous SBH.....	14
III. PHYSICAL AND CHEMICAL PERSPECTIVES ON INTERFACE-DIPOLE FORMATION.....	17
A. Electrostatics at solid interfaces: Energy levels and their “hosts”.....	17
B. Formation of electronic states at epitaxial MS interfaces	24
C. Charge transfer in molecules	30
D. Estimation of interface dipole	32
E. Non-uniform MS interfaces and defects	36
F. Nanostructures and nano-scale contacts	39
IV. MODIFICATION OF SBH.....	41
A. SBH modification with molecular dipoles..	41
B. SBH modification with thin layer of insulating material	44
C. SBH modification with atomic monolayer (s)	46
V. CONCLUSIONS.....	49

I. INTRODUCTION

The electrical current flowing across the interface between a metal and a semiconductor is usually non-linear against the applied bias voltage, as the result of a discontinuity on the energy scale of the electronic states responsible for conduction in the two materials. In Fig. 1, a band diagram of the interface is sketched to show this discontinuity. Delocalized electronic states around the Fermi level (FL) are responsible for electrical conduction in the metal, drawn on the left, but these states are not coupled to any delocalized electronic states in the semiconductor drawn on the right. The set of electronic states responsible for electrical conduction in the semiconductor depends on the doping type of the semiconductor. For n-type semiconductors, the electrons near its conduction band minimum (CBM) are primarily responsible for electrical conduction, and for p-type semiconductors, holes near the valence band maximum (VBM) carry most of the current. Because of the presence of the fundamental band gap, the lowest-lying states for n-type semiconductor that can communicate with electrons in the metal are now at an energy $\Phi_{B,n}^0$ above the FL, as shown in the figure. For electronic transport across the metal-semiconductor (MS) interface, this energy offset, known as the n-type Schottky barrier height (SBH), manifests itself as a potential energy barrier that leads to rectifying behavior between the metal and the n-type semiconductor, i.e., the flow of electrons from the semiconductor to the metal is easier than conduction in the opposite direction. If the semiconductor in contact with the metal is doped p-type, the energy difference between the FL and the VBM, marked as $\Phi_{B,p}^0$, is now the energy barrier, i.e., the p-type SBH, that controls the transport of holes across this MS interface. Because the current flow across an MS interface depends exponentially on the magnitude of the SBH at common

^{a)}rtung@brooklyn.cuny.edu

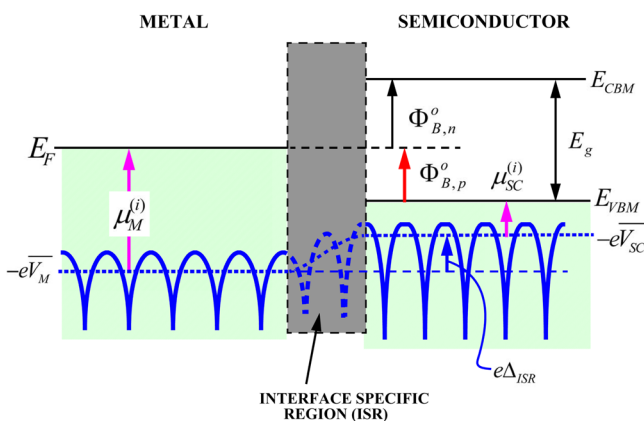


FIG. 1. Band diagram at a metal-semiconductor interface. The electrostatic potential energy, $-eV(\vec{r})$, is drawn as curve lines. Dotted lines indicate average electrostatic potential.

applied voltages, the SBH is clearly the most important property of an MS interface that decides its electrical characteristics. From a scientific perspective, the explanation of the alignment condition between the energy bands across an MS interface represents an interesting challenge, and there is a long history of extensive scientific investigations attempting to meet that challenge. As a matter of fact, the formation mechanism of the SBH has been an area of very active research in condensed matter physics and surface science, dating back at least sixty years. There were annual conferences dedicated to this topic and focused sessions at every large international meeting on electronic materials in the 1970s and 1980s to address the SBH “mystery.” This intense scientific interest in the SBH still paled in comparison with the pressure and demand within the semiconductor industry to solve the contact problem for various devices. In terms of applications, the magnitude of the SBH is of overriding importance for electronic devices, and “solving the contact problem” essentially means to be able to control, or “tune,” the SBH for the MS interfaces of any desirable device. Such a technology-related problem should not be difficult to solve if the formation mechanism of the SBH is thoroughly understood. With so much effort that has gone into SBH research, and given the astonishingly sophisticated state of today’s semiconductor devices and fabrication technologies, it seems a sure bet that the formation mechanism of the SBH should be, by now, a well understood subject theoretically and the magnitude of the SBH is a quantity that can be skillfully controlled technologically. However, a glimpse into most recent literature on the SBH and ohmic contacts still finds a wide spectrum of conflicting opinions and models, with which SBH data are interpreted. Also, except for sporadic demonstrations of strategies capable of altering the SBH in isolated cases, techniques effective in achieving desired SBH for any semiconductor system in general are still lacking. It seems only natural to ask “why haven’t we learned more about the SBH after all the scientific and technological investigations?”

The lack of a coherent explanation of a wide spectrum of experimentally observed SBH data and the lack of control over the magnitude of the SBH, despite decades of intensive investigations, speak volumes about the difficult and complex nature of the SBH problem itself. The main sticking point can

be traced to a sharp dependence of the SBH on the atomic structure of the MS interface, which has slowly yet surely been established through careful experimental and theoretical investigations. Compounding that dependence by a lack of control and understanding of the atomic structure at common MS interfaces routinely fabricated in the laboratories, and the SBH researchers really had an uphill battle on their hands. Presently, short of full-fledged numerical calculations, there are still no comprehensive and quantitative theories on the formation of interface dipole to explicitly address this most crucial part, i.e., the structural dependence, of the SBH. On the other hand, simple models of SBH are the ones that are easy to understand, easy to use, and the only ones that have been treated in standard textbooks.^{1–3} Even though it has been pointed out that the basic assumptions made in simple models of the SBH are at odds with what *ab initio* calculations revealed about real MS interfaces,⁴ researchers still cling to them out of convenience and are hesitant to look beyond them for a more complete and realistic view of the SBH, presumably one that’s built on the rigor of quantum mechanics. This gap between the complexity of the problem and the simplicity of the models it has continued to be compared with has been the main obstacle to SBH research that really shouldn’t have been let happen. Continued research and technology development efforts in the same mode will almost certainly leave us in the doldrums, which we cannot afford to do at a time when the continued advances in technologies and the searches for novel devices demand an immediate solution to the contact issue.

The main purpose of this review article is to point out, through an examination of experimental and theoretical results on atomically controlled MS interfaces and known fundamental principles, that a nearly complete quantum-mechanics-based picture of SBH formation can already be constructed. However, as is often the problem with quantum descriptions of any realistic and practical phenomena, the formation of the SBH turns out to be intricately dependent on the specifics of the MS interface under study. Therefore, quantum description of the SBH in general cannot be formulated into simple analytic equations that are applicable for all MS systems, especially since there are usually so many important details about any MS interface that are not experimentally known. However, if one is willing to look beyond the inconvenience of not having a short answer for every SBH situation waiting to be explained, there are actually several basic principles that transcend all interface specificities and it is the interplay of these overarching principles under different circumstances that lead MS interfaces to display a wide range of intriguing and sometimes puzzling SBH behavior. These basic rules, which traditionally belong to, and are discussed in, their respective disciplines of electrostatics, quantum theory of solids, chemical bond formation, quantum transport, etc., together describe the formation of the SBH and therefore they should also form the knowledge base with which we understand SBH data and tackle technological SBH problems. In Sec. III, we will introduce each of these principles in their traditional settings and discuss in detail the specific roles each plays in the SBH. As the prospects for ever finding one fixed rule for the entire field of MS interfaces look very dim, these concepts are the only faithful ones that we can fall back on

and the ones that we would need to put together for specific MS interface, under the known circumstances surrounding its formation, in order to make sense of its particular SBH behavior. Putting together separate ideas from their varied origins is mainly what this article intends to do. We will go over the basic concepts that are important for the SBH, examine real examples to see what roles these concepts play in shaping the actual experimental observations. The concepts that are fundamentally important for a sound description of the SBH come from the realms of both “physics” and “chemistry.” Therefore, when an esteemed Editor of this journal suggested the current title for this article, which contains both of these buzzwords, the author gratefully agreed. This turned out to be far better than any title for this article the author had thought of on his own! The plan of this review article is as follows: We will summarize what has been discovered about the SBH through experiments and theoretical calculations, both historically and recently, in Sec. II, where we will also go over the philosophy and circumstances behind some simple models of the SBH. Since most of the discussions here are on topics that have already been covered in some detail in prior reviews, Sec. II will be brief in places but will serve the function of directing interested readers to original work for further reading. Section III will be devoted to in-depth discussions of classical and quantum concepts that are essential and necessary in order to properly analyze the formation of interface dipole for specific MS system. Section IV will examine recent experimental and theoretical work on SBH adjustment at technologically important interfaces, from the perspective of the physics and chemistry expected at these MS interfaces.

II. REVIEW OF SBH RESULTS

A. SBH formation without chemistry: Schottky-Mott rule

In-depth discussions and explanations of the magnitude of the SBH usually begin with a consideration of the Schottky-Mott Rule,^{5,6} which is an excellent practice because the Schottky-Mott Rule is a stalwart reminder of the critical role played by electrostatics in all energy-level-alignment types of problem, including the SBH. When a crystal is in isolation, the positions of its internal energy bands can be referenced to the “vacuum level” outside, as illustrated in Fig. 2(a), which shows that the energy difference between the vacuum level and the Fermi level of an isolated metal is the metal work function, ϕ_M . Hidden in a band diagram like this

are the facts that a surface of the solid has been created and that the surface has specific orientation, atomic structure(s), and electronic structures that likely influence the work function. What should also be pointed out is that the relevant “vacuum level” here is the rest energy of an electron placed just outside the crystal surface, and that only in cases where the long-range electric field vanishes identically in vacuum can this level be equated with the vacuum level at infinity.^{4,7} In Fig. 2(a), the bands of an isolated semiconductor are also sketched, with the CBM of the semiconductor drawn at an energy χ_{SC} (semiconductor electron affinity) below the vacuum level. Again, we should keep mind that χ_{SC} depends on the specifics of the semiconductor surface. The Schottky-Mott Rule prescribes that the alignment condition for the energy bands when the two crystals are each in their isolated state should also prevail over the intimate MS interface between these two crystals. From Fig. 2(a), before the two crystals make contact with each other, the CBM of the semiconductor is at an energy $\phi_M - \chi_{SC}$ above the metal FL. If, after the metal and the semiconductor make contact and form an interface, the CBM is still found to be so positioned with respect to the FL, then we say that the Schottky-Mott Rule,

$$\Phi_{B,n}^o = \phi_M - \chi_{SC} \quad (\text{Schottky - Mott}), \quad (1)$$

is observed for this MS interface. Or, equivalently, the p-type SBH is said to obey the Schottky-Mott Rule, if it is found that

$$\Phi_{B,p}^o = I_{SC} - \phi_M \quad (\text{Schottky - Mott}). \quad (2)$$

The underlying idea behind the Schottky-Mott Rule, and the related Anderson Rule for heterojunction band offset,⁸ is the “superposition principle” of electrostatic potential. In practice, these theories seem as simple as “lining up the vacuum levels outside the two surfaces.” Schematically shown in Fig. 2(a) is the distribution of the electrostatic potential energy near the free surfaces of the two crystals. In the interior of each crystal, the electrostatic potential is periodic, arising from the periodic distribution of electronic and nuclear charge. The average electrostatic potential energy per unit cell for the metal, when referenced to the vacuum level, is assumed to be $-e\bar{V}_M$. In a bulk crystal, all the energy levels and bands have definite and fixed relationship with respect to the electrostatic potential of the crystal. We may identify the Fermi energy of the metal relative to its average potential energy as its internal chemical potential, $\mu_M^{(i)}$, i.e.,

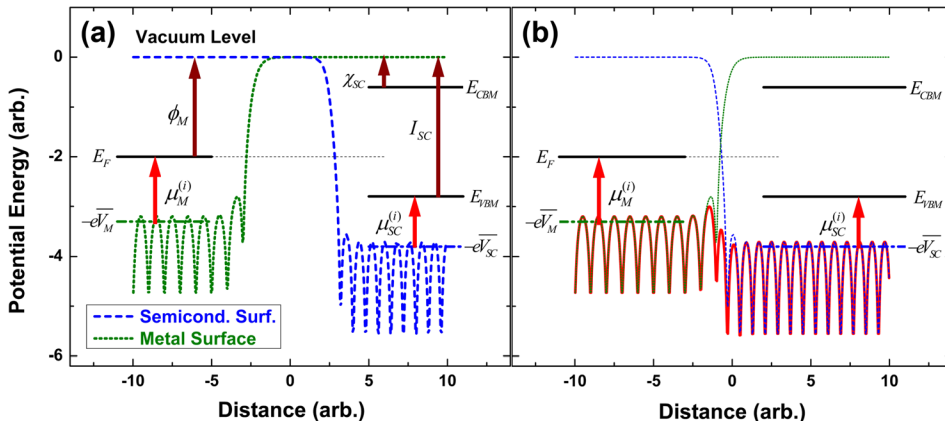


FIG. 2. Potential energy for isolated metal surface (dotted) and semiconductor surface (dashed) plotted on the same energy scale. (a) When the two crystals are far apart. (b) When the two crystals are next to each other. The solid line is the sum of the two individual potential energies. Note the relative position of the semiconductor potential to the metal potential remains unchanged, independent of the distance separating the two crystals.

$$E_F = -e\bar{V}_M + \mu_M^{(i)}. \quad (3)$$

Note that $\mu_M^{(i)}$ is calculable with quantum mechanics and is a pure bulk quantity that does not depend on the structure of the crystal surface, while the other two terms in Eq. (3) depend on the specifics of the metal surface. Also note the electrostatic potential energy arises only from Coulomb interaction, i.e., the average electrostatic energy increases by $q\bar{V}_M$ when a test charge q of any kind enters from vacuum into the metallic crystal. Surface scientists have preferred to break down this drop in potential energy from the exterior upon entry into the metal crystal, $-e\bar{V}_M$, into a surface dipole contribution that depends on the structure of the surface and a bulk contribution which does not.^{9,10} However, a surface dipole cannot be uniquely defined, mainly because the “bulk contribution” cannot be uniquely defined,¹¹ as discussed later. From the distribution of the electrostatic potential energy near the surface of a semiconductor shown in Fig. 2(a), we can also define an average electrostatic potential energy, $-e\bar{V}_{SC}$, for the interior of the semiconductor. Some clarification should be made about the electrostatic potential inside a semiconductor, which wasn’t necessary for metallic crystals. Due to incomplete screening, long-range electric field can be present inside a semiconductor, or any insulating material, making it possible for the electric potential energy to vary with position. The $-e\bar{V}_{SC}$ shown in Fig. 2(a) refers to the average potential energy in the “near-surface” region of the semiconductor. The VBM of the semiconductor, being the highest occupied state in the semiconductor, is the sum of the average electrostatic potential energy of the crystal and its internal chemical potential,

$$E_{VBM} = -e\bar{V}_{SC} + \mu_{SC}^{(i)}. \quad (4)$$

While the metal and semiconductor are separated, as shown in Fig. 2(a), the difference between the average electrostatic potential energy of the metal and that of the semiconductor is $-e\bar{V}_M + e\bar{V}_{SC}$. If the charge distribution of both the metal and the semiconductor is held fixed, and the two crystals are brought together, the potential energy difference will remain the same, as graphically demonstrated in Fig. 2(b). This is necessarily the case because the electrostatic potential energy arises only from charge distribution and obeys superposition principle. Therefore, under the condition that charge rearrangement can be strictly avoided during MS interface formation, the band alignment condition for the isolated crystals carries over to the final interface, i.e., the Schottky-Mott Rule will hold. One thus deduces that the Schottky-Mott Rule describes the SBH of the metaphysical, non-interacting MS interfaces, put together without charge or atomic relaxation. Because of such, the Schottky-Mott Rule has very limited relevance for real MS interfaces and is not expected to be able to account for experimentally observed SBH. However, this Rule is a worthwhile indicator of the electrostatics in the system before interface chemistry takes over.

B. What makes SBH mysterious: Interface chemistry

Ever since Schottky diodes became available for experimental investigation decades ago, it was clear that the

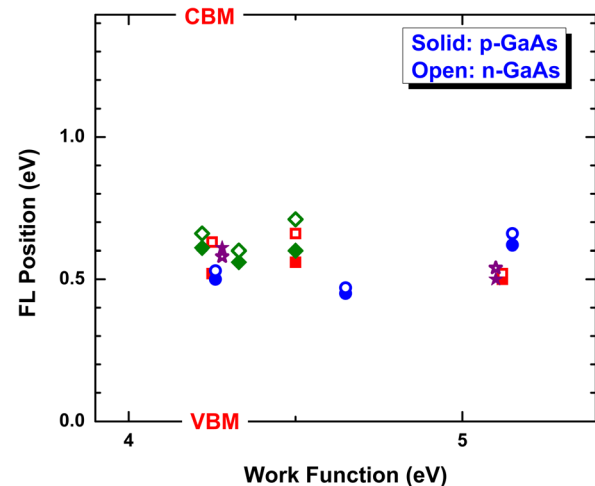


FIG. 3. Fermi level position of ideal metal contacts to GaAs. Filled symbols represent SBH measured by I-V method on p-type GaAs, while open symbols are the difference between the band gap and the n-type SBH measured by I-V. Corrections for the effect of image force have been included. Adapted from Ref. 12.

idealistic, non-interacting picture of the MS interface suggested by the Schottky-Mott Rule was in error. Shown in Fig. 3 are FL positions in the band gap found for various metals evaporated in ultrahigh vacuum (UHV) on n- and p-type GaAs (100) surface, plotted against the work function of the metal.¹² In this particular case, there is no clear dependence of the SBH on the metal work function. The absence of a strong dependence of the SBH on the metal work function was an unexpected and sensational phenomenon that was observed on various covalent semiconductors. This phenomenon was given the name “Fermi level pinning” and captured much of researchers’ attention and imagination for the last quarter of the 20th century. The reason that the Schottky-Mott theory fails is obvious: the charge distribution at real MS interfaces is significantly different from a simple superposition of the charge distributions on the original surfaces. In reality, during the formation of an MS interface, the metal and the semiconductor come to within close range of each other. From quantum mechanics, we know that when an atom is brought so close to another atom such that some orbitals from the atoms significantly overlapped, these isolated orbitals are no longer eigenstates of the system. Instead, molecular orbitals would form which could lead to chemical bonds. The chemistry at MS interfaces should not be any different, because metals and semiconductors are made of atoms. Electronic states that used to belong to only the semiconductor or only the metal have to be modified, to some degree, so that they can exist in the combined, larger quantum mechanical system. States that are related to the surfaces of the two crystals will not survive the formation of the MS interface, at least not without serious modifications. New “interface states” that are localized in the interface region and are dependent on the interface atomic structure may form. Because of chemistry, the actual charge distribution at an MS interface will be quite different from a linear superposition of the charge distributions on the two starting surfaces, as depicted in Fig. 2(b). One can attribute the net change in the potential energy as a result of charge rearrangement at the interface to the formation of an additional “interface dipole” eD_{int} , namely,

$$\Phi_{B,n}^o = \phi_M - \chi_{SC} + eD_{int}, \quad (5)$$

where $\Phi_{B,n}^o$ is the n-type SBH actually observed from an MS interface. We caution that there are many definitions of interface dipole and that the use of this term without a prior definition would be meaningless. The interface dipole can be largely viewed as the result of a transfer of charge between the metal and the semiconductor. While the direction of the charge transfer is usually self-evident, the exact amount of charge transferred, on the other hand, cannot be determined unambiguously. This is because at an MS interface there is no rigorous way to define where the metal begins and the semiconductor ends! It is only by artificial means that a charge transfer can be determined or defined. We shall adopt the convention that a “positive” interface dipole arises when an amount of electron is transferred from the metal to the semiconductor. Since the Schottky-Mott relationship is almost never observed in experiment, it can be concluded that the interface dipole does not vanish and is actually quite significant for the vast majority of MS interfaces. The formation of dipole at MS interfaces thus becomes the main focus of research and development work in SBH. It is not much of an exaggeration to say that “the formation of interface dipole is the entire topic of the SBH.” Casting the formation mechanism of the interface dipole in the light of basic physical and chemical principles is the main focus of Sec. III.

C. Fermi level pinning and simple SBH models

There is an element of timing in all simple models of the SBH that cannot be ignored. These models were all proposed at a time in the history of SBH research when the dominant experimental finding was the FL pinning phenomenon and the sole motivation for SBH theories seemed to be the explanation of this effect. The investigation of the “pinning strength” at a semiconductor (surface) was popular at the time, as this was believed to be a parameter that revealed the FL pinning mechanism. SBH data of various metals measured on one semiconductor were customarily plotted against the work function of the metal, such as shown in Figs. 3 and 4, the latter shows experimentally observed SBH for metals and metal silicides on n-type Si.^{13,14} The data presented in plots like these were typically fitted linearly to deduce a slope of the n-type SBH against the metal work function. This slope is called the “interface behavior parameter,” or the “S parameter” of the semiconductor

$$S_\Phi \equiv \frac{\partial \Phi_{B,n}^o}{\partial \phi_M} = 1 + \frac{e\partial D_{int}}{\partial \phi_M}, \quad (6)$$

which is regarded as a measure of the ability of a semiconductor surface to screen out external (metallic) influences. If the Schottky-Mott Rule were observed for a semiconductor surface ($D_{int} = 0$), i.e., no pinning, an S-parameter of 1 would be deduced. As can be seen from Fig. 4, the SBH on Si shows some correlation with the metal work function, but there is much scatter in the data and the overall trend of the data is far from the dashed line with the slope of unity drawn on the same figure to represent the Schottky-Mott prediction.

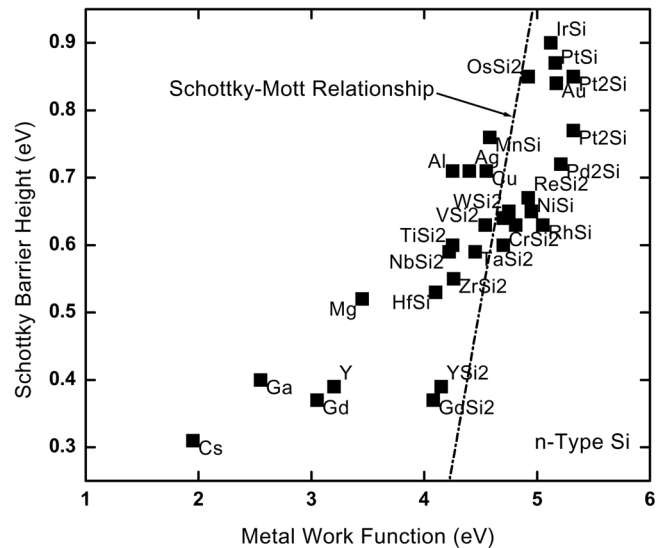


FIG. 4. Experimental Schottky-barrier height on n-type Si.^{13,14} The straight line marks the prediction of the Schottky-Mott rule. Reprinted with permission from R. T. Tung, J. Vac. Sci. Technol. B **11**, 1546–1552 (1993). Copyright 1993 American Vacuum Society.¹⁵

A linear fit of the set of the experimental data shown^{13–15} would render an S parameter of ~ 0.2 for Si, the small value for which would imply that the FL is “strongly pinned” for Si interfaces. Other covalent semiconductors, such as Ge, GaAs, InP, etc., are also marked by small S-parameters or weak dependencies of the SBH on the metal work function, whereas compound semiconductors with larger ionicity tend to have larger S-parameters, although there are exceptions. How the S-parameters found for different semiconductors correlate with specific properties, such as the ionicity,¹⁶ the polarizability,¹⁷ or the dielectric constant,¹⁸ of the semiconductors also became the subject of discussions and debates in the literature. These research activities of attempting to experimentally establish a strength-of-pinning from the SBH dependence on the metal work function and then, from that, empirically deducing the SBH formation mechanism are unwittingly at the mercy of many other factors at the MS interface to “remain the same” to be meaningful. For example, although the data in Fig. 3 seem to suggest that the dependence of the SBH on the metal work function is weak, the SBH of the various metals nevertheless varies over a range of >0.2 eV in a manner unrelated to the work function. It is also known that SBH measurement of supposedly the same MS interface often exhibited very significant variations in the magnitude of the SBH and/or the details of the junction characteristics, as a result of differences in surface preparation, treatment, and measurement technique. Theoretical and experimental investigations in the last decade of the 20th century would reveal that the electrical characteristics found for most of the (polycrystalline) MS interfaces involved in these empirical studies actually exhibited clear evidence for SBH inhomogeneity.^{19,20} In other words, the FL was not uniquely positioned at most of these MS interfaces but rather varied locally, and the measured, supposedly singular, SBH for the entire MS interface was actually just an average among a significant range in the SBH for that interface.

The widespread observation of SBH inhomogeneity indicates that the FL is “unpinned” within most MS interfaces, making the dedicated efforts at the time to find the “pinning” mechanism ill-advised. Given these additional bits of information, it only makes sense today for us to look at plots such as Figs. 3 and 4 with some caution. First of all, since each “point” on these plots actually represents a range of SBH, there is at least one other parameter, in addition to the metal work function, that controls the SBH, i.e., D_{int} in Eq. (5) cannot be a single-valued function of ϕ_M . As $\Phi_{B,n}^o$ depends on multiple variables, the partial derivative in Eq. (6), mathematically speaking, should be taken with the other variable(s) held fixed, and the value of S_Φ would depend on the value of the other parameter, as well as ϕ_M . It is not surprising then that quite different S_Φ values were deduced from analysis of experimental data obtained by different laboratories or under different processing conditions. The message one gets from plots such as Fig. 4 should not be that the S-parameter is such and such for this semiconductor, but rather something that inspires the question “beside the work function and the electron affinity, what other factors are important for the SBH that are making the local SBH changing?” Without a knowledge of all the parameters that control the SBH, the value of the S-parameter itself has little meaning. It seems that the investigation of the reason(s) for the SBH to be locally varying would more directly reveal the microscopic formation mechanism of the SBH than making much of the slopes in plots such as Figs. 3 and 4.

At the time when researchers attempted to solve the mystery of FL-pinning at MS interfaces, a different phenomenon, unfortunately by the same nickname, was also a topic of much interest and investigation. The pinning of the FL in the band gap at the free and adsorbate-covered surfaces of semiconductors was extensively investigated and, by then, well understood to be driven mainly by the overall neutrality of the semiconductor surface.²¹ When the periodic structure of a crystal lattice is terminated at a surface, electronic states particular to the surface are created. The FL for the semiconductor surface should always be positioned such that, just when all electronic states below the FL are occupied, the surface is electrically neutral. The reason for the neutrality requirement is obvious: excess charge on the surface costs energy, in the absence of external free charge. For the FL of semiconductor surface therefore, the energetic position of electronic states in the surface region is of primary importance. Surface electronic structure depends on the atomic structure of the surface, and conversely, the atomic structure of the surface is dictated by surface energy, to which the distribution of surface electronic states make a major contribution. Electronic states found at the surface can be true surface states, which exist only in the gaps of the bulk energy band structure and decay in amplitude away from the surface, both toward vacuum and toward the bulk crystal. They can also be tails of the Bloch states of the semiconductor crystal, which generally decay toward the vacuum but could have enhanced intensity in the surface region, in which case they are known as surface resonance states. These aspects of surface electronic structure are similar to what will be described for the MS interfaces in Sec. III B. Uniform

semiconductor surfaces typically feature dangling bond states from the surface atoms, which broaden into two-dimensional (2D) surface state bands in the fundamental gap of the semiconductor. The charge neutrality level (CNL) of electronic states in the surface region is then the FL for the surface. We should stress here that the CNL is an energy level that is defined by the charge neutrality condition for all electronic states in the entire surface region and not a level that can be revealed through analysis of only the charge distribution of electronic states in the gap. There is no particular neutrality requirement that needs to be satisfied by the “gap states” alone. Most frequently for semiconductor surfaces, the CNL is indeed found to lie in the gap of the bulk band structure, thus effectively “pinning” the surface FL inside the band gap. There are exceptions, the most prominent of which are the cleaved, non-polar {110} surfaces of some III-V compound semiconductors,^{22,23} which feature no surface state bands in the fundamental band gap. In principle, therefore, neutrality at these cleaved surfaces is satisfied if the FL is anywhere within the band gap.²⁴

The dominant role played by the CNL in pinning the FL position for semiconductor surfaces did not go unnoticed to researchers looking for an explanation for FL pinning at MS interfaces. The first of the proposals to involve the same mechanism in the explanation of both “FL pinning” effects came from Bardeen,²⁵ who suggested that the work function difference between a metal and a semiconductor with surface states could be compensated by an exchange of charge between the metal and the semiconductor surface states. This idea was developed into a quantitative model for the SBH by placing the metal not in direct physical contact with the semiconductor, but at a small gap distance away from it.²⁶ The schematic shown in Fig. 5 is the “fixed-separation

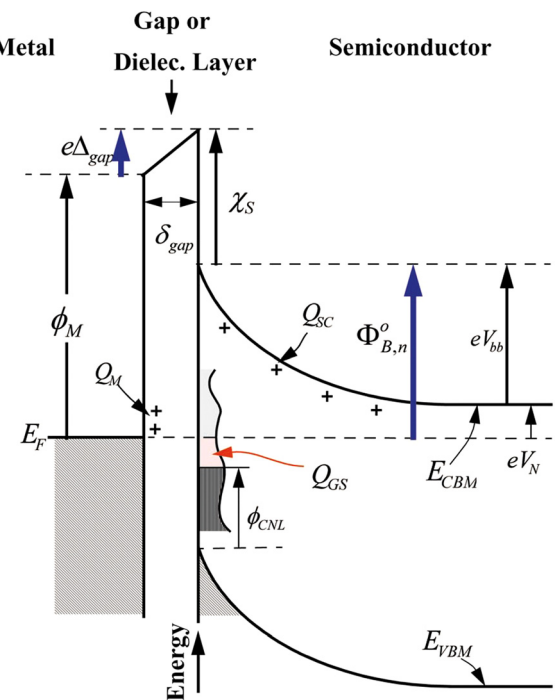


FIG. 5. The fixed separation model for SBH formation. Electronic states, with a characteristic CNL and density of states, are assumed to reside on the semiconductor surface, which is held at a fixed distance from the metal.

model” of interface dipole formation,^{4,26} which has been used not only for surface states but also for other types of interface states, including metal-induced gap states, defect states, etc. The small gap is imagined to be an (uncharged) oxide or dielectric layer that does not affect the surface states of either the semiconductor or the metal. Under these conditions, the n-type SBH can be deduced to be²⁶

$$\Phi_{B,n}^o = S_{GS}(\phi_M - \chi_{SC}) + (1 - S_{GS})(E_g - \phi_{CNL}), \quad (7)$$

where ϕ_{CNL} is the energy of the CNL, measured with respect to the VBM, S_{GS} is a constant in this theoretical model, given by

$$S_{GS} = \left(1 + \frac{e^2 \delta_{gap} D_{GS}}{\epsilon_{int}} \right)^{-1}, \quad (8)$$

which could be identified with the S-parameter experimentally deduced for the semiconductor, and D_{GS} , δ_{gap} , ϵ_{int} are, respectively, the density of surface states, the thickness of the gap, and the dielectric constant of the gap material. The slight separation between the metal and the semiconductor, $\sim 1\text{--}2\text{ nm}$, avoids the problem that the electronic structure of both the metal and the semiconductor should be significantly modified upon contact and, at the same time, allow some chemistry expected at MS interface, i.e., the charge exchange between the metal and the semiconductor, to take place. As can be deduced from the form of Eq. (7), the dependence of the SBH on the metal work function in this model is reduced by a factor of S_{GS}^{-1} , which could be a large number for a significant density of surface states, D_{GS} . Therefore, with a high density of surface states, the interface FL is expected to be strongly pinned, near the position of the CNL, as shown in Fig. 6. With two free parameters, D_{GS} and ϕ_{CNL} , to play with, Eq. (7) can explain any linear relationship found in SBH vs. work function plots such as Fig. 4. The artificial insertion of a dielectric layer at the MS interface might seem reasonable in the early days of SBH research when the cleanliness of semiconductor surface was suspect, but it makes no sense today as high resolution characterization techniques routinely reveal that MS interfaces fabricated with proper care are invariably intimate. One should note that even in the case that a thin dielectric layer truly separates the metal and the semiconductor as assumed in Fig. 5, the distribution of states at either the semiconductor-dielectric or the metal-dielectric interfaces cannot remain unchanged from the surface states on, respectively, the semiconductor and the metal. As explained in Sec. III B, the electronic states at these interfaces would depend on the band structure of the dielectric layer as well as the atomic structure of the two dielectric interfaces! Furthermore, there could be significant dipoles associated with both the semiconductor-dielectric and the metal-dielectric interfaces which would render the baseline condition for the band diagram, i.e., the use of ϕ_M and χ_S in Fig. 5, inappropriate (cf. Fig. 47). A convenience afforded by the fixed separation models, which is also presumably the most attractive motivation for these models, is that there is no mistaking which part of the interface belongs to the metal, which part belongs to the semiconductor, and the amount of

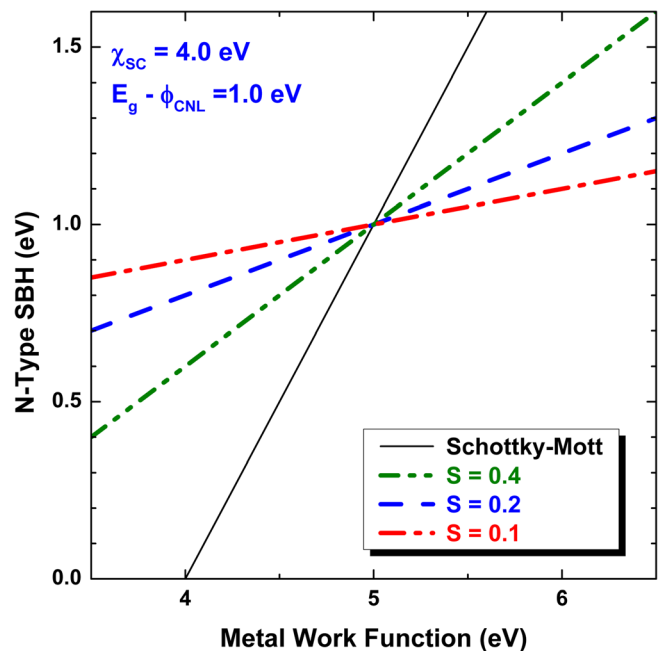


FIG. 6. Prediction from SBH models that assume a fixed separation between interface states and metal. The intercept of lines plotted with different S-parameters is at a metal work function corresponding to the difference between the CNL and the vacuum level, $\chi_{SC} + (E_g - \phi_{CNL})$, which is 5.0 eV for the present example, and at an n-type SBH of $E_g - \phi_{CNL}$, which is 1 eV in this example.

net charge on either side. At intimate MS interfaces, such unambiguous distinction would not be possible, which is a fact that makes the requirement of charge neutrality a meaningful concept only for the entire MS interface, and a meaningless one for only one (the semiconductor) part of the interface. We also note that the derivation of Eq. (7) presumes that the metal has nearly perfect screening and allows no penetration of the electric field inside,²⁷ i.e., the density of states at the metal-dielectric interface is assumed to be infinite. This is another feature common to all simple SBH models that is in disagreement with result from *ab initio* calculations, discussed below. While there is little doubt that a band diagram such as Fig. 5 can explain the weak dependence of the SBH on metal work function, the question has always been whether such a simple picture of the charge distribution at MS interfaces is realistic enough to be worthwhile considering.

Surface states in the band gap of the isolated semiconductor cannot remain at intimate MS interfaces,²⁸ because Bloch states from the metal are present at these energies. Inside the band gap of the semiconductor, metal wave functions cannot propagate into, but rather have to decay toward, the semiconductor. The tails of these wave functions penetrate a small distance into the semiconductor and are known as metal-induced gap states (MIGS). As a result of MIGS, there is a spillage of negative charge from the metal into the semiconductor side of the interface in this energy range. This gives the appearance of charge transfer, albeit unidirectional, between states near the FL of the metal and the MIGS in the semiconductor. Since the MIGS can be rationalized as what evolves from the surface states on the original semiconductor, there is the expectation that the CNL concept

is still applicable to the distribution of MIGSs at MS interfaces.^{29,30} To make use of the CNL concept for MIGS in simple models, however, it is necessary to justify that the distribution of the MIGS is independent of the metal. The idea was put forward that, even though a band gap exists for a bulk semiconductor, movement of the Fermi level inside the band gap at the interface of a semiconductor still leads to local charging.³¹ The distribution of induced gap states is then argued to be an intrinsic property of the semiconductor and, thus, is independent of the nature of the interface, being the same for MS interfaces and for semiconductor heterojunctions.^{27,32} Under these assumptions, the exchange of charge between the metal and the MIGS is envisioned to provide the dipole which screens the work function difference between the metal and the semiconductor. A distribution of MIGS, with a characteristic CNL, is assumed to be placed at a fixed distance, e.g., the decay length of typical MIGS, away from the metal to accommodate the charge transfer. Therefore, the band diagram by which an MIGS-based model is used to analyze the SBH is exactly as that already shown in Fig. 5 for surface states, and the specific predictions in an MIGS model for the SBH and the pinning strength are exactly those already given in Eqs. (7) and (8). There are many proposals on what the CNL should be for MIGS formed in the gap of a semiconductor. Tersoff argued that the CNL should be the energy level of the evanescent state with equal conduction and valence band character.³⁰ In one dimension, this is the branch point of the complex band structure. Arguments were also given as to why this level roughly corresponds to the midgap level of the indirect band gap.³² Cardonna and Christensen proposed that the midgap state at the Penn gap, called the “dielectric midgap energy” (DME), is the intrinsic CNL of the semiconductor.³³ Harrison and Tersoff drew from the tight-binding concept to propose that the average hybrid energy in the semiconductor, i.e., the dangling bond orbital energy, should act as the CNL.³⁴ There is also an empirical rule on the CNL from a compilation of experimental data.³⁵ From the perspective of quantum chemistry, the electronic wave functions in a region occupied by a material can always be expanded in terms of atomic orbitals of that material, because the orbitals form a complete set. The wave functions in the semiconductor material at the immediate MS interface can also be rigorously expanded in wave functions for the bulk semiconductor crystal, because the bulk wave functions, of all energies including unbound states, also form a complete set. The expectation is thus understandable that the semiconductor region at the MS interface will become neutral when certain energy is reached. However, this argument falls apart if the contributions from higher lying states are appreciable, which is almost inevitable when metal with orbitals of very different symmetries becomes the neighbor of the semiconductor.

Many aspects of the MIGS model are vague. For example, “the exchange of charge between the metal and the MIGS” has often been stated as the mechanism for interface dipole formation. This has two obvious problems: (1) The semiconductor does not have a density of electrons with energy in the bandgap. Therefore, there cannot be a transfer of electrons from the semiconductor to the metal around the

FL. Through the formation of MIGS, the transfer of charge around the FL can only be uni-directional. This is why early investigations of the role played by MIGS in SBH were under the banner of the “negative charge model.”^{36–38} (2) Because MIGSs are not isolated states but extensions of Bloch states in the metal, it is not possible to add or remove MIGS from the semiconductor side without adding or removing states on the metal side. They are parts of the same state. There is nothing to exchange! As explained below, the charge transfer between the metal and the semiconductor actually takes place through the entire energy range(s) of occupied states in the metal and the semiconductor, of which states inside the band gap represent only a small portion. How the MIGS theory is used to generate interface dipole is a carbon copy of how the fixed-separation model works, as shown in Fig. 5, with the exception that the gap states in the semiconductor are MIGS rather than surface states. Therefore, the shortcomings of the fixed separation model discussed above are also inherited by the MIGS model. Like the former, the MIGS model is unable to account for the large scatter in SBH data and the inhomogeneity of MS interfaces. In addition, some of the most basic assumptions of the MIGS models, such as the assumption on the independence of the MIGS distribution on the metal and the assumption that the CNL is an innate property of the semiconductor, are in disagreement with the result of *ab initio* calculations.^{4,39} It thus seems that the MIGS models have little connection with processes at real MS interfaces. Notwithstanding these known problems, pinning by MIGS has become, by far, the most frequently invoked model when SBH data are discussed in the literature. A browse into these publications often finds that it is the ability to use the linear dependence of the fixed-separation model, Fig. 6 and Eq. (7), which attracted the comparison with the MIGS model. In such comparisons, what the “MIGS model” represents is only the phenomenological aspect of its theoretical prediction and has little to do with the hypotheses within the model that led to the prediction.

D. Epitaxial MS interfaces and theoretical calculations

In order to fabricate an epitaxial MS interface, the crystal structures of the metal and the semiconductor must be similar and the lattice parameters of the two must be closely matched. That does not happen very often in nature, and therefore high quality epitaxial MS interfaces that have been experimentally produced are very few in number. However, once such single crystal interfaces are produced, the SBHs measured at these MS interfaces offer the most direct clues to the formation mechanism of the SBH. This is because the atomic structure is homogeneous at these MS interfaces and thus is clearly and solely responsible for the observed SBH. Most notable among epitaxial MS interfaces are the type A and type B $\text{NiSi}_2/\text{Si}(111)$ interfaces, both of which can be fabricated with very high structural perfection^{40,41} and their atomic structures have been carefully determined by high-resolution electron microscopy and other technique to be 7-fold coordinated.^{42–46} These two interface atomic structures are similar in immediate bonding arrangement and differ

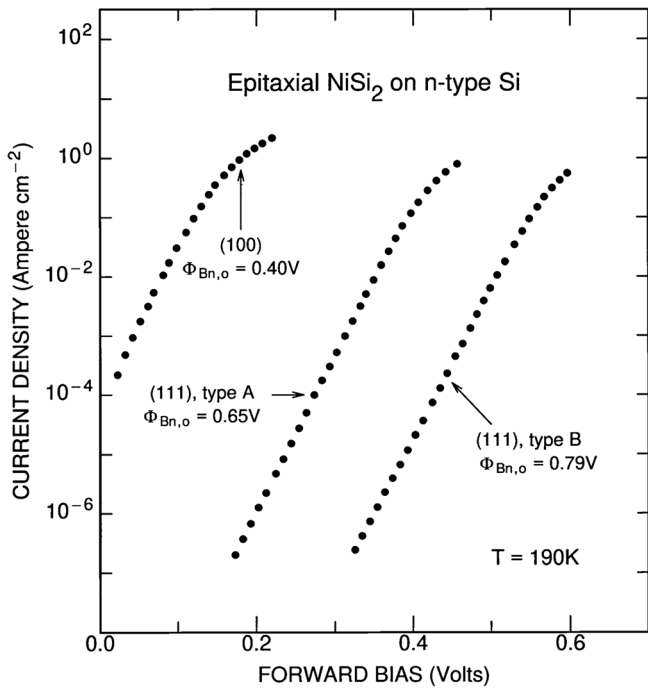


FIG. 7. I-V characteristics of single crystal NiSi_2 Schottky diodes on n-type Si, recorded at 190 K. Reprinted with permission from R. T. Tung, J. Vac. Sci. Technol. B **11**, 1546–1552 (1993). Copyright 1993 American Vacuum Society.¹⁵

only in distances for second-nearest-neighbor and beyond,⁴³ yet experiments showed that there was a difference of 0.14 eV in the SBHs of these two interfaces,⁴⁷ after an early experimental mistake⁴⁸ was identified. The NiSi_2/Si

(100) interface was another epitaxial MS interface that could be fabricated with near perfection in its crystalline order^{53,54} and its interface atomic structure was determined by high resolution electron microscopy.^{43,55} The n-type SBH of this NiSi_2 interface was found to be about 0.40 eV lower than that at the type B $\text{NiSi}_2/\text{Si}(111)$ interface,⁵⁶ as shown in Fig. 7. The experimental discovery of this huge variation in the SBH with orientation between a single phase of the silicide, NiSi_2 , and Si was in stark contrast to the opinion prevailing at the time that the SBHs for silicides were independent of the substrate orientation, crystalline phase, and stoichiometry.^{57,58} *Ab initio* calculations,^{59–61} based on the experimentally determined structure, yielded SBH results which were in excellent agreement with the trend experimentally observed for the two $\text{NiSi}_2/\text{Si}(111)$ interfaces.⁶⁰ One should note that even though the SBH difference was reproduced, the absolute values of the SBH from these calculations were not accurate, because of the problem with the local density approximation (LDA) employed in these calculations. The A- and B-type comparison filtered out systematic errors in the calculations, leaving the essence of the SBH formation mechanism bare to the view of researchers who study their interface electronic structures. The projected density of states for each layer for the two epitaxial $\text{NiSi}_2/\text{Si}(111)$ interfaces are shown in Fig. 8. Although the densities of MIGS were high at both interfaces,⁶⁰ calculations found no easily identifiable feature in the energetic distribution of these states to suggest a “pinning” of the FL. Actually, the role played by MIGS in determining the FL position could not be established in these calculations.^{59,60} The interface dipole arises from charge distribution of all electronic states below the

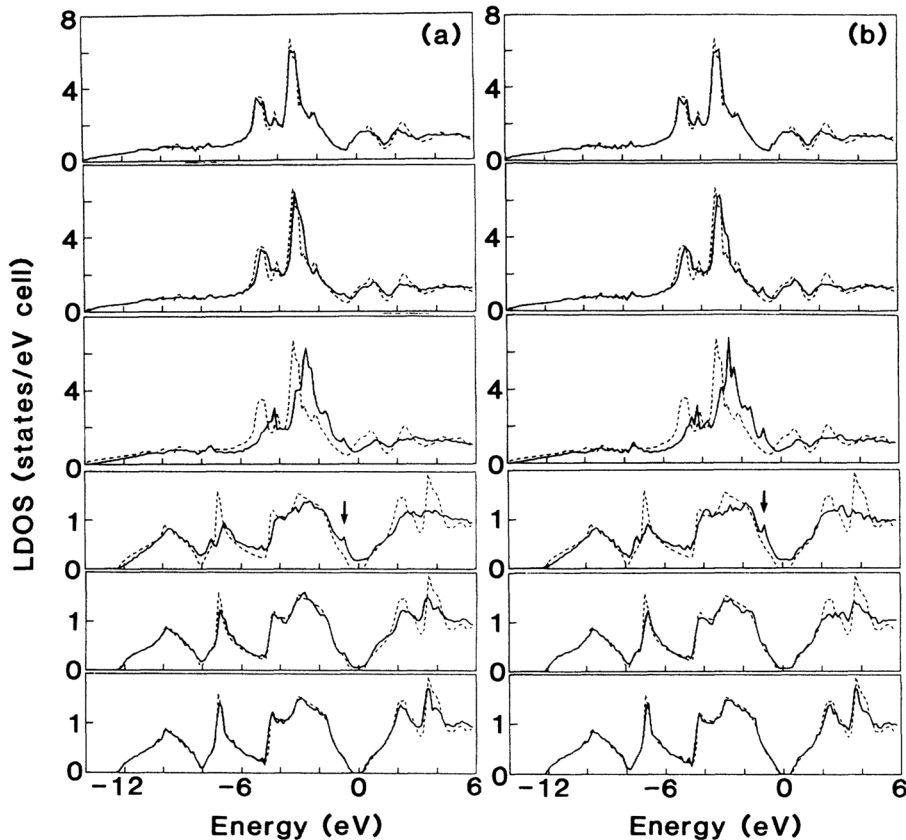


FIG. 8. Local density of states (LDOS) of the $\text{NiSi}_2/\text{Si}(111)$ interface obtained with 12/11 supercells: (a) of the type-A interface, (b) of the type-B interface. From top to bottom, they are sixth NiSi_2 layer, second NiSi_2 layer, first NiSi_2 layer, first Si_2 layer, second Si_2 layer, and sixth Si_2 layer from the interface. The dotted lines are bulk density of states of Si and NiSi_2 . The arrows indicate interface states. The zero energy point indicates the Fermi energy of the supercell. Reprinted with permission from H. Fujitani and S. Asano, Phys. Rev. B **42**, 1696–1704 (1990). Copyright 1990 by The American Physical Society.⁶⁰

Fermi level, of which the charge due to MIGS is only a small part. There are significant differences in the distribution of MIGS at these two interfaces, reflecting an expected dependence of the MIGS characteristics on the interface structure. The potential due to all charges at the two interfaces in Fig. 9 (Ref. 60) reveals that the local charge varies rapidly at the MS interface and extends a small distance into both the Si and the NiSi_2 . Two somewhat surprising features in Fig. 9 for both the A- and the B-type interfaces should be noted: (1) The potential does not simply decay into the metal (NiSi_2), but rather goes through some rapid changes inside the metal before decaying. This very significant chemical shift inside the metal can also be clearly observed in Fig. 8 by comparing the main features of the dashed curve (bulk NiSi_2 DOS) with the solid curve (interface NiSi_2 DOS) in the third panel from the top. Such a behavior is inconsistent with the expectation that the metal simply screens out the disturbance due to the presence of the semiconductor. (2) The total depth of potential variation is longer into the metal (~ 0.9 nm) than it is into Si (~ 0.5 nm), which is inconsistent with the suggestion from the MIGS model that the formation of the interface dipole is one-sided (longer into the semiconductor), because of the long tails of MIGS.³⁶

CoSi_2 is technologically more attractive^{62,63} because of its lower resistivity than NiSi_2 . Single-crystal $\text{CoSi}_2/\text{Si}(111)$ interfaces could be fabricated, albeit only with the type B orientation.^{64–66} Experimental and theoretical studies have indicated that the 8-fold model is most likely the structure for well-annealed, type B $\text{CoSi}_2/\text{Si}(111)$ interface.⁶⁴ However, it is also known that the interfacial structure of type B $\text{CoSi}_2/\text{Si}(111)$ may vary according to preparation. Evidence for 7-fold coordinated structure has been obtained from layers that have only been annealed to lower temperatures. The SBH of well-annealed type B CoSi_2 layers is in the range of 0.65–0.70 eV on n-type Si, which is usually attributed to the 8-fold structure. On the other hand, CoSi_2 layers grown at lower temperatures show considerable variation in their SBH, including an n-type SBH as low as 0.27 eV.^{67,68} Electronic structure calculations of the $\text{CoSi}_2/\text{Si}(111)$ interfaces showed that the SBH could vary by as much as ~ 0.6 eV with the assumed atomic structure and orientation of the interface. In particular, the n-type SBH for the 7-

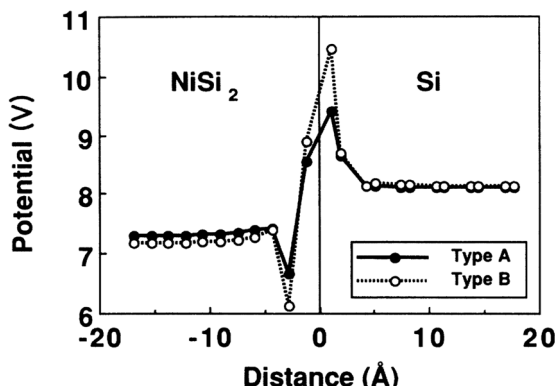


FIG. 9. Potential in each Si site. This was calculated by Madelung constants and charges in other atomic spheres. The center line is the interface. Reprinted with permission from H. Fujitani and S. Asano, Phys. Rev. B 42, 1696–1704 (1990). Copyright 1990 by The American Physical Society.⁶⁰

fold B-type interface was calculated to be lower than the 8-fold B-type interface, by ~ 0.1 –0.4 eV, depending on computation details, in agreement with the experimentally observed trend. The SBH of epitaxial $\text{CoSi}_2/\text{Si}(100)$ interface⁶⁹ is usually found not to differ much from that observed for polycrystalline CoSi_2 , ~ 0.7 eV. A 2×1 reconstruction is often observed at the interfaces of epitaxial CoSi_2 , although its structure has not been definitively determined.^{69–71} The existence of more than one stable structures has been suggested by HREM studies of the $\text{CoSi}_2/\text{Si}(100)$ interface.^{72,73} In particular, the SBHs of the two interfaces (upper and lower) of buried, epitaxial Si/ $\text{CoSi}_2/\text{Si}(100)$ structures were found to be different,⁷³ a dependence which was attributed to the difference in the observed interface structures.⁶⁸ Theoretical calculations showed that the SBH of the $\text{CoSi}_2/\text{Si}(100)$ interface depends on the assumed interface structure (cf. Fig. 29 below).^{74–76} However, the n-type SBH for 6-fold coordinated interface was calculated to be about ~ 0.3 eV larger than that for the 8-fold coordinated interface,⁷⁶ opposite to the trend experimentally deduced.⁷³

On compound semiconductor surfaces, epitaxial metallic compounds that have been successfully fabricated included elemental metals such as Al and Fe,^{77,78} and two groups of cubic materials with the CsCl and the rock salt structures.^{79–81} The interfaces between epitaxial Al and GaAs(100) were studied by a number of techniques.^{82,83} MBE prepared GaAs(100) surfaces may have a variety of reconstructions which are associated with different surface stoichiometry.⁸⁴ Some studies found that the SBH of epitaxial metal was a function of the original surface reconstruction/stoichiometry of the GaAs (100)^{85,86} and the ZnSe(100),⁸⁷ which was suggestive of a possible correlation of the interface structure and SBH. However, this correlation was not always found.^{88–90} Possible interface structures and electronic structures of the Al/GaAs system have been theoretically investigated.^{39,91,92} Needs *et al.* found the SBH at epitaxial Al/GaAs(110) interface to vary by as much as 0.7 eV with a change in the interface structure.⁹¹ A much smaller variation, ~ 0.1 eV, was found by Bardi *et al.* who noticed the importance of interface relaxation.⁹² In addition, experimentally observed dependence of the SBH of epitaxial Al/ $\text{Al}_{1-x}\text{Ga}_{1-x}\text{As}(100)$ interface on the alloy composition was reproduced by a linear response theory calculation.⁹² For the epitaxial Al/GaAs(100) interface, Dandrea and Duke provided detailed analysis of the distribution of MIGS's as a function of interface structure.³⁹ The density of MIGS was calculated to be above the 1×10^{14} $\text{cm}^{-2} \text{eV}^{-1}$ level, usually considered high enough to pin the Fermi level. However, the SBH was found to vary by 0.23 eV for the Al-Ga and Al-As bonded interfaces. The MIGS were incapable of pinning the Fermi level because the electronic charge density in other energy range changed by the order of 6×10^{14} $\text{cm}^{-2} \text{eV}^{-1}$ over the interface plane and overwhelmed MIGS screening. These resulted show a lack of direct connection between the Fermi level in the gap and the neutrality of the semiconductor. The interfaces between GaAs (AlAs) and a number of epitaxial intermetallic compounds have been examined by HREM.^{93,94} However, the atomic structures of these interfaces have not been firmly established. Evidence for a reconstruction has been observed at the

interface between NiAl and overgrown GaAs. The SBH of various structures involving epitaxial metallic compounds has been studied in detail. It was found that buried NiAl has a different SBH with respect to the overgrown (AlAs)GaAs than that on an (AlAs)GaAs substrate.⁹⁵ The observed SBH also seems to depend on the thickness of the NiAl and CoAl layers.⁹⁶ Furthermore, evidence for inhomogeneous SBH was found for these interfaces. The most spectacular result from these epitaxial metallic compound interfaces is the observation of a dependence of the SBH on epitaxial orientation,^{97,98} observed at the lattice-matched $\text{Sc}_{1-x}\text{Er}_x\text{As}/\text{GaAs}$ systems,^{97,98} and shown in Fig. 10. It shows that annealing may lead to significant changes in the observed SBH. The SBH of the ternary compound $\text{Sc}_{0.32}\text{Er}_{0.68}\text{As}$ varies by as much as 0.4 eV when the n-type GaAs orientation is changed from (100) to (111).⁹⁸ The electronic structure at ErAs/GaAs interfaces has been investigated in detail.^{99,100} There are two possible 1×1 structures for the ErAs/GaAs(100) interface, the Ga-terminated (the “chain model”), which is in agreement with experiment, and the As-terminated (the “shadow model”). Straight calculations for these two un-reconstructed interfaces showed that the FL was pinned at close to the CBM and VBM, respectively. The buckling of the two kinds of atoms in the mixed (Er + As) plane was responsible for a very large adjustment (>1 eV) in the interface dipole.¹⁰⁰ The p-type SBH calculated for a 2×2 reconstructed, and yet energetically more favorable, (100) interface structure was lower than that calculated for the ErAs/GaAs(110) interface by about 0.2 eV, in agreement with experimental result shown in Fig. 10.

If either the metal or the semiconductor forming an MS interface is a compound phase, there is always a choice on whether the interface is terminated on anions or cations,

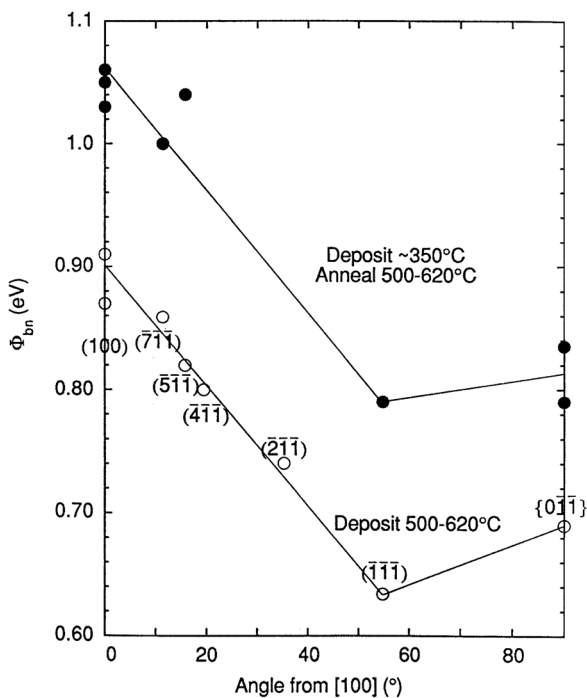


FIG. 10. Schottky barrier height versus substrate orientation for lattice matched $\text{Sc}_{1-x}\text{Er}_x\text{As}/\text{GaAs}\{\text{h}11\}$ diodes. Reprinted with permission from Palmstrom *et al.*, J. Vac. Sci. Technol. A **10**, 1946–1953 (1992). Copyright 1992 American Vacuum Society.⁹⁸

except for non-polar interfaces. The type of silicide interfaces, e.g., 8-fold or 6-fold, described above is a subtle example of this termination issue. For every compound semiconductor studied by numerical calculations, termination at polar interfaces has been a prominent parameter that leads to different SBHs, e.g., for $\text{GaAs}(100)$,³⁹ $\text{GaN}(100)$,¹⁰¹ and $\text{ZnSe}(100)$ ⁸⁷ interfaces. General considerations would suggest that, everything else being equal, the anion-terminated interface should have a smaller n-type SBH than the one terminated on cations. Furthermore, the SBH difference between the cation- and anion-terminated interfaces should increase with semiconductor ionicity. A systematic study of these issues was conducted by Berthod *et al.*,¹⁰² who calculated the electronic structures at the unrelaxed interfaces of Al with different terminations of the lattice-matched, (100)-oriented, Ge, GaAs, AlAs, and ZnSe crystals. The calculated SBHs were shown to be in reasonable agreement with experiment. Furthermore, the possibility was explored, of explaining the calculated SBH within a model^{103,104} assuming “linear response” of the interface charge distribution to “external disturbance” in the form of changes in the nuclear charge (or, more precisely, the pseudo-potential) of atoms at the interface. To determine the systematics of dielectric response from the electronic distribution at the MS interface, a “test charge sheet,” in the form of a dilute mixture in the pseudo-potential of the atoms on a selected plane, was first placed at different depth on the semiconductor side to induce a change in the potential drop across the MS interface. The result of this clever “numerical experiment,”^{102,105} shown in Fig. 11, represented the linear response with which the difference in the cation- and anion-terminated SBH was compared. Excellent agreement was found for the Al/GaAs(100) and the Al/ZnSe(100) systems, while for the Al/AlAs(100) interface the trend in the calculated SBH was predicted in the right order of magnitude by the model. In general, this work suggested that the concept of image-charge screening, classically only valid at macroscopic dimensions, could be extended to distances shorter than the decay length of the MIGS. This is an excellent work that is a great assistance to the understanding of the interplay between chemistry and electrostatics at the MS interface.^{102,106} Note that even though the interface charge distribution seems to respond linearly to small changes in the nuclear (pseudo-)potential, this is largely an electrostatic effect. The baseline (the non-polar version) of these MS systems, on which the numerical experiments were conducted, already had interface dipoles, via quantum mechanical calculations, that satisfied the chemical (or bond-forming, energy-minimizing) aspect of the interface interaction.¹⁰² It would not be right to conclude from the image-force picture that the act of bond formation between the metal and the semiconductor could also be treated by a linear response model. One wouldn’t know where to begin, in that case.

A technologically important group of semiconductors whose SBH has been discovered to depend on the surface termination is silicon carbide.^{107–112} The SBH of two polytypes of the SiC family, 3C-SiC and 6H-SiC, have been studied in detail. Experimentally, the dependence on the starting surface termination for the individual metal has been strong,

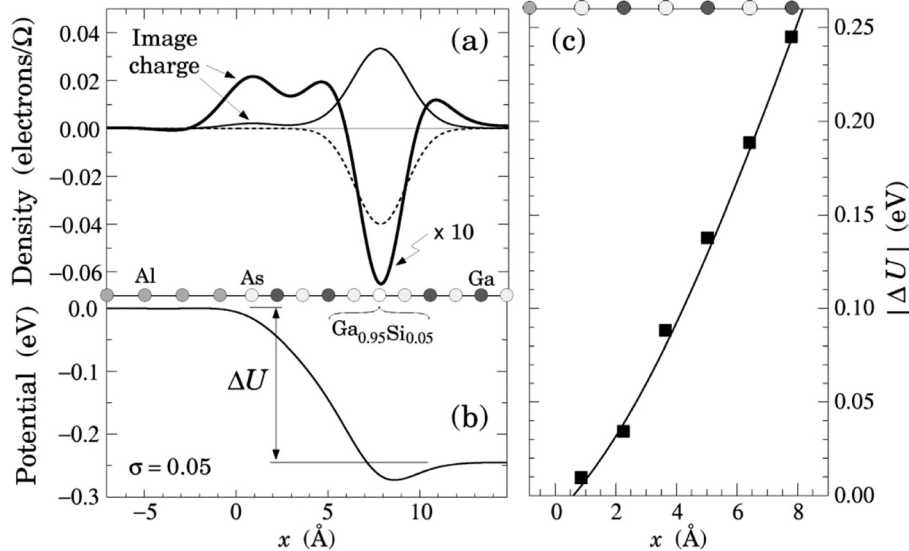


FIG. 11. (a) Macroscopic average of the electronic (thin solid line) and ionic (dotted line) charge densities induced by a plane of $\langle \text{Ga}_{0.95}\text{Si}_{0.05} \rangle$ virtual ions in the As-terminated Al/GaAs(100) junction. A Gaussian filter function was used for the macroscopic average. The thick solid line is the sum of the electronic and ionic densities, scaled by a factor of 10. (b) Macroscopic average of the corresponding induced total electrostatic potential. The resulting potential difference ΔU is also indicated. (c) Schottky barrier modification $|\Delta U|$ (filled squares) obtained for a surface charge $\sigma = 0.05$ as a function of its position within the semiconductor, in the As-terminated Al/GaAs junction. The symbols give the results of the self-consistent calculations. The solid line corresponds to the prediction with $x_0 = 0.06$ nm. The calculations were done in a 7 + 21 supercell. Reprinted with permission from Berthod *et al.*, Phys. Rev. B **68**, 085323 (2003). Copyright 2003 American Physical Society.¹⁰²

although a systematic correlation has been lacking.^{107–109} It is not known the extent to which the original surface termination has survived at the final MS interfaces. These MS interfaces typically do not have good lattice matches and are not expected to accommodate epitaxial growth. However, theoretical calculations have been carried out by artificially placing metal atoms on strained lattice sites, which typically found that the C-terminated surfaces were more chemically reactive, and the dependence on metal work function stronger, than the Si-terminated surfaces.^{113–115} As shown by the summary in Fig. 12, the n-type SBH on C-terminated SiC is systematically larger than that found on Si-terminated SiC. Oxide semiconductors/insulators with the perovskite structure (ABO_3) are of great interest for a wide range of current and future applications.^{116,117} Along the normal (100) direction, a perovskite crystal can end on an AO surface plane, where A represents a 2+ cations such as Sr and Ca, or a BO_2 plane, where B is a 4+ cation such as Ti or Si. Because of the ionicity of the compound, these two surface terminations could offer different band alignment conditions.¹¹⁸ Theoretical calculations of the

electronic structure at the interface between SrTiO_3 (100) (STO) band various metals showed that the SBH has a wider range of variation (~ 0.7 eV) on SrO-terminated surface than the range (0.3 eV) observed on TiO_2 -terminated surface.¹¹⁹ For each individual metal, however, the effect of the surface termination on the SBH is present but not very significant (≤ 0.3 eV). An interesting insight into the formation mechanism of the SBH was offered in these calculations through a break-down of the final SBH into stages. The alignment condition between metals and STO was calculated as the difference at the free surface stage ("stage 0"), at a stage when the surfaces of the STO and the Pt were individually constrained to their eventual, relaxed, atomic arrangement at the interface ("stage 1"), and then at the final equilibrated relaxed interface structure ("stage 2"). This analysis showed that even though the two different surface terminations led to very significant differences (> 1 eV) in the alignment conditions at stages 0 and 1, the rearrangement in the spatial distribution electronic density when the metal and the semiconductor made contact in stage 2 would dominate and render the SBHs on the two

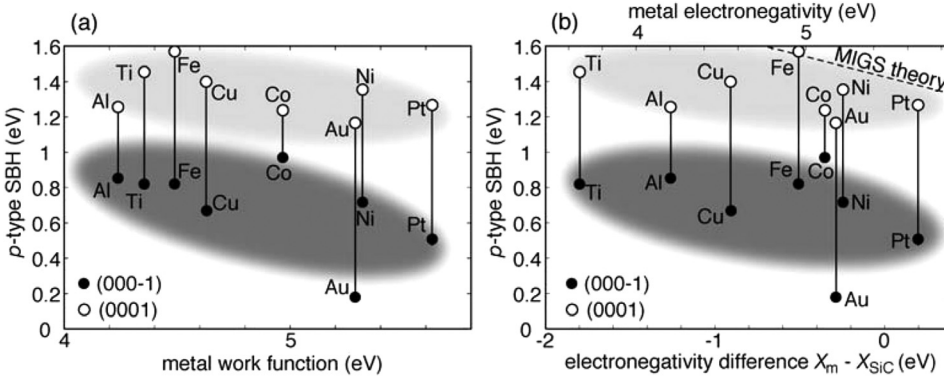


FIG. 12. SBH plots as a function of (a) metal work function and (b) Miedema's metal electronegativity. The data of metal work functions and electronegativities were determined by experimental results. The dashed line in the panel (b) is the line by the MIGS-and-electronegativity concept, along which experimental values of Si-terminated interfaces are located. Reprinted with permission from Tanaka *et al.*, Phys. Status Solidi C **4**, 2972–2976 (2007). Copyright 2007 John Wiley and Sons.¹¹⁵

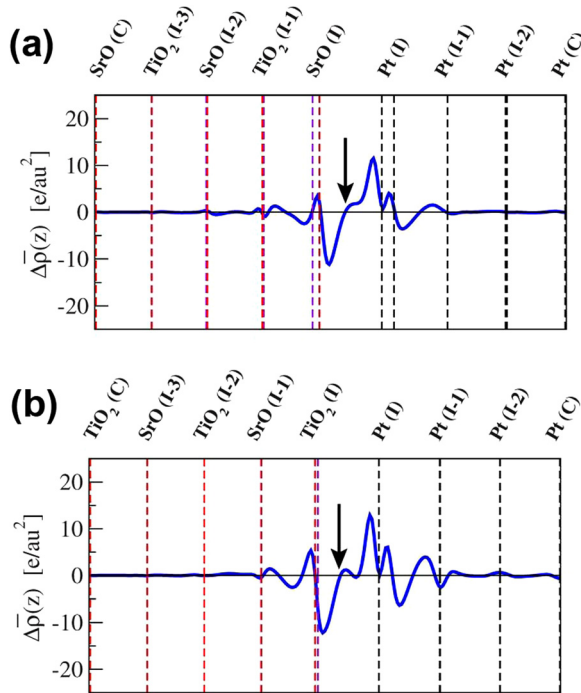


FIG. 13. Differences of the planar averaged charge densities from the interface and slab calculations for seven-layer Pt films on (a) SrO- and (b) TiSi2-terminated STO (only one half of each mirror-symmetric supercell is shown). The vertical dashed lines mark the positions of atomic layers (I and C denote interface and center of the slab, respectively); the arrows indicate the interface position. Reprinted with permission from Mrovec *et al.*, Phys. Rev. B **79**, 245121 (2009). Copyright 2006 American Physical Society.¹¹⁹

surface terminations similar.¹¹⁹ The rationale for this stage analysis was to separate out the effect due to atomic rearrangement during the formation of the MS interface from that due to the relaxation of the electronic density. Both of these relaxations are results of chemical bond formation. Another

interesting aspect of the formation of SBH that was demonstrated in these calculations concerned the spatial extent of charge rearrangement at the MS interface. As shown in Fig. 13, the modification of charge density during bond formation extended roughly equal distances into the metal and the STO for both surface terminations. Actually, if anything, the extension of the disturbance of the interface into Pt was a little longer than that into STO. This roughly equal participation in the depth of the MS interface from the metal and the semiconductor is similar to that found for silicide interfaces⁶⁰ shown in Fig. 9, and also that for other oxides (see Fig. 14(b)). Experimentally, it is known that the observed SBH on STO can be affected by the oxidation condition of the interface,¹²⁰ which is a result also found at many other oxide interfaces. As implied by the more than one dashed vertical lines in Fig. 13 representing atomic positions, crystal planes (with mixed atomic species) that are flat in a bulk crystal could have different perpendicular shifts at the interface due to reduced symmetry in the bonding geometry. Such corrugations, or “rumpling,” within the atomic planes of some binary alkaline earth crystalline oxides has been shown to have a significant effect on the magnitude of the SBH.^{121–123} Electronic structure calculation of approximately lattice-matched interfaces of BaO, CaO, and SrO with different metals and metal “intralayers” failed to produce a clear dependence of the SBH on the metal work function.¹²¹ However, a dependence of the SBH on the rumpling parameter of the fully relaxed MS interface was noticed, as shown in Fig. 14(a). The interface rumpling here is defined as half the difference in the interplanar distance (between the 1st and the 2nd oxide planes at the interface) for oxygen atoms and that for the alkaline earth metal atoms, normalized by the bulk interplanar distance. Notice that a positive rumpling parameter indicates a shift of the (oxygen) anions toward the metal and/or a shift of the (alkaline earth metal) cations toward the oxide, creating an

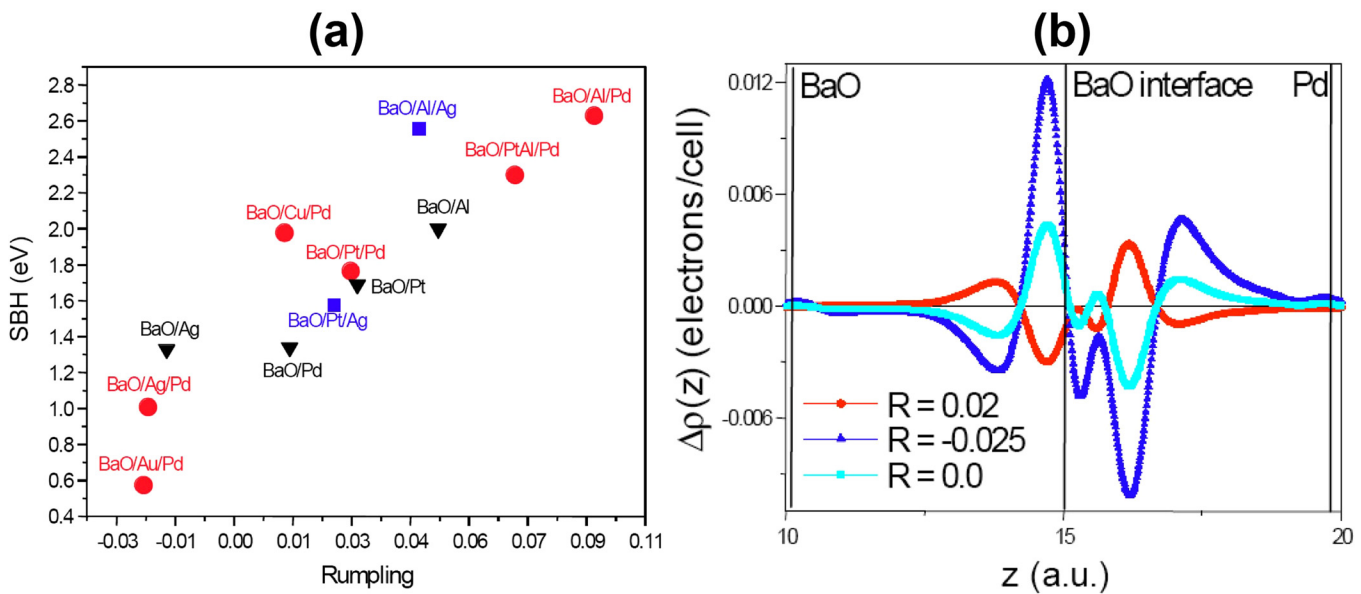


FIG. 14. (a) SBH versus rumpling of the first oxide layer at the interface with different metals (black triangles) and metal interlayers (circles and squares). (b) Lateral average of the electronic charge difference for three rumpling values: 0.02, -0.025 , and 0.0 in BaO/Pd. Very similar results are obtained for CaO/Si. Vertical lines indicate the position of the different atomic planes as labeled in the picture. Reprinted with permission from M. Nunez and M. B. Nardelli, Phys. Rev. B **73**, 235422 (2006). Copyright 2006 American Physical Society.¹²¹

additional dipole with a sign that is in agreement with the observed trend in the p-type SBH shown in Fig. 14(a). The rumpling parameter seemed to be an indicator of the strength of the interaction between the metal and the oxide. To further explore the role played by rumpling, this parameter was deliberately changed at the interface (to non-optimized atomic structure) leading to approximately linear change in the calculated SBH.¹²¹ As shown in Fig. 14(b), the depth/length of the charge transfer remained little changed, while the magnitude and even the polarity of the charge transfer could be adjusted.

Very consistent results have been seen from all the first principles calculations on the SBH of epitaxial MS interfaces. They can be summarized as follows: (1) The SBH depends on the atomic structure of the interface. (2) The distribution of MIGS and the location of the CNL are intrinsic properties of the semiconductor, but depend on the interface structure. (3) The distribution of all charges, including MIGS, states below the VBM, and states in the metal, determines the interface dipole. The sharp dependence of the SBH on the interface structure, experimentally and theoretically found for epitaxial MS interfaces, clearly put the explanation of the microscopic mechanism of SBH formation out of the reach of simple models.

E. Inhomogeneous SBH

The vast majority of MS interfaces studied experimentally are non-epitaxial and therefore have atomic structure that varies from place to place. The interface dipole and the SBH at these interfaces are expected to vary locally. Evidence for the presence of inhomogeneity in the SBH's was recognized and reported only sporadically before the 1990s,^{124–126} and serious attention was not paid to the issue of SBH inhomogeneity. The development of the ballistic electron emission microscopy (BEEM) technique^{127,128} provided the spatial resolution needed to examine the distribution of local SBH underneath ultrathin metal layers. Occasionally, large-scale variations (0.7–1.1 eV) of the SBH were observed at compound semiconductor.¹²⁹ The amplitude of SBH modulations was found to depend on the doping level of the semiconductor,¹³⁰ being apparently more uniform on lightly doped semiconductors^{128,130,131} than on heavily doped semiconductors. The reason for the dependence of the apparent SBH on the doping level is potential “pinch-off,”¹³² taking place not at the

immediate MS interface but in the space charge region some distance in front of the MS interface. This effect involves no special physics and is just a consequence of the band-bending (electrostatic potential) near an inhomogeneous SBH needing to satisfy the Poisson's equation. When a region with locally lower SBH is small in size compared with the depletion width, electronic transport across this region of the interface is not determined by the local SBH, as for uniform MS interfaces, but rather by the transport of carriers across the (inhomogeneous) space charge region. Illustrated in Fig. 15 are potentials with different doping levels, in front of MS interfaces with identical inhomogeneous interface SBH profile. The key parameter that controls the electron transport at an inhomogeneous MS interface is the “saddle-point potential” energy, which decreases with the doping level, as illustrated in Fig. 15, thus accounting for the doping level dependence of BEEM.¹³⁰ Direct evidence for the potential pinch-off effect has been observed by BEEM in artificially generated inhomogeneous SBs^{133,134} and also at semiconductor/liquid interfaces.^{135,136} An analytic theory of the potential distribution and the electron transport at inhomogeneous SBH was developed^{20,132} and was shown to accurately describe the results of experiments with known inhomogeneous SBHs⁵⁶ and the results of numerical simulations.¹⁹ Potential pinch-off can mask the rapid fluctuations of local SBH and was a major reason why inhomogeneous SBH could escape experimental detection for so long and why this issue was largely ignored historically. It was only after all the ramifications of potential pinch-off were understood that it became clear how severe and widespread the SBH inhomogeneity problem really was in polycrystalline Schottky diodes.¹⁹

The most intriguing dependence of the saddle-point potential for a low-SBH region is the one on the applied bias. As shown in Fig. 16, with an applied forward (reverse) bias, the saddle-point potential energy increases (decreases). In reverse bias, the effective SBH decreases with voltage, leading to unsaturated reverse current. Enhanced current at large reverse leakage current has often been observed experimentally. As pointed out,²⁰ the traditional explanation based on negative charge of the MIGS tails³⁷ was incompatible with the entirety of available experimental data. Rather, the much varied behavior of reverse current at similarly processed MS interfaces was in better agreement with the voltage dependence of the saddle-point potential for inhomogeneous

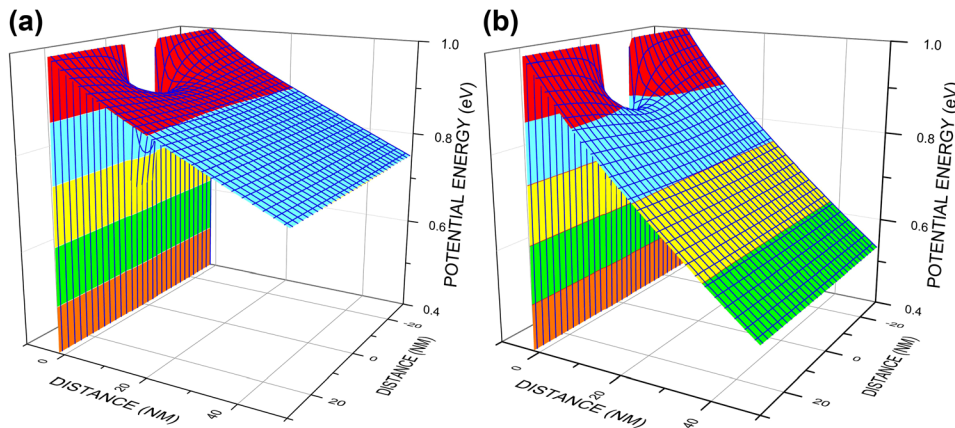


FIG. 15. Potential distribution in front of a low-SBH patch for (a) lightly doped semiconductor and (b) more heavily doped semiconductor.

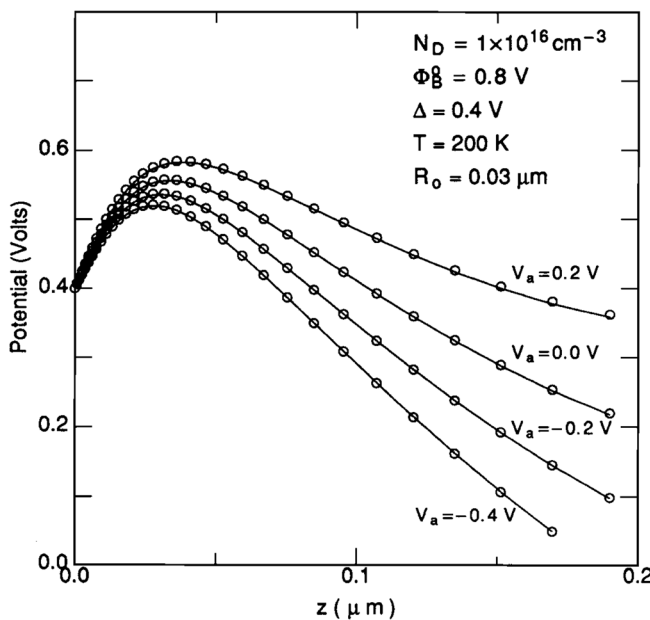


FIG. 16. Numerically simulated potential distribution (shown as circles) along $r=0$ of the low-SBH patch at different biases across the MS contact. The potential based on the analytic theory is shown as the solid lines. Reprinted with permission from J. Appl. Phys. **70**, 7403–7424 (1991). Copyright 1991 AIP Publishing LLC.¹⁹

SBH.^{19,20} At forward applied bias, the rise in the saddle-point potential leads to an increase in the effective SBH that controls the current transport with the applied voltage. This is manifested in a slower-than-normal rate of increase in the current with forward bias, i.e., an ideality factor that exceeds unity, which is a phenomenon commonly observed in the studies of SBH. Before the bias-dependence of the saddle-point potential was pointed out, there had been many explanations of the non-ideal I-V characteristics, including image force lowering,¹³⁷ generation-recombination, interface states (negative charge),^{138,139} and tunneling,^{140,141} all of which could explain a greater-than-unity ideality factor. However, the facts that experimentally observed I-V traces often contained kinks and shoulders, the measured I-V characteristics could be significantly different for diodes similarly fabricated, and the measured ideality factor displayed various dependencies on temperature made clear that it would be impossible to explain the wide range of junction current behavior with uniform SBH. SBH inhomogeneity is the most

likely cause for experimentally observed greater-than-unity ideality factors.

When the interface SBH is non-uniform, the current transport across the MS interface is spatially inhomogeneous. As just explained, the inhomogeneous distribution of the electrostatic potential in the space charge region leads to the formation of saddle-points that exert actual control over electronic transport across the entire junction. The analytic expressions derived for the locations and the potential energies of saddle points, as a function of interface SBH profile, doping level, temperature and the applied bias, pertains to a space charge region with artificially homogenized distribution of dopants. In other words, the charges due to exposed dopants are assumed to be smeared into a density of charge that is homogeneous in the space charge region. In reality, however, charges due to exposed dopants are approximately point charges fixed at discrete lattice sites. The discrete nature of dopant charges (or other charged defects) can have a very profound effect on the saddle-point potential and on the current transport at real MS interfaces. Particularly, how far the discrete dopant atom(s) are from the location of a saddle point can have a very significant influence on the actual energy barrier that controls the electronic transport with this low-SBH region. As illustrated in Fig. 17, the presence of a charged defect near the saddle-point significantly modifies the potential distribution. Therefore, it can be concluded that a non-uniform MS interface will appear leakier on more heavily doped semiconductor not only because of an increased average electric field near the MS interface, but also because of additional SBH lowering from dopant ions being accidentally placed near the critical saddle points. With a current flowing at an inhomogeneous MS interface, locations near the saddle-points become “hot spots” with current density often orders of magnitude greater than that averaged over the entire MS interface. There are a few interesting consequences of such a localized “current crowding” phenomenon, one of which concerns the “spreading” series resistance and is an issue that has already been addressed theoretically.^{19,20} When the electronic transport at an inhomogeneous MS interface is dominated by the current flow in small and dispersed low-SBH patches, the total junction current can be written as a linear sum of the current to each patch^{19,20}

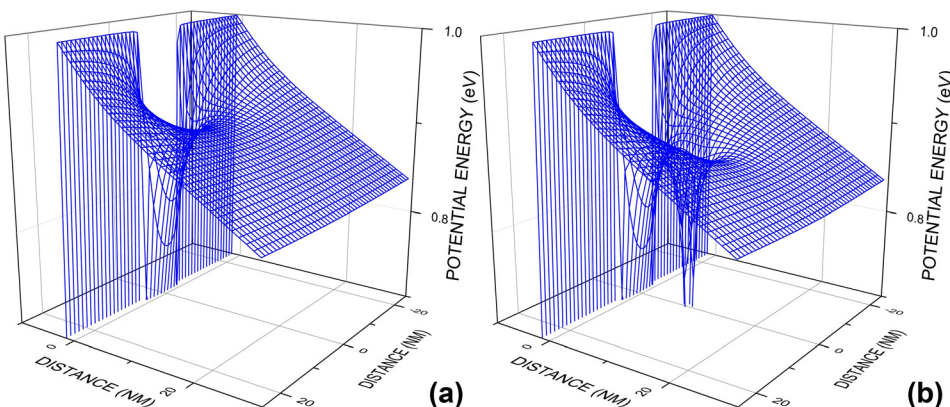


FIG. 17. (a) Potential distribution near a low-SBH patch. (b) Potential distribution when a fixed charge is located near the location of the saddle-point.

$$I(V_a) = \sum_i I_i(V_a) \\ = A^{**} T^2 \sum_i A_i(V_a) \exp \frac{-\Phi_i(V_a)}{k_B T} \left[\exp \frac{e(V_a - I_i R_i)}{k_B T} - 1 \right], \quad (9)$$

where V_a and A^{**} are the applied voltage and the Richardson constant, respectively. Φ_i , A_i , I_i , and R_i are, respectively, the SBH, the area, the current, and the series resistance of the i -th conducting patch. The series resistance associated with an independent patch, assumed circular in shape, has been found empirically to be¹⁴²

$$R_i \approx \frac{\rho}{2\sqrt{A_i \pi}} \arctan \frac{2t_{layer}}{\sqrt{A_i / \pi}}, \quad (10)$$

where ρ is the electrical resistivity, and t_{layer} the layer thickness, of the semiconductor. Note that the series resistance for a patch can vary from essentially uniform in nature ($= \rho t_{layer} / A_i$) when $\sqrt{A_i} > t_{layer}$, to essentially spreading in nature ($= \rho (16A_i / \pi)^{-1/2}$), as for a point contact, when $\sqrt{A_i} \ll t_{layer}$.^{143,144} Calculation with the analytic form of the series resistance, Eq. (10), has been shown to reproduce experimental I-V characteristics and also results in close agreement with full-fledged semiconductor numerical simulation package.^{19,20} The current crowding may also cause the density of carriers in the vicinity of the saddle-point to far exceed that corresponding to the equilibrium majority-carrier quasi-Fermi-level of the space charge region. In the simulation of the current flow at an inhomogeneous SBH, this represents a small complication as the quasi-Fermi-level is likely laterally inhomogeneous. However, there are also real and observable consequences of current crowding. As discussed earlier, electron transport is greatly facilitated by the accidental placement of dopant ion(s) near the saddle-point, which is the location of current crowding. What this implies is that at forward bias the capture rate of majority carriers by the exposed dopant near the saddle-point is greatly enhanced. One consequence of carrier capture near the saddle point is the negation of the additional SBH lowering due to discrete dopants and an increase in the effective SBH. In other words, the ideality factor of this particular current component may be very large statistically, due to the dependence of the statistically averaged charge state of such defects on the applied bias. Another consequence of the capture and emission of carriers near the saddle-points is “noisy” junction current in the time domain.

When the MS interface is non-uniform, even the simple task of reporting the SBH deduced by experiments becomes non-trivial. Frequently, the SBH determined experimentally depends on the technique of measurement, e.g., SBH measured by C-V often exceeds that measured for the same diode by photo-response or I-V techniques.^{145–147} That this is a necessary consequence of SBH inhomogeneity has long been realized.^{148–150} For certain types of work, only the result of one type of SBH measurement is important, e.g., I-V measurement for ohmic contact development. For other types of applications and investigations, the entire profile of the SBH

distribution at an MS interface is of interest, in which case the experimental techniques and conditions that are needed to provide the desired, complete information should be carefully thought out. When the semiconductor is uniformly doped, C-V measurement usually renders the arithmetic average of the distribution of the SBH profile at the MS interface, which is a good starting point. To help with the reduction of the in-phase component of the current in C-V measurement, a common trick is to conduct the measurement at low temperatures. There are also other pitfalls with C-V measurements that should be avoided.^{151,152} Because of the exponential dependence of the magnitude of junction current on the SBH, $\exp[-\Phi_B/(k_B T)]$, I-V measurement is dominated by the portions of the MS interface with lower-than-average SBH; and the lower the measurement temperature, the more pronounced the dominance of the low SBH patches. The upper-half of the SBH distribution of an MS interface is not accessible experimentally by I-V measurements, except by special techniques with spatial resolution such as BEEM or electron-beam induced conduction (EBIC). However, since the upper-half for one type of doped semiconductor, e.g., n-type, is the lower-half in SBH distribution for the other type of doping, e.g., p-type. In routine studies, the I-V characteristics on both types of semiconductor form a complete picture of the full SBH distribution. In addition, the pinch-off effect at inhomogeneous MS interfaces can be reduced by the use of more heavily doped semiconductor. To circumvent the uncertainties in both the effective area responsible for current transport at inhomogeneous MS interfaces and the appropriate Richardson constant to use, study of junction current as a function of temperature, i.e., activation-energy analysis, is an effective technique. For certain distribution in the inhomogeneous SBH, the Richardson plot of a diode may be curved, as shown in Fig. 18, in which case the slope deduced at the low measuring temperatures represents an upper limit to the minimum in the distribution of the interface SBH. An additional uncertainty one can avoid in I-V measurement of inhomogeneous interfaces concerns the contribution due to series resistance (cf. Eqs. (9) and (10)), which vanishes identically at zero current (zero-bias). Instead of plotting the logarithmic of the forward-bias junction current against voltage, which renders the current at

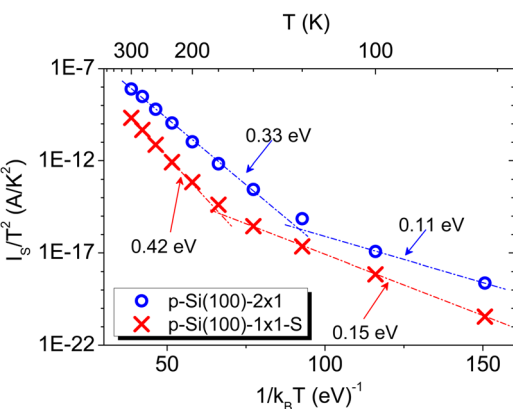


FIG. 18. Richardson's plots of the saturation currents of Ag Schottky barriers formed on clean and S-terminated Si(100) surfaces. Adapted from Ref. 143.

small biases range unusable for analysis, a logarithmic plot of the quantity $I/\{1 - \exp[-eV_a/(k_B T)]\}$ against the applied bias⁸⁹ allows the current in the entire bias range to become usable as shown in Fig. 19.¹⁴³ Therefore, activation energy study of junction current obtained at a fixed (non-zero) bias should be avoided, in favor of the analysis of the logarithmic of the quantity $I/\{1 - \exp[-eV_a/(k_B T)]\}$ interpolated to zero-bias, as done for Fig. 18. Taking into consideration of various known factors, the most revealing investigation of the full range of SBH distribution of an MS interface, assuming that the same MS structure can be reproduced on different types of semiconductor, consists of studying I-V results, obtained at low applied bias voltage, on both types of moderately doped semiconductor. Reporting of SBH measured for inhomogeneous MS interfaces should consist of results obtained by various techniques under different conditions. It is generally inadequate to report a single SBH value for any inhomogeneous interface.

III. PHYSICAL AND CHEMICAL PERSPECTIVES ON INTERFACE-DIPOLE FORMATION

A. Electrostatics at solid interfaces: Energy levels and their “hosts”

The SBH problem, which can be roughly stated as “How the bands of a semiconductor are aligned with those of a metal at an interface?”, constitutes a small, albeit very important, part of a much broader area of scientific research on the “alignment of energy levels” between different materials. Included in this broader area are topics that are also of interest to materials scientists and device engineers, such as the alignment of energy levels at semiconductor-semiconductor, metal-insulator, semiconductor-oxide, metal-polymer, metal-electrolyte, etc., interfaces. The physics and chemistry that govern band alignment at these solid or condensed matter interfaces are expected to be similar. But also related to this general area of research are topics that aren’t usually associated with the SBH, such as “the electron transfer rate between donor ions and acceptor ions in an electrochemical solution” or “the rate of a (bio-)chemical reaction.” The

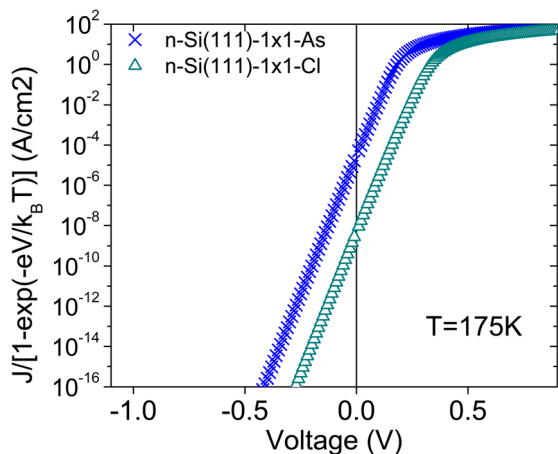


FIG. 19. Logarithmic plot of $I/\{1 - \exp[-eV_a/(k_B T)]\}$ vs. V of experimental data, obtained at 175 K, for Ag Schottky diodes fabricated on As- and Cl-terminated n-type Si(111) surfaces. Adapted from Ref. 143. This figure should be compared with Fig. 51 below, where the same data are plotted in the conventional log(I) vs. V format.

common thread that connects all of these fields of research is the critical importance of the relative position of the energy levels in one material to the energy levels in the second material in deciding the current flow or charge transfer rate between the two materials. In these problems, of interest is the relative position/shift between two sets of energy levels, belonging to two different substances physically located very close or right next to each other. Despite their spatial proximity, the two sets of energy levels must maintain their separate individuality for a study of their relative alignment condition to make sense. For example, asking the question of “how do the valence atomic levels on a carbon atom compare with those on an oxygen atom” would not make sense if the two atoms together formed a CO molecule, because in that case the molecular orbitals can no longer be regarded or associated exclusively with only one atom. Looking at Fig. 1, we notice that the energy bands for either the metal or the semiconductor are not drawn inside the interface specific region (ISR), even though the ISR for an abrupt MS interface may contain physically nothing more than the metal crystal lattice and the semiconductor crystal lattice all the way up to the plane that separates the two. The reason that the energy bands for the individual crystals should be drawn only outside of the ISR is obvious: the electronic states inside the ISR are characteristic of the coupling between the metal and the semiconductor and cannot be exclusively identified with either side. Therefore, as far as the SBH is concerned, the material inside the ISR can be thought of as a third substance (neither the metal nor the semiconductor) whose levels on the energy scale *per se* are not directly linked to the SBH. Rather, the relevant aspect of the electronic states in the ISR is their “spatial” distribution, which causes shifts in the relevant energy levels elsewhere, in the two regions just right and just left of the ISR. From Fig. 1, the p-type SBH can be written in terms of the average potential energy at two specific places

$$\Phi_{B,p}^{(0)} = (-e\bar{V}_{M-I} + \mu_M^{(i)}) - (-e\bar{V}_{S-I} + \mu_{SC}^{(i)}), \quad (11)$$

where $-e\bar{V}_{M-I}$ is the average potential energy near the metal-ISR boundary, $-e\bar{V}_{S-I}$ is the average potential energy near the semiconductor-ISR boundary, and the $\mu^{(i)}$ ’s, as before, are the internal chemical potential for the two bulk solids. As vividly demonstrated by the form of Eq. (11), the electrostatic potential of the crystal is of paramount importance to any energy alignment problem. It is thus worthwhile to delve deeper into the issue of electrostatics of crystalline materials.

The potential energy due to all the charges in a solid, from ions and electrons, as well as charges external to the solid, can be written as

$$-eV(\vec{r}) = e^2 \sum_j \int d\vec{r}' \frac{|\psi_j(\vec{r}')|^2}{4\pi\epsilon_0 |\vec{r} - \vec{r}'|} - \sum_j^{ion} \frac{Z_j e^2}{4\pi\epsilon_0 |\vec{r} - \vec{R}_j|} - eV_{ext}(\vec{r}), \quad (12)$$

where ψ_j ’s are single electron wave functions, \vec{R}_j ’s are the positions of the positive ions in the crystal, and V_{ext} is the electrostatic potential due to external sources. For a large and perfect crystal, the potential in the interior portion of the

crystal is expected to be periodic. The average potential energy at any point \vec{r} inside the crystal can be defined as that spatially averaged over the volume of a unit cell

$$-e\bar{V}(\vec{r}) = \frac{-e}{\Omega_{cell}} \int_{W-S} V(\vec{r} + \vec{r}') d\vec{r}', \quad (13)$$

where Ω_{cell} is the volume of the unit cell and the integration is carried over a unit cell centered about \vec{r} . A convenient shape for the integration is the Wigner-Seitz cell, although any acceptable choice for the unit cell will give the same answer as long as $\bar{V}(\vec{r})$ is a slowly varying function in a crystal. There are other weighting strategies that may be used to smooth out the periodic oscillations and define the average potential.¹⁰⁵ One may wonder, in the absence of external charges ($V_{ext} = 0$ in Eq. (12)), what would be the average potential energy $-e\bar{V}(\vec{r})$ due to the (infinite) crystal itself. This seems like a reasonable question to ask and is one that has been asked many times in the literature, as the answer seems to provide some “baseline” condition for the crystal potential. After a highly publicized debate in the literature,^{153–155} it is now clear that the average potential of an infinite crystal has no physical meaning,^{156,157} because the structure of the surface assumed for the crystal, as its dimensions approach infinity, actually determines the average potential of the “infinite” crystal. In other words, the surface contribution to the crystal potential energy does not vanish but becomes a constant, as the crystal approaches infinity. The easiest way to describe and understand the surface effect is to look at well-known results concerning “model solids.”^{10,158} A model solid is an artificial object with a charge distribution which mimics that of a real solid, except that its charge distribution can be arbitrarily specified.^{159,160} Such an object is not a real crystal because its charge distribution, especially that near the edge of the model solid, is not governed by Schrödinger equation. Nevertheless, the electrostatic potential of a model solid, being solution to the Poisson’s equation, is invaluable for the analysis of electrostatics of solids. To reproduce the crystal potential inside a real solid, we can construct a model solid by attaching identical cells of (fixed) charge distribution to every three dimensional crystal lattice point, as schematically shown in Fig. 20. For simplicity, we shall choose a unit cell with vanishing net charge, net dipole, and net quadrupole moments, and also satisfies the requirement that the placement of one cell at every lattice point seamlessly recreates the charge distribution of a real solid. For a crystal of high symmetry, such as cubic or hcp, a unit cell with these properties can always be found and, in fact, there are always many such choices. The advantage of choosing a cell with these properties is that the electrostatic potential of each cell is very short-ranged, falling off more rapidly than r^{-5} .¹⁶¹ This means that cells a few lattice spacings away will have little contribution to the local electric potential. The average potential inside a large model solid so constructed is a constant and is independent of the shape (or size) of the model solid. In fact, the average potential energy of a model solid is simply and uniquely related to the spatial distribution of charge within the unit cell (model-solid cell) used to construct the model solid.

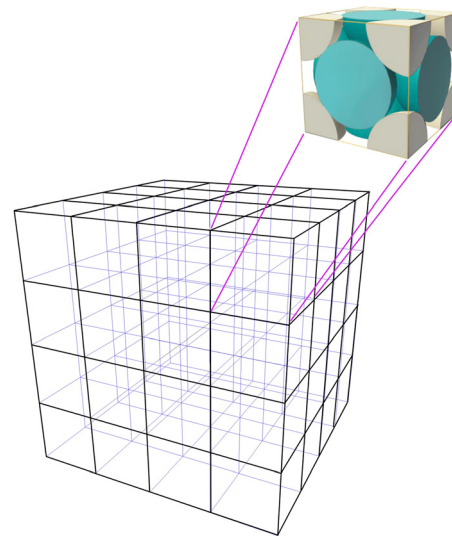


FIG. 20. The construction of model-solid from “cells” with vanishing lower order moments. A Wigner-Seitz cell is shown as the building block.

After a particular charge distribution for the model-solid cell, ρ_{MSCell} , is chosen, the electrostatic potential in the model solid is given by

$$V_{ModSol}(\vec{r}) = \frac{1}{4\pi\epsilon_0} \sum_i^{MSCell} \int_0^{\vec{R}_i} d\vec{r}' \frac{\rho_{MSCell}(\vec{r}')}{|\vec{r} - \vec{r}' - \vec{R}_i|}, \quad (14)$$

where \vec{R}_i ’s are points of the Bravais lattice. Note that the integration in \vec{r}' is only over the volume of one model-solid cell centered about $\vec{r}' = 0$, and that ρ_{MSCell} contains not only the dispersed negative density due to electrons but also positive delta-function(s) due to the nuclei. To calculate the average electrostatic potential of a model solid, one integrates Eq. (14) over a unit cell in \vec{r} coordinates and divides by the volume. Because of the superposition principle of electrostatic potential, the average electrostatic potential in the interior of a model solid is simply

$$\overline{V_{ModSol}} = \frac{1}{4\pi\epsilon_0\Omega_{cell}} \int d\vec{r} \int_{cell}^{cell} d\vec{r}' \frac{\rho_{MSCell}(\vec{r}')}{|\vec{r} - \vec{r}'|}. \quad (15)$$

It can be shown¹⁶² that the above integral renders

$$\overline{V_{ModSol}} = -\frac{\Theta_{MSCell}}{6\epsilon_0\Omega_{cell}}, \quad (16)$$

where the spherapole (trace of the second order density matrix) of the unit cell, Θ_{MSCell} , is given by

$$\Theta_{MSCell} = \int_{MSCell} \rho_{MSCell}(\vec{r}) r^2 d\vec{r}. \quad (17)$$

One cautions that the average electrostatic potential, per cell, is a constant and given by Eq. (16), only if the lower order moments of the chosen $\rho_{MSCell}(\vec{r})$ vanish. Note also that a different choice of the cell density would produce a different model solid potential via Eq. (17). Any difference in the

model solid potential is obviously a result of different surface termination, as can be verified by using “Wigner solids” as examples. A Wigner solid, as schematically shown in Fig. 21, is made up of a periodic lattice of (positive) point charges with a neutralizing uniform background of (negative) charge.^{153,156} Assume that we have a proton placed on every lattice site of a simple cube with a lattice constant of the Bohr radius, a_0 , and a uniform, compensating density of electrons throughout the lattice. The obvious choice for a unit cell is the Wigner-Seitz cell about the point charge, which consists of a proton ($+e$) at the origin (its center) and is in the shape of a cube of a_0 on each side, with a uniform charge density of $-ea_0^{-3}$. This choice of the unit cell would render an average model solid potential energy of $-\pi/6$ a.u. (atomic unit, Hartree = 27.2 eV) according to Eqs. (16) and (17). Another conceivable choice for the unit cell of the Wigner solid is a solid cube of uniform negative charge density with eight point charges of $+e/8$, one on each corner of the cube. Obviously, the net charge, dipole, and quadrupole moments also all vanish for such a Wigner-Seitz cell centered about the body center of the cube, for which the average potential energy is calculated to be $+\pi/3$ a.u. This difference in average potential energy can be easily demonstrated to be identical to the potential energy drop across the “difference layer” between the two Wigner solid surfaces. For example, the potential difference along the cubic (001) direction across one-half the length of the unit cell can be calculated to be $\pi/2$ a.u. It should be noted that even though the two cells chosen above are the only two available non-overlapping cells with vanishing lower multipole moments, there are actually many (infinite) other choices of “overlapping” unit cells that are also valid. For example, a cell with the positive point charge $+e$ at the origin and a linearly graded distribution of negative charge density

$$\rho_{MSCell}^{graded}(x, y, z) = (-ea_0^{-6})(a_0 - abs(x))(a_0 - abs(y)) \times (a_0 - abs(z)), \quad -a_0 \leq x, y, z \leq a_0, \quad (18)$$

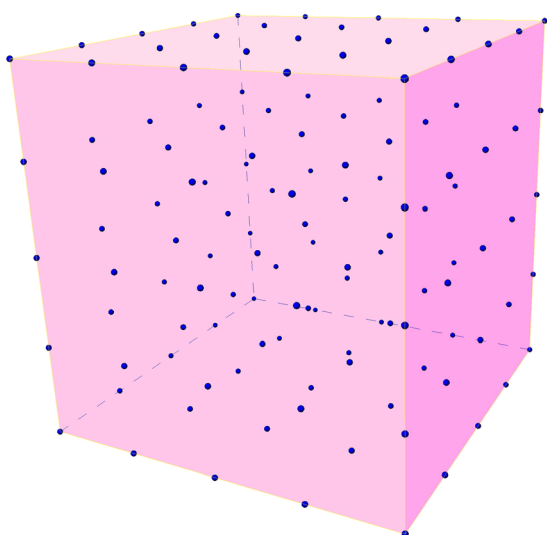


FIG. 21. Schematic of a Wigner solid.

seamlessly recreates the Wigner-solid and has vanishing lower moments. A model solid generated with such a cell has an average potential energy of $-\pi/3$ a.u., even more negative than non-overlapping cells. These examples illustrate the facts that the potential of a model solid is completely arbitrary and that the potential of an infinite solid cannot be defined without a knowledge of the surface structure.¹⁵⁶

If the surfaces of a real solid have charge distribution exactly the same way as a model solid, then obviously the electronic states inside can be referenced directly to the true vacuum level at infinity. For example if a metal were terminated exactly the same way a model solid built from $\rho_{MSCell}^{(metal)}$ cells is, its Fermi level would be

$$E_F^{(ModSol)} = -e\overline{V_{ModSol}^{(metal)}} + \mu_M^{(i)} \quad (\text{model solid}), \quad (19)$$

with respect to the vacuum level.¹⁰ And for a semiconductor model solid built from cells with density $\rho_{MSCell}^{(SC)}(\vec{r})$, its VBM would be

$$E_{VBM}^{(ModSol)} = -e\overline{V_{ModSol}^{(SC)}} + \mu_{SC}^{(i)} \quad (\text{model solid}), \quad (20)$$

with respect to the vacuum level at infinity. The model-solid result, Eq. (16), is very helpful in the analysis of the average potential energy at points near the MS interface, cf. Eq. (11). We know that if the sign of a certain charge distribution is reversed, the potential also reverses its sign. Therefore, if in the interior of a model solid a (small) number of unit cells of charge is removed, the average potential in the “hollow” or “void” left inside the model solid **vanishes** because of the superposition principle of electrostatics. In other words, if an integer number of cells of $\rho_{MSCell}(\vec{r})$ were removed around a location inside a (model) solid, while keeping the charge distribution elsewhere frozen, the local average potential **decreases** by $\overline{V_{ModSol}}$. We shall call the potential inside the void created by removing a few unit cells of ρ_{MSCell} from a (real) charge distribution the local “empty potential” $V_{MT}(\vec{r})$. In other words,

$$V_{MT}(\vec{r}) = \overline{V(\vec{r})} - \overline{V_{ModSol}}. \quad (21)$$

The empty potential naturally depends on the charge distribution of ρ_{MSCell} . The few cells of charge that are removed from the crystal, with its periodic potential inside, can be viewed as the “host” of the electronic states of the crystal, with its energy levels referenced to the vacuum level via Eq. (19) or Eq. (20). This scenario is schematically demonstrated in Fig. 22. Empty potential is the electrostatic potential at any point in a crystal solid that is NOT due to the local periodic density of charge of the crystal itself, but due to other sources such as the surfaces, the interface, defects, free charge, external charge, etc. When the “host” is put back to the “hollow” in the crystal that it came from, these energy levels are simply shifted by the slow-varying empty-potential in the empty space, from superposition principle. For example, the Fermi level in a metal crystal is

$$E_F = E_F^{(ModSol)} - eV_{MT}(\vec{r}), \quad (22)$$

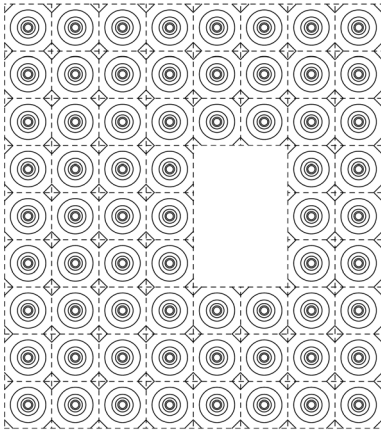


FIG. 22. Charges of a few cells are removed from the charge distribution of a crystal. The potential in the empty space created is the empty potential and is of a value that is reduced by V_{ModSol} from the original average of the full potential. In this specific example where a few cells are removed from a model solid built from the same type of cells, the empty potential vanishes inside the void.

which should be a constant inside a metal ($V_{MT}(\vec{r}) = V_{MT}$), and the VBM of a semiconductor crystal is

$$E_{VBM}(\vec{r}) = E_{VBM}^{(ModSol)} - eV_{MT}(\vec{r}), \quad (23)$$

which may be position-dependent. As usual, the energy level positions in Eqs. (22) and (23) are referenced to the zero in the electrostatic potential energy. We stress that the writing of Eqs. (22) and (23) amounts to nothing more than a re-definition of the energy levels in terms of the empty potential. However, empty potential turns out to be a friendlier and much more transparent reference to use for the analysis of energy level alignment problems than the average of the full periodic potential of a crystal. Before moving on, an issue that should be mentioned is that, as the form of Eq. (15) suggests, the above analysis, strictly speaking, pertains only to the full potential and the full charge distribution of a solid, e.g., from an all-electrons calculation. If numerical computations of bulk solids made use of pseudo-potentials, which is a very common practice at the present, results discussed above would however remain valid, provided some modifications, detailed elsewhere,¹⁶³ were included.

Consider the case when a model solid of metal is placed near a semiconductor model solid, as shown in Fig. 23(a). Because the electric field from symmetric cells is short-ranged and can be regarded as vanishing identically outside the model solid, the empty potential inside either model solid vanishes independent of the relative position or orientation of the two model solids. For this arrangement, the p-type SBH is simply

$$\Phi_{B,p}^{(0)} = E_F^{(ModSol)} - E_{VBM}^{(ModSol)}. \quad (\text{two bare model solids}). \quad (24)$$

When it comes to the analysis of the distribution of electrostatic potential and the SBH near a real MS interface, Eq. (24) now provides a definitive reference. From the charge distribution at an MS interface, Fig. 23(b), it is clear

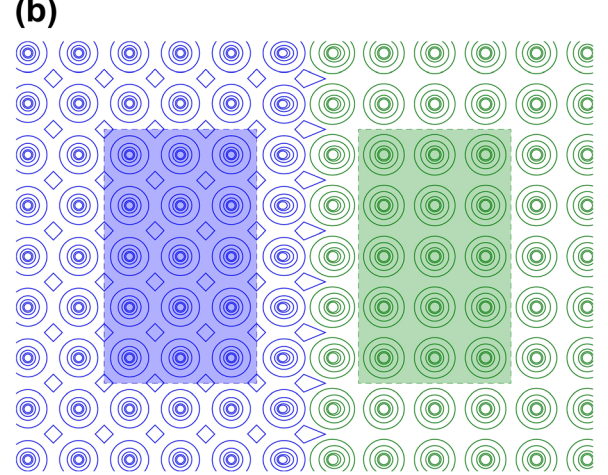
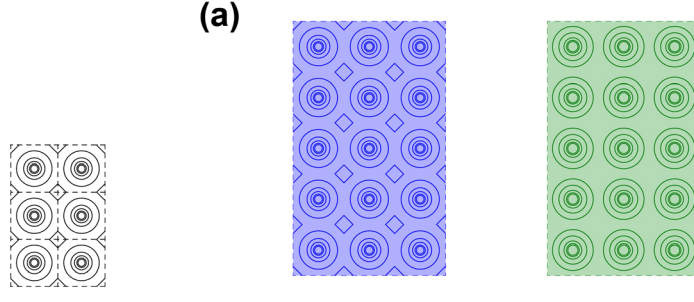


FIG. 23. (a) When two model solids are by themselves and near each other, the empty potential vanishes inside both model solids regardless of the separation or the relative orientation. (b) At an interface, the empty potentials inside the shaded regions differ by the dipole of the charge distribution in the region (ISR) between them.

that Eq. (24) would have held if not for the possible dipole due to the presence of the charge distribution in the unshaded region (ISR). Note that charge distribution far away from the interface region can shift the empty potentials in both shaded regions, but cannot lead to a difference in the two. We further note that any part of the charge distribution inside the ISR that is overall neutral and locally symmetric, such as a layer of unit cells with undistorted (bulk) charge distribution, cannot lead to a difference in the empty potentials either. Therefore, it is only the change/difference in the charge distribution from the bulk charge distribution of either crystal that can lead to a shift in the SBH from Eq. (24). In other words,

$$\Phi_{B,p}^{(0)} = E_F^{(ModSol)} - E_{VBM}^{(ModSol)} - e(\Delta V)_{ISR}, \quad (25)$$

where the potential drop across the ISR, $(\Delta V)_{ISR}$, is given by

$$(\Delta V)_{ISR} = \frac{1}{\epsilon_0} \int_{ISR} \rho(z) z dz = \frac{1}{\epsilon_0} \int_{ISR} \delta\rho(z) z dz, \quad (26)$$

where $\delta\rho(z)$ is the difference between the ISR planar-average charge distribution $\rho(z)$ and reference bulk charge distribution

$$\rho(z) = \frac{1}{A_{2D}} \iint_{2D_cell} \rho(x, y, z) dx dy. \quad (27)$$

We remind ourselves that the choices of the cells to construct the two model solids now also define the boundary of the ISR. To make $(\Delta V)_{ISR}$ easier to handle by chemical principles and ideas, the cell for the metal and that for the semiconductor should be chosen consistently. For elemental metals with a monatomic unit cell, the use of the Wigner-Seitz cell about the nucleus is an obvious and reasonable choice, as this ends the model solid on the same boundaries that separate the “atoms” in the crystal. Common elemental semiconductors, Si, Ge, and α -Sn, have the diamond lattice, with a basis for the unit cell. A model solid can be constructed with a Wigner-Seitz cell (for the fcc lattice) centered about the mid-point between nearest neighbors. However, more convenience is afforded if cells centered about the nucleus are used. Because of symmetry, the two atoms in a unit cell of the diamond structure are topologically inequivalent, but electrically equivalent. The diamond lattice can be partitioned into spaces in closest proximity to each atom, treating the two atomic sites in a unit cell on equal footing. These two types of “proximity cells,” each with the volume of $1/8$ of the conventional fcc unit cell, can be used to stack together a model solid. The shapes of these two proximity cells, which are related to each other through inversion, are shown in Figs. 24(a) and 24(c). The relationship of a proximity cell to the atomic positions is roughly sketched in Fig. 24(b). It can be verified that the model solid would have an average electrostatic potential given by (16) and (17), where the integration is taken over one proximity cell only and the cell volume is taken to be that of one proximity cell. The simplicity in this result is the consequence of a property of the spherapole, Eq. (17): When the charge distribution of a model-solid-cell can be partitioned into several sub-cells, each with vanishing lower moments, the spherapole of the model-solid-cell is a simple sum of the spherapoles of the sub-cells. This is another way of saying that the value of the spherapole calculated in Eq. (17) does not depend on the choice of the origin. Model solids constructed using both types of proximity cells would put the representation of the (elemental) semiconductor crystal on par with the metal model solid. The preference for terminating/building both crystals with cells centered about nucleus is obviously an attempt to preserve the notion of “atoms” in a solid, about which most of the chemical concepts evolve.

There are many more compound semiconductors/insulators than there are elemental semiconductors. Common crystal structures for these compounds include zinc blende, perovskite, hexagonal, and fluorite. Because of the ionic nature of these crystal structures, the best choice for the model

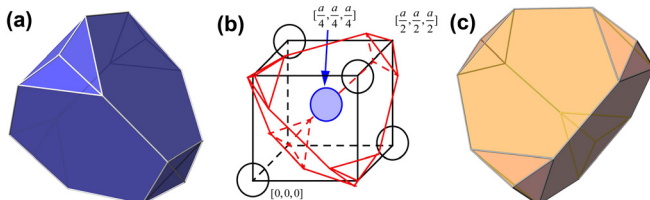


FIG. 24. “Proximity cells” for atoms in the diamond and zinc-blende lattices. (a) and (c) Proximity cells for anions and cations, respectively, of the zinc-blende lattice. A schematic of $1/8$ of the conventional unit cell is drawn in (b) to indicate the orientation of the proximity cells.

solid is not definable *per se* but is dependent on the kind of MS interface structure to be analyzed. Below we shall briefly describe how several model solids might be constructed each for the zinc blende and perovskite crystals to be friendly with different stacking sequences at the MS interface. For the zinc blende structure, the most straightforward choice for the construction of a model solid would be the Wigner-Seitz cell centered about either the cation or the anion, although these choices do not appear particularly chemistry-friendly, as nuclei are exposed on the surface (corner) of such a cell. A more chemistry-friendly choice would be to first construct proximity cells for both the cation and anion, a step which leads to cells identical to those already shown in Figs. 24(a) and 24(c). The sum of one each of the cation-centered proximity cell (CPC) and the anion-centered proximity cell (APC) would constitute one whole unit cell. However, to make the lower-order moments of the model-solid-cell vanish, one may place a CPC at the origin and place four APC’s, each with $1/4$ of its full density, at the nearest neighbor positions, as shown in Fig. 25(a). This is obviously an arrangement that will generate a model solid with the periodic charge distribution of the bulk crystal and, at the same time, have rapidly decaying potential outside the cells. Let the net charge and the spherapole of the stand-alone CPC be q_{cpc} (typically positive) and Θ_{cpc} , respectively; and for the APC: $q_{apc} (= -q_{cpc})$ and Θ_{apc} . The spherapole of a cation-centered model-solid-cell is

$$\Theta_{ccmsc} = \Theta_{cpc} + \Theta_{apc} - q_{cpc}(\sqrt{3}a/4)^2, \quad (28)$$

where $\sqrt{3}a/4$ is the distance between neighboring cation-anion pair. From Eq. (16), the average potential for a model solid constructed with cation(Ga)-centered model-solid cells (CCMSC) is

$$\overline{V_{ModSol}^{(ccmsc)}} = -\frac{\Theta_{ccmsc}}{6\epsilon_0(a^3/4)}. \quad (29)$$

Alternatively, one could have placed an APC at the center of the MSC and put four quarter-strength CPCs at nearest neighbor position, as schematically shown in Fig. 25(b). A moment’s consideration tells us that the spherapole for such an anion-centered MSC (ACMSC) is

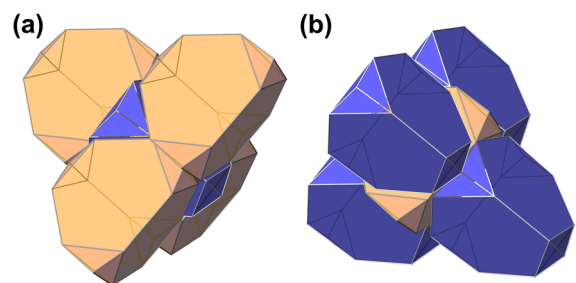


FIG. 25. Two ways to construct a proximity-cell-based model-solid-cell for the zinc blende structure. For a cation-centered construction, a full charge density of cation proximity cell is placed at the center and four cells, each with $1/4$ the charge density of an anion proximity cell, are placed at the corners. An anion-centered model-solid-cell can be constructed by placing an anion proximity cell at the center and surrounding it with four $1/4$ -strength cation proximity cells.

$$\Theta_{acmsc} = \Theta_{cpc} + \Theta_{apc} + q_{cpc}(\sqrt{3}a/4)^2, \quad (30)$$

which can give its model solid potential through an equation analogous to Eq. (29). The average model-solid potentials of common compound semiconductors are shown in Table I.¹⁶³ As expected the model solids constructed with proximity cells have lower potential energies than that constructed with Wigner-Seitz cells. Also, the cation-centered model solids have lower potential energies than the anion-centered model solids, consistent with Eq. (28). We should remember that proximity cell is simple but not the only way to represent the chemical identity of an “atom” in a crystal. Defining atoms in a molecule is a well-studied topic in molecular chemistry, for which many proposals exist.^{164–168} These prescriptions in quantum chemistry may provide more chemical flavor in the construction of model solids. However, one notes that these methods are more involved, sometimes yield very different definitions of atoms,¹⁶⁹ and are not based on strict rigor. On the other hand, the proximity cells for cations and anions are equal in size by definition, the size for the anion will typically exceed that for the cation in the same compound when one of these other methods is used to partition the solid.^{164–168} With a specific definition, the anions and cations can be used to construct model solid according to the same procedures. For example, a cation defined by Bader’s atoms-in-molecules (AIM) theory¹⁶⁵ is placed at the center and four anions, each with $\frac{1}{4}$ of the charge density, are placed at the corners, to form a CCMSC with the AIM method. Model-solid potentials calculated with the AIM method are also shown in Table I. Note that for the same semiconductor, the number of valence electrons on the AIM-defined cation, as a result of its smaller size, is significantly smaller than that in the cation proximity cell. Therefore, the difference between the potentials for cation-centered and anion-centered model-solids of a compound is much larger for AIM construction than proximity cell construction.

Except for the non-polar (110) surface, model solids of the zinc blende crystal structure constructed from any of the methods described above cannot lead to a surface terminated on a full layer of either cations or anions. Instead, a fraction of a monolayer of ions (or proximity cells) has to terminate any polar surface of the zinc blende model-solid. For

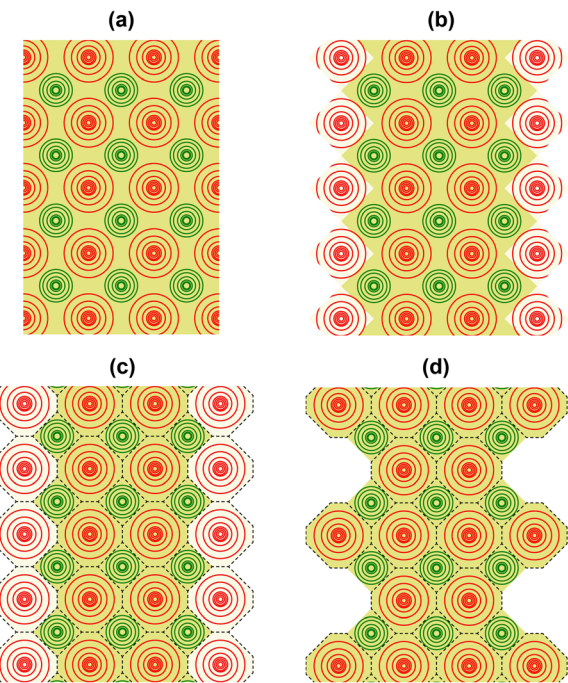


FIG. 26. Schematic diagrams of model solids in the shape of semi-infinite vertical slabs consisting of three (100) layers of cation-centered model-solid cells. Cations are drawn smaller than anions. (a) Wigner-Seitz cell, (b) proximity cell, (c) ions defined by quantum chemistry methods such as Bader’s atoms-in-molecules. In (b) and (c), darker-shaded regions represent full charge density and lighter-shaded regions represent $\frac{1}{2}$ charge density. The average potential for the model solid in (c) is identical to that for the model solid in (d), when a full monolayer of $\frac{1}{2}$ strength anions on the surface of (c) is replaced by one-half monolayer of complete anions in (d).

example, zinc blende model solid built from CCMSCs ends with one-half monolayer of anions on $\{100\}$ type surfaces and three-quarters monolayer of anions on $\{\bar{1}\bar{1}\bar{1}\}$. This is a necessary consequence dictated by electrostatics: because the ion (or proximity cell) for an ionic compound has net charge, beginning the surface with a full layer of either cations or anions necessarily leads to long-range potential in the solid and a situation unsuitable for meaningful analyses.¹⁷⁰ Shown in Fig. 26 are schematic diagrams of several possible cation-terminations of the zinc-blende model-solids on the (100) surface. As can be verified, the net potential drop across any of these slabs is zero, reflecting the suitability of

TABLE I. Model solid potential energies for common III-V compound semiconductors constructed with three different types of model solid cells.¹⁶³ (Cation #Elec.: number of electrons on cation, 3 = neutral; A-: anion-centered; C-: cation-centered.)

Latt. Const.	Cation #Elec.	Bader AIM		Cation #Elec.	Proximity cell		Wigner-Seitz cell		VBM w.r.t. Avg. PE	
		C- Model solid (eV)	A- Model solid (eV)		C- Model solid (eV)	A- Model solid (eV)	C- Model solid (eV)	A- Model solid (eV)		
AIP	5.45	1.015	-17.200	-0.714	2.690	-9.193	-6.619	4.932	1.519	9.840
AlAs	5.64	1.127	-16.223	-1.187	2.818	-8.446	-6.986	5.016	1.176	9.863
AlSb	6.12	1.430	-14.036	-2.426	3.207	-6.494	-8.027	5.425	0.353	9.815
GaP	5.43	2.291	-10.919	-5.008	2.878	-8.336	-7.323	5.316	1.221	10.477
GaAs	5.63	2.427	-9.996	-5.386	3.007	-7.535	-7.595	5.409	0.914	10.450
GaSb	6.09	2.752	-8.220	-6.377	3.397	-5.687	-8.639	5.792	0.055	10.365
InP	5.87	2.307	-9.684	-4.340	2.549	-8.717	-5.241	4.268	1.886	8.210
InAs	6.06	2.415	-9.022	-4.654	2.683	-7.989	-5.621	4.415	1.570	8.176
InSb	6.48	2.665	-7.826	-5.489	3.059	-6.392	-6.809	4.893	0.725	8.493

these model-solids as reference for interface analysis. Which of these “constructions” should be used in actual SBH analysis depends on the way the interface chemistry is handled, as explained in detail in Sec. III E. Here, we only examine the “canonical” (without interface chemistry) energy level alignment condition for polar interfaces. If an MS interface is known to be fabricated with metal deposition over an anion-terminated (100) surface, e.g., As-stabilized GaAs(100), then the use of CCMSC would lead to the situation depicted in Fig. 27(a), where we have assumed the metal to have a monatomic unit cell. Because no atoms (proximity cells) are distorted from their bulk state, Fig. 27(a) represents a MS interface without interaction or charge transfer. Under this condition, the empty potential is the same for the two crystals and the p-type SBH is given by

$$\Phi_{B,p}^{(0)} = E_F^{(ModSol)} - E_{VBM}^{(ccm sc)},$$

(non-interacting anion-terminated zinc blende). (31)

If it bothers to see missing atoms at the interface, one may imagine these voids filled with neutral atoms to recreate the arrangement of atoms expected at this MS interface, as shown in Fig. 27(b). The symmetry in the charge distribution of neutral atoms guarantees that the electrostatic effect of these atoms fades rapidly. Therefore, electrostatics in the solids is the same with (Fig. 27(b)) or without them (Fig. 27(a)). If one is interested in analyzing the SBH at an interface fabricated by metal deposition over a cation-terminated semiconductor (100) surface, a reasonable starting configuration pits the model solid constructed with ACMSC’s against the metal model solid, for which the non-interacting SBH is

$$\Phi_{B,p}^{(0)} = E_F^{(ModSol)} - E_{VBM}^{(acmsc)},$$

(non-interacting cation-terminated zinc blende). (32)

Using similar arguments as just demonstrated for the zinc blende (001) surface, one can deduce that the baseline condition for a metal interface with the anion-terminated $\{\bar{1}\bar{1}\bar{1}\}$, also known as the $\{111\}B$ surface, is that given in Eq. (32),

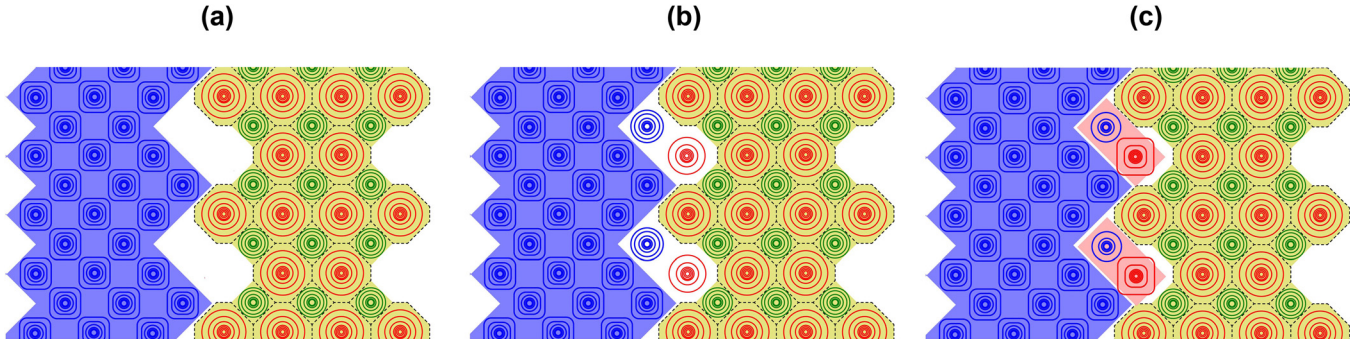


FIG. 27. (a) Model solids of an elemental metal and a compound semiconductor are placed next to each other to set the baseline condition for a polar interface. (b) Neutral atoms are used to fill absences in the charge density. The empty potential vanishes inside either model solid in both (a) and (b). In (c), charge exchange between neutral atoms due to bond formation may be estimated by methods in molecular chemistry to simulate the relative shift in the empty potentials of the two model solids.

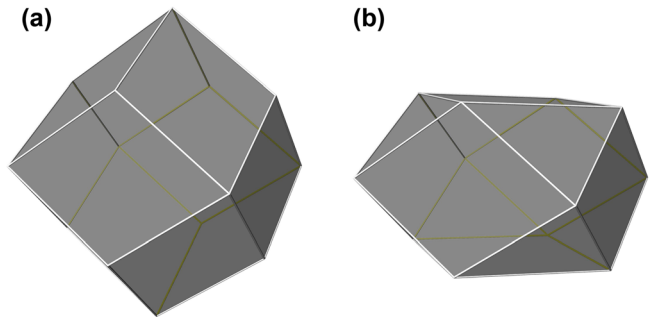


FIG. 28. Shapes of proximity cells for the perovskite lattice structure (ABO₃): (a) A (2+) atoms and (b) oxygen atoms.

while the baseline SBH with the $\{111\}$ is given by Eq. (31). Therefore, without MS interaction, the p-type SBH fabricated on anion-terminated surfaces would exceed that on cation-terminated surfaces by

$$\Phi_{B,p}^{(cation-term.ZB)} - \Phi_{B,p}^{(anion-term.ZB)} = \frac{eq_{cpc}}{4\epsilon_0 a}. \quad (33)$$

The non-polar (110) surface of the zinc blende crystal can be represented by a model solid potential of

$$\overline{V_{ModSol}^{(110)}} = -\frac{\Theta_{cpc} + \Theta_{apc}}{6\epsilon_0(a^3/4)}. \quad (34)$$

As expected, this non-polar surface has a potential which is the average of the cation-terminated surface and anion-terminated surface.

The perovskite structure and its derivatives are important structures occupied by many technologically important materials. The SBH to perovskite oxide is of great interest to a wide range of possible applications. In an ABO₃ cubic unit cell, there is a nominally 2+ (A) ion, a 4+ (B) ion, and three 2- oxygen (O) ions, about which three different types of proximity cells can be sketched out. A simple cube with the same orientation as the unit cell but with $a/2$ on each side, is found to be the proximity cell centered on B-atom. The proximity cell centered on A-atom, shown in Fig. 28 (a), also has the full point group symmetry of the cube, as it is of the exact shape and size of the Wigner-Seitz cell for

an f.c.c. lattice with the same lattice parameter. Shown in Fig. 28(b) is an oxygen-centered proximity cell, which has the same mid-section as Fig. 28(a) but with both the top and the bottom chopped off. There are three different orientations of the oxygen proximity cell, with the square facets oriented to mate with B-centered proximity cells and the diamond-shaped facets face the A-centered proximity cells. There are two convenient choices for the model-solid-cell, centered on A and B, respectively. To construct an “A”-centered model solid cell, we put an A proximity cell at the origin, eight B-centered proximity cells, at 1/8 of the full density, at the eight body-centered positions, and twelve 1/4-strength oxygen proximity cells at midpoints between B-cells. The spherapole of this “A”MSC is

$$\Theta_{Amsc} = \Theta_{Apc} + \Theta_{Bpc} + 3\Theta_{Opc} + q_{Bpc}(\sqrt{3}a/2)^2 - (q_{Apc} + q_{Bpc})(a/\sqrt{2})^2, \quad (35)$$

where Θ_{Apc} , Θ_{Bpc} , Θ_{Opc} are the spherapoles of A-cell, B-cell, and oxygen-cell, respectively, and q_{Apc} , q_{Bpc} are the net charge of A-cell and B-cell, respectively. Similarly, for the “B”-centered MSC, which includes a B-cell at the origin, eight 1/8-strength “A” cells at the body-centered positions, and six 1/2-strength O-cells at the $\langle 1/2, 0, 0 \rangle$ type positions, the spherapole is

$$\Theta_{Bmsc} = \Theta_{Apc} + \Theta_{Bpc} + 3\Theta_{Opc} + q_{Apc}(\sqrt{3}a/2)^2 - (q_{Apc} + q_{Bpc})(a/2)^2. \quad (36)$$

The most common orientation employed for perovskite oxides is the $\{100\}$, for which there are two possible terminations for a flat surface: a layer of AO or a layer of BO_2 . Surfaces with either termination may be prepared by modern epitaxial techniques and used to fabricate Schottky barriers.¹¹⁹ To analyze interfaces with an AO layer at the interface, the model solid constructed from B-centered MSC’s is used, which creates a surface with 1/2 of the AO proximity cells removed. As in the case of zinc blende (100), the absence of a fraction of the proximity cells at the perovskite surface preserves surface neutrality. And, to analyze an interface with a BO_2 termination, the potential of an “A”-centered model solid serves as a useful reference for the non-interactive interface. It is interesting to notice that, in the absence of interface chemistry, the p-type SBH for the AO-terminated surface differs from that for the BO_2 -terminated surface by

$$\Phi_{B,p}^{(\text{BO}_2\text{-term.})} - \Phi_{B,p}^{(\text{AO-term.})} = \frac{e}{6\epsilon_0 a} (q_{Apc} - q_{Bpc}/2). \quad (37)$$

The chemistry between the metal and the oxide termination layer usually reduce this difference in SBH at the actual interfaces.

Generally speaking, the philosophy of establishing a baseline alignment condition for the bands of the metal and the semiconductor based on atoms in their bulk-like state seems more intuitive than say the philosophy behind the Schottky-Mott Rule. With the discussion so far in this section, we are actually in position to analyze what the Schottky-Mott

Rule really implies about the magnitude of the interface dipole. We first notice that while a metal crystal is in isolation, its measured work function, ϕ_M (defined positive), is the difference between the vacuum level just outside the metal and the E_F of the metal. From Eq. (22), we know that inside this isolated metal crystal, the empty potential energy is a constant

$$-eV_{MT}^{(\text{MetalSurf})} = -\phi_M - E_F^{(\text{ModSol})}, \quad (38)$$

which is a positive quantity ($V_{MT}^{(\text{MetalSurf})} < 0$). In the above equation, it is implied that a particular cell has been chosen to construct the metallic model solid. If we define $-E_F^{(\text{ModSol})}$ as the bulk contribution to the work function, the empty potential energy, $-eV_{MT}^{(\text{MetalSurf})}$, is then identified as the dipole due to the formation of the metal surface, i.e., the surface dipole. Likewise, for an isolated semiconductor crystal with an experimentally measured ionization potential of $I^{(\text{SC-surf})}$, the empty potential at the near surface region of the semiconductor crystal is (cf. Eq. (23))

$$-eV_{MT}^{(\text{SC-surf})} = -I^{(\text{SC-surf})} - E_{VBM}^{(\text{ModSol})}, \quad (39)$$

which can be regarded as the surface dipole of the free surface of the semiconductor. When the Schottky-Mott relationship holds, we write

$$\Phi_{B,p}^{(0)} = I^{(\text{SC-surf})} - \phi_M \quad (\text{Schottky - Mott}). \quad (40)$$

Plugging in Eqs. (25), (38), and (39) into Eq. (40), one finds that

$$-e(\Delta V)_{ISR} = eV_{MT}^{(\text{SC-surf})} - eV_{MT}^{(\text{MetalSurf})} \quad (\text{Schottky - Mott}). \quad (41)$$

In other words, the Schottky-Mott Rule holds when the interface dipole is the difference between the dipoles of the two free surfaces. Note that this conclusion is reached, independent of the way the model solids are defined for the metal and the semiconductor.

B. Formation of electronic states at epitaxial MS interfaces

The distribution of charge at real MS interfaces is different from the abrupt termination depicted in Fig. 27(b). Generally speaking, the distribution of electronic charge is the sum of the individual densities of all the occupied electronic states at the interface, while the characteristics of the available electronic states depend on the arrangement of the positive ions at the interface. Conversely, the positions of the ions relax to configurations favored by the total energy associated with the electronic structure. This complex, self-consistent, process depends on every detail of the interface and can be quite individualistic and unfit for generalization. In this section, we shall be concerned with only one small aspect of this process, namely, the formation of electronic states from known and fixed atomic positions at the interface. For simplicity, we shall also initially restrict ourselves to epitaxial interfaces. Our discussion shall pertain to

essentially the very last step in a real electronic structure calculation, i.e., when the electronic states calculated actually self-consistently generate the charge distribution assumed for the calculation (from the previous iteration)! Within either the Hartree-Fock formalism or the Density Functional Theory (Kohn-Sham), this step involves finding solutions to the single-electron Schrödinger equation,

$$\left[-\frac{\hbar^2}{2m} \nabla^2 - eV(\vec{r}) \right] \varphi_i(\vec{r}) = \varepsilon_i \varphi_i(\vec{r}), \quad (42)$$

where the potential $V(\vec{r})$ contains the Coulomb interaction with all charges in the system and also exchange-correlation interactions. Even though the entire process of electronic structure calculation is routinely carried out in all modern electronic structure software packages for any given arrangement of atoms, a discussion of the physics of this process as it specifically applies to MS interfaces has not appeared in print, to the best of our knowledge. Although there are similarities with how the electronic structure at solid surfaces is calculated, on which detailed accounts are available.^{21,171} An understanding of the requirements on the interface states from quantum mechanics is crucial in distinguishing what may be assumed of the electronic states at an MS interface and what may not.¹⁷²

Assume that we have a semi-infinite MS interface with metal atoms occupying the space $z < 0$ and semiconductor atoms occupying $z > 0$. Since we assume that all the atomic positions and the electrostatic potential of the entire interface are known, we can choose an ISR as the region $z_{M-ISR} \leq z \leq z_{SC-ISR}$ such that the potential/charge distribution at $z < z_{M-ISR}$ is identical to that in the bulk metal and the potential/charge distribution at $z_{SC-ISR} < z$ is identical to that in bulk semiconductor. $|z_{M-ISR}|$ and z_{SC-ISR} should be chosen to have the above described properties, but also as small as possible for simplicity, and typically they are < 1 nm for physically abrupt interfaces. The common 2D unit cell for both the semiconductor and the metal, which may be viewed as rectangular in shape without loss of generality, has an area of $|\vec{a}_1 \times \vec{a}_2| = a_1 a_2$. We apply the Born-von Karman periodic boundary condition (PBC) in 2D with a box of area $(N_1 a_1) \cdot (N_2 a_2)$ to define a mesh of N_{2D} ($= N_1 \cdot N_2$) distinct $\vec{k}_{||}$'s that are allowed in a 2D Brillouin zone (2DBZ), which has a total area of $4\pi^2/(a_1 a_2)$ in reciprocal space. As the entire epitaxial MS interface is assumed to be periodic in x-y directions, the known potential at any z can be expanded in plane waves with the periodicity of the 2D unit cell,

$$V(\vec{r}_{||}, z) = \sum_{\vec{K}_{||}} U_{\vec{K}_{||}}(z) e^{i\vec{K}_{||} \cdot \vec{r}_{||}}, \quad (43)$$

where $\vec{K}_{||}$'s are the 2D reciprocal lattice vectors, including 0, and note that the Fourier coefficients, $U_{\vec{K}_{||}}(z)$'s, have explicit z -dependence. Inside either of the bulk regions, $U_{\vec{K}_{||}}(z)$ has the z periodicity of the respective crystal. However, there is no particular symmetry for $U_{\vec{K}_{||}}(z)$ inside the ISR. Because of the in-plane periodicity, Bloch theorem holds true in x and y directions. Inside the ISR, wave function with a specific $\vec{k}_{||}$ can be written as

$$\varphi_{\vec{k}_{||}}(\vec{r}_{||}, z) = e^{i\vec{k}_{||} \cdot \vec{r}_{||}} \sum_{\vec{K}_{||}} w_{\vec{k}_{||}, \vec{K}_{||}}^{ISR}(z) e^{i\vec{K}_{||} \cdot \vec{r}_{||}}, \\ z_{M-ISR} \leq z \leq z_{SC-ISR}, \quad (44)$$

where band and spin indices have been suppressed. Equations (43) and (44) can be plugged into Eq. (42) to yield coupled equations for the $w_{\vec{k}_{||}, \vec{K}_{||}}^{ISR}$ coefficients,

$$\left[\frac{\hbar^2}{2m} \left(|\vec{k}_{||} + \vec{K}_{||}|^2 - \frac{\partial^2}{\partial z^2} \right) - \varepsilon_{\vec{k}_{||}} \right] w_{\vec{k}_{||}, \vec{K}_{||}}^{ISR}(z) \\ = e \sum_{\vec{K}'_{||}} U_{\vec{K}_{||} - \vec{K}'_{||}}(z) w_{\vec{k}_{||}, \vec{K}'_{||}}^{ISR}(z). \quad (45)$$

In theory, the sums over the 2D reciprocal lattice vectors in Eqs. (43)–(45) have infinite number of terms. However, finer spatial details are unimportant especially when pseudopotentials are used, justifying the termination of these summations at some appropriate cut-off energy in actual computations. Therefore, these sums have, in fact, a fixed number (N) of terms. Since Eq. (45) is a second-order differential equation, the complete solution for the ISR region can be written down if a total of $2N$ independent boundary values are supplied from the M-ISR and the SC-ISR interfaces. $\varphi_{\vec{k}_{||}}$ in the ISR thus serves as the link between state(s) in the semiconductor and those in the metal, with the same energy and $\vec{k}_{||}$, through matching of the value and slope of the wave function at z_{M-ISR} and z_{SC-ISR} . How the numerical solutions to all the $w_{\vec{k}_{||}, \vec{K}_{||}}^{ISR}(z)$ in Eq. (45) may be obtained is perhaps best visualized by imagining setting up a grid in z for a finite-element analysis, e.g., all points with values $z_{m+1} = z_m + \delta z$ are on the grid. In this analysis, the second derivative in Eq. (45) becomes simply

$$\left[\partial^2 w_{\vec{k}_{||}, \vec{K}_{||}}^{ISR}(z) / \partial z^2 \right]_{z=z_m} = \left[w_{\vec{k}_{||}, \vec{K}_{||}}^{ISR}(z_{m+1}) + w_{\vec{k}_{||}, \vec{K}_{||}}^{ISR}(z_{m-1}) \right. \\ \left. - 2w_{\vec{k}_{||}, \vec{K}_{||}}^{ISR}(z_m) \right] / (\delta z)^2. \quad (46)$$

One thus sees that if all the $w_{\vec{k}_{||}, \vec{K}_{||}}^{ISR}$'s on two consecutive grid points, e.g., z_m and z_{m-1} , are known (for a total of $2N$ boundary values), then the solutions to Eq. (45) can be generated for points z_{m+1} and z_{m-2} ; and from there on, throughout the entire grid for the ISR.

In the metal region, $z \leq z_{M-ISR}$, the potential is 3D periodic and identical to that in a bulk crystal, except for a possible rigid shift due to the dipole of ISR. It is clear that any bulk Bloch function $\psi_{\vec{k}_{||}}^{M-Bloch}$ with the same energy (after the rigid shift) and $\vec{k}_{||}$ would satisfy the Schrödinger equation in this region. A general form for the full MS wave function in this region is, therefore,

$$\varphi_{\vec{k}_{||}, e_i}(\vec{r}) = \sum_{\vec{k}_j} b_{\vec{k}_j}^M \psi_{\vec{k}_j}^{M-Bloch}(\vec{r}), \quad z \leq z_{M-ISR}, \quad (47)$$

where the sum is over all the Bloch states with the same energy and $\vec{k}_{||}$ ($\vec{k}_j = \vec{k}_{||} + \vec{k}_{\perp,j}$). Because a 3D energy band of

the bulk crystal is periodic in the repeated-zone representation, a straight line through the (3D) Brillouin zone typically intersects with an equi-energy surface at two points or a few pairs of points. Since the band index is suppressed in Eq. (47), we should generalize and include all such intersections with all the bands. Only in rare cases are an odd number of points encountered. This happens when the straight line is tangent to part of the equi-energy surface. Such cases are unimportant for MS interface electronics, as the lone state either is static or involves an electron traveling parallel to the interface (with its group velocity in the plane of the interface). What is important and happens quite frequently is the case when the $\vec{k}_{\parallel} = \text{const}$ straight line intersects with no part of the equi-energy surface of interest in any of the bands. Obviously, this happens when the chosen energy ε_i is in a gap between bands of the metal, or the entire $\vec{k}_{\parallel} = \text{const}$ line is inside a pocket of the Brillouin zone, i.e., a “mini-gap,” missed by the relevant equi-energy surface, which resides elsewhere in the zone. As can be seen from Fig. 29 (a), which shows the bulk energy bands of the CoSi₂ projected along the {100} direction,⁷⁶ there are many “pockets” of these mini-gaps at specific energy and location in the 2DBZ. Inside these mini-gaps, there is no solution to the Schrödinger equation for the metal that satisfies the PBC. Other types of solutions, i.e., non-Bloch, may still be found. This should be obvious from Eq. (45), the general form of which can also be used for bulk metal or semiconductor. As before, a supply of 2N boundary values will allow a solution to be generated. What are the forms of these non-Bloch solutions? It is difficult to generalize because there are different reasons for the presence of (mini) band gaps. Below, we examine the forms of solutions in just one type of band gap, for nearly free electrons, and surmise that similar conclusions can be drawn for other types of band gap. In the nearly free electron theory, the potential is assumed to be so weak that it does not influence either the plane wave nature of the free electron wave functions, $\psi_{\vec{k}_j}^{M,\text{Bloch}}(\vec{r}) \propto e^{i\vec{k}_j \cdot \vec{r}}$, or its

energy dispersion, $\varepsilon_j = \frac{\hbar^2 k_j^2}{2m}$, EXCEPT when \vec{k}_j is near a Brillouin zone boundary.¹⁶¹ Close to a Bragg plane, $\vec{k}_j \cdot \vec{K} \approx \frac{1}{2} K^2$, two related, unperturbed plane wave states are nearly degenerate, $|\vec{k}_j|^2 \approx |\vec{k}_j - \vec{K}|^2$. Therefore, the coupling between these two plane wave components cannot be ignored, even if the coupling potential energy between them is weak $|eU_{\vec{K}}| \ll \hbar^2 k_j^2 / (2m)$. Writing $\psi_{\vec{k}_j}^{M,\text{Bloch}}(\vec{r})$ as a linear combination of the two plane waves and plugging into the Schrödinger equation, one gets

$$\begin{aligned} \varepsilon_j = & \frac{1}{2} \left(\frac{\hbar^2 k_j^2}{2m} + \frac{\hbar^2 |\vec{k}_j - \vec{K}|^2}{2m} \right) \\ & \pm \sqrt{\left(\frac{\hbar^2 k_j^2}{4m} - \frac{\hbar^2 |\vec{k}_j - \vec{K}|^2}{4m} \right)^2 + e^2 U_{\vec{K}}^2}, \end{aligned} \quad (48)$$

as the eigenvalues. Indeed, the two-fold degeneracy is removed and a gap of $|2eU_{\vec{K}}|$ is opened up at the Bragg plane. On the Bragg plane, the two solutions are known to be^{161,171}

$$\psi_{\vec{k}_j=\vec{K}/2}^{M,\text{Bloch}}(\vec{r}) \propto \sin\left(\frac{\vec{K}}{2} \cdot \vec{r}\right) \quad \text{and} \quad \cos\left(\frac{\vec{K}}{2} \cdot \vec{r}\right). \quad (49)$$

The sign of the coupling energy, $-eU_{\vec{K}}$, determines which of the two solutions corresponds to which root in Eq. (48). Our interest in this exercise has been to examine the kind of non-Bloch solutions that may survive near an interface. For that purpose, we let \vec{K} be a primary lattice vector for the 2D reciprocal lattice, $\vec{K} = \vec{K}_{\parallel}$, and ignore all other Fourier components of the potential except $-eU_{\vec{K}_{\parallel}}$. We assume the Fourier energy term to be positive, i.e., $|U_{\vec{K}_{\parallel}}| = -U_{\vec{K}_{\parallel}}$, thus identifying $\cos(\vec{K}_{\parallel}/2) \cdot \vec{r}$ with the higher of the eigenvalues in (48). We now look for a solution with a (forbidden) energy just below the top of the band gap ($\varepsilon_{\text{gap-top}}$)

$$\varepsilon_{\text{forbid}} = \frac{\hbar^2 |\vec{K}_{\parallel}|^2}{2m} - eU_{\vec{K}} - \frac{\hbar^2 \kappa^2}{2m} = \varepsilon_{\text{gap-top}} - \frac{\hbar^2 \kappa^2}{2m}, \quad (50)$$

where κ is purely real and $\frac{\hbar^2 \kappa^2}{2m}$ is small compared with $-eU_{\vec{K}_{\parallel}}$. Because we know that plugging $\cos(\vec{K}_{\parallel}/2) \cdot \vec{r}$, which has no z-dependence, into the Schrödinger equation would render an eigenvalue of $\varepsilon_{\text{gap-top}}$, we try the same wave function but with an artificially added z-dependence

$$\psi_{\vec{K}_{\parallel}/2}^{\text{gap}} = \cos\left(\frac{\vec{K}_{\parallel}}{2} \cdot \vec{r}\right) e^{\kappa z}, \quad (51)$$

and discover that indeed this is a solution with the desired energy of Eq. (50). The reason that these two possible solutions, with positive and negative values of κ , are not allowed under the PBC is now clear: they diverge in the positive z and negative z directions, respectively. Near an interface or a surface, however, one of the two solutions, the one that decays toward the bulk crystal, is allowed. Note that the closer to the edge of the gap, the longer the decay length. The fact that there are a diverging state and a converging state in the gap, at any energy and \vec{k}_{\parallel} , is expected to have general validity beyond the nearly free electron model.

We've examined the forms of solution of the Schrödinger equation for the ISR and the bulk metal. A separate discussion for the bulk semiconductor region is unnecessary, as the relevant equations would be identical to those for the bulk metal, except for a change in the designation index. A solution to the Schrödinger equation for the entire MS interface is found if these “regional” wave functions can match in both their values and gradients at the boundaries. From above discussions, there are four different cases concerning the formation of interface state that can be distinguished: (1) there are Bloch states in the bulk metal with a given \vec{k}_{\parallel} and at a specific $\varepsilon_{\vec{k}_{\parallel}}$, but no such Bloch states are available in the semiconductor; (2) there are Bloch states in the semiconductor, but not in the metal; (3) there are Bloch states in both the metal and the semiconductor; and (4) there are no Bloch states with the $\varepsilon_{\vec{k}_{\parallel}}$ and \vec{k}_{\parallel} in either the metal or the semiconductor. In Fig. 29, there are bulk states for CoSi₂ at the \bar{M} point and at ~ 5 eV below the Fermi level,⁷⁶ but there are no bulk states for the Si; thus serving as an example of Case (1). In Case (1), the semiconductor cannot support extended propagating states and therefore the wave function

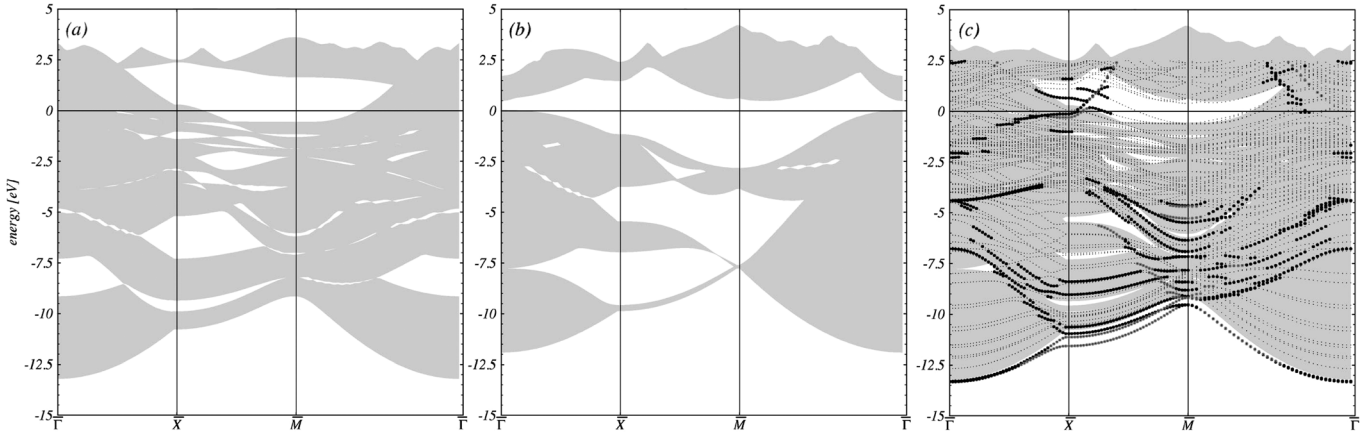


FIG. 29. Bulk bands projected along {100} orientation of (a) CoSi₂ and (b) Si. (c) Energy bands for the CoSi₂/Si(100) interface with the C8 interface type (8-fold coordinated). Shaded area in (c): sum of projected bands of (a) and (b). Interface states localized at positions Si_C(I) (Si interface site of CoSi₂ block): black circles; and Si(I) (Si interface site of Si block): grey circles. All other states: small dots. Fermi energy is defined by zero of energy in all cases. Reprinted with permission from R. Stadler and R. Podloucky, Phys. Rev. B **62**, 2209–2219 (2000). Copyright 2000 American Physical Society.⁷⁶

has to be of a form that decays exponential toward the semiconductor, i.e., κ is negative in a wave function similar in form to Eq. (51). The known form of the semiconductor wave function completely specifies the 2N boundary values at $z = z_{SC-ISR}$, except for a normalization factor. Therefore, the form of the wave function in the ISR is exactly known. For the metal, we assume that two Bloch states are available, one “incoming” toward the ISR and one outgoing from the ISR, i.e.,

$$\varphi_{\vec{k}_{||},\vec{r}}(\vec{r}) = a_{in}^M \psi_{in}^{M-Bloch}(\vec{r}) + b_{out}^M \psi_{out}^{M-Bloch}(\vec{r}), \quad z \leq z_{M-ISR}. \quad (52)$$

As these two solutions form a complete set of the solution to the Schrödinger equation for the bulk like potential, a combination of the two can always be found that will match the value and gradient of the wave function for ISR at $z = z_{M-ISR}$. Therefore, there is only one degree of freedom left, which is the normalization of the entire wave function. Because the interface is assumed to be between two infinite crystals, the normalization condition needs to be applied only for the infinite metal crystal in Case (1). The normalization process for Bloch electrons, e.g., $\psi_{in}^{M-Bloch}$, $\psi_{out}^{M-Bloch}$, etc., is that one electron per unit cell per spin is rendered by one complete band.¹⁶¹ Therefore, a wave function for the entire MS interface is normalized if

$$|a_{in}^M|^2 + |b_{out}^M|^2 = 2. \quad (53)$$

The reason that the right hand side of Eq. (53) is 2 rather than 1 has nothing to do with spin (the present work completely ignores spin). It has to do with the fact that the z dimension of the PBC used for the metal crystal is only one-half the length of the entire region that encompasses both the metal and the semiconductor. Therefore summing only over states allowed in the PBC for the metal crystal will miss one-half the states allowed for the entire region. A remedy, shown in Eq. (53), is to let each allowed bulk state double its intensity in order to continue to contribute one electron per unit cell per band. A consideration from the prospective of the time-dependent

Schrödinger equation suggests that $|a_{in}^M|^2 = |b_{out}^M|^2 = 1$, i.e., the linear combination in Eq. (52) actually produces a standing wave in the z -direction. This is consistent with the fact that electrons in the metal cannot have a net flux into or out of the semiconductor, which does not have bulk states at this energy and $\vec{k}_{||}$. As these states for the MS interface are normalized to recreate the bulk electron density for the metal, the weight of these wave functions in the ISR is known to be finite but otherwise unconstrained. The intensity of the wave function usually decays monotonically from the metal into the ISR. However, at certain energy and $\vec{k}_{||}$, the intensity in the ISR could peak and far exceed that in the metal, forming what is known as an “interface resonance” state, in analogy with the formation of surface resonance states theoretically and experimentally well-studied for metal surfaces. In Fig. 30(a), the calculated charge density at the epitaxial NiPtGe/GaAs (100) interface,¹⁷³ for an interface band in the fundamental band gap of GaAs is shown. The electron density due to this particular 2D band of MIGS is seen to display resonant character at the interface. The condition for the formation of interface resonances is very much dependent on the atomic arrangement in the ISR. In summary, for Case (1), there will always be a state for the MS interface that is in the form of a standing wave in the metal, of unspecified intensity in the ISR, and decays toward the semiconductor. If the energy of this state is in the fundamental gap of the semiconductor, such a state is referred as MIGS. The formation of interface states for Case (2) is described in exactly the same fashion as for Case (1) and, therefore, the same results and conclusions can be drawn about electronic states at the MS interface for Case (2). For example, the $\bar{\Gamma}$ point at ~ 0.85 eV below the Fermi level in Fig. 29 belongs to Case (2), for which there are semiconductor-induced gap states (SIGS!?) that decay toward the metal.

When there are bulk states, at specific energy and $\vec{k}_{||}$, for both bulk semiconductor and metal as in Case (3), the wave function for the metal region can still be written in general as Eq. (52). We also assume that there are only two Bloch states in the semiconductor, allowing the wave function in the semiconductor region to be written as

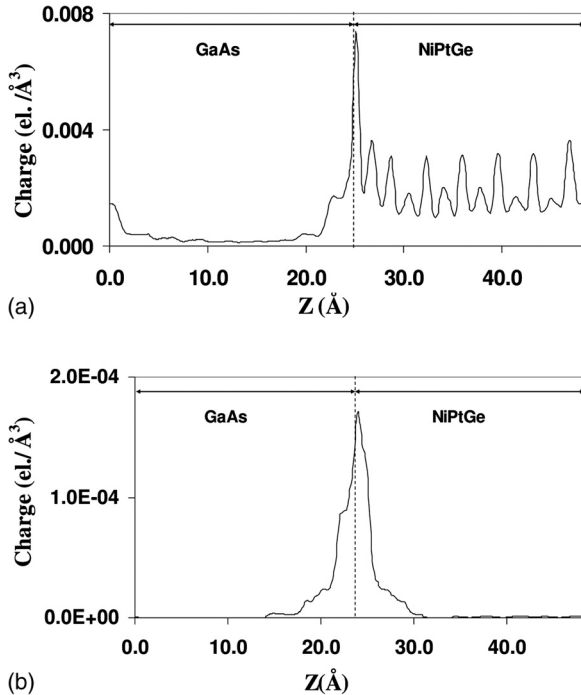


FIG. 30. (a) Calculated charge density (planar average) at the epitaxial NiPtGe/GaAs(100) interface, along the slab axis for an interface band in the fundamental band gap of GaAs. The electron density on GaAs side is due to MIGS. (b) Charge density along the slab axis for a 2D interface band in the gaps of both GaAs and NiPtGe, at ~ 8.0 eV below the Fermi level. The vertical dotted lines indicate the interface position that is defined to be halfway between As and Ge atoms at the interface. Reprinted with permission from Niranjan *et al.*, Phys. Rev. B **77**, 155316 (2008). Copyright 2008 American Physical Society.¹⁷³

$$\varphi_{\vec{k}_{||,e_i}}(\vec{r}) = a_{in}^{SC} \psi_{in}^{SC-Bloch}(\vec{r}) + b_{out}^{SC} \psi_{out}^{SC-Bloch}(\vec{r}),$$

$$z_{SC-ISR} \leq z. \quad (54)$$

Since an identification of the semiconductor wave function at the $z = z_{SC-ISR}$ interface sufficiently specifies the boundary condition for the ISR and, therefore, uniquely define the wave function at the $z = z_{M-ISR}$ interface through Eq. (45), the Bloch functions in the metal region are coupled to the Bloch functions on the side of the semiconductor. Following the treatments in quantum transport theories,^{174,175} we write

$$\begin{pmatrix} \sqrt{|v_z^M|} b_{out}^M \\ \sqrt{|v_z^{SC}|} b_{out}^{SC} \end{pmatrix} = \begin{pmatrix} s_{M-M} & s_{M-SC} \\ s_{SC-M} & s_{SC-SC} \end{pmatrix} \begin{pmatrix} \sqrt{|v_z^M|} a_{in}^M \\ \sqrt{|v_z^{SC}|} a_{in}^{SC} \end{pmatrix}, \quad (55)$$

where v_z^M and v_z^{SC} are the group velocities $= \hbar^{-1}(\partial \epsilon / \partial k_z)_{\vec{k}_{||}}$ for the metal and the semiconductor bulk bands, respectively, and the s 's are fixed coefficients obtained from the Schrödinger equation for the ISR, Eq. (45), relating the outgoing “current amplitudes” to the incoming current amplitudes. In the matrix form, the above equation can be written as

$$\vec{A}_{\vec{k}_{||,e}} = \vec{S}_{\vec{k}_{||,e}} \vec{B}_{\vec{k}_{||,e}}, \quad (56)$$

where $\vec{S}_{\vec{k}_{||,e}}$ is the scattering matrix, or S-matrix, and $\vec{A}_{\vec{k}_{||,e}}$ and $\vec{B}_{\vec{k}_{||,e}}$ are single-column vectors representing the incoming and

outgoing current amplitudes. Because the flux of electrons associated with an electronic state, i.e., the number of electrons per time per unit area on an x-y plane, is the product of the perpendicular velocity and the density of electrons, i.e., the absolute square of the wave function, the inclusion of the $\sqrt{v_z}$ factor ensures that the S-matrix relates vectors of conserved quantity. Because the total flux is conserved

$$|\vec{A}_{\vec{k}_{||,e}}|^2 = |\vec{B}_{\vec{k}_{||,e}}|^2, \quad (57)$$

the S-matrix is unitary

$$|s_{M-M}|^2 + |s_{M-SC}|^2 = |s_{SC-M}|^2 + |s_{SC-SC}|^2 = 1, \quad (58)$$

and the conjugate transpose of the S-matrix is its own inverse matrix

$$\vec{S}_{\vec{k}_{||,e}}^+ \vec{S}_{\vec{k}_{||,e}} = \vec{S}_{\vec{k}_{||,e}} \vec{S}_{\vec{k}_{||,e}}^+ = \vec{1}. \quad (59)$$

There are many equivalent ways to write the two degenerate and orthogonal states for the MS interface at a specific $\vec{k}_{||}$ of Case (3). The most straightforward choice may be the pair of states $a_{in}^M = 0$ and $a_{in}^{SC} = 0$, the schematics of which are shown in Fig. 31. As already mentioned, the allowed states in the MS interface are normalized such that one complete band will render one electron per spin per unit cell for either the metal or the semiconductor. This makes for some tricky normalization requirements for Case (3). For example, the normalization conditions for the wave function without an incoming semiconductor wave ($a_{in}^{SC} = 0$) according to Eqs. (58) and (59) can be the following:

$$|a_{in}^M|^2 = 1 \quad (60)$$

and

$$|b_{out}^M|^2 + |v_z^{SC}/v_z^M| \cdot |b_{out}^{SC}|^2 = 1. \quad (61)$$

The appearance of a $|v_z^{SC}/v_z^M|$ factor in the normalization condition seems odd, but actually makes perfect sense.

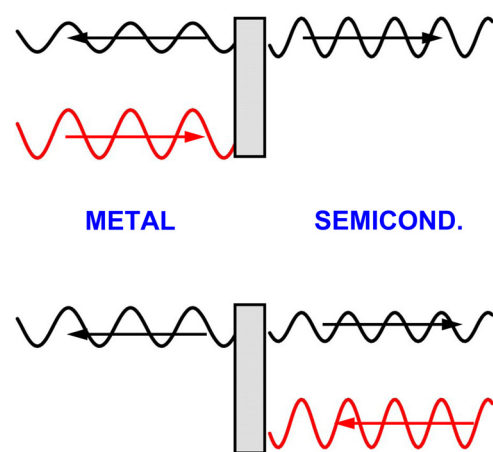


FIG. 31. Two orthogonal eigenstates of the MS interface from coupling between bulk states of the metal and the semiconductor with the same energy and $k_{||}$.

Although the two dimensional Brillouin zone of the two crystals are of the same area and have the same number of allowed $\vec{k}_{||}$'s, the density of states in the Brillouin zone for the bulk metal and the bulk semiconductor are unspecified in the k_z direction. By writing (60) in the usual normalization form, it is implied that a range in k_z (or energy) has been chosen, which holds exactly one pair of allowed Bloch \vec{k} states (in and out) in the metal Brillouin zone. The number of states in the semiconductor Brillouin zone that can match the metallic state in the implicit range of energy is none other than $|v_z^M/v_z^{SC}|$! It is thus clear that the way these bulk-coupled states should be normalized depends on eventually how the density of charge is summed. Conditions specified in Eqs. (53), (60), and (61) are appropriate when the density of states in the reciprocal space of the bulk metal is used for integration/summation. Rest assured that a normalization scheme consistent with the integration method of all states for Cases (1-3) always leads to a neutral metal region and a neutral semiconductor region at the same time. As for Cases (1) and (2), the amplitude of the wave function inside the ISR for Case (3) follows no specific rules. Interface resonances may take place at certain energy and $\vec{k}_{||}$, the nature of which is sensitive to the interface atomic structure. The strength of the coupling between the metal and the semiconductor is reflected in the off-diagonal S-matrix elements $|s_{M-SC}| (= |s_{SC-M}|)$. When the coupling at certain energy and $\vec{k}_{||}$ is weak, $|s_{M-SC}| \ll 1$, electronic transport across the MS interface is impeded, with $|s_{M-SC}|^2$ being related to the tunneling probability across the ISR. Electron transport can be small for wide ranges of energy and $\vec{k}_{||}$'s, e.g., when the metal and semiconductor bulk bands belong to different symmetry groups, or when a thin insulating layer is present in the ISR.

If there are no bulk Bloch states in either the semiconductor or the metal at specific energy and $\vec{k}_{||}$, i.e., Case (4), such as at the \bar{M} point at the Fermi level (or ~ 10 eV below the FL) in Fig. 29, the only acceptable form of the wave function for the metallic region is the kind that decays toward negative z ; and the acceptable form of the wave function for the semiconductor region is the type that decays toward large positive z . Having either one of these two types of wave function already supplies sufficient boundary values to define the wave function in the ISR to within a normalization factor. The fact that the Dirichlet and the Neumann conditions are both defined at all the exterior boundaries of the ISR represents a gross over-constraint on the wave function in the ISR. Therefore, there is usually not any solution allowed at the specified energy and $\vec{k}_{||}$, except in rare incidents when the oversupplied boundary conditions are redundant or internally consistent. Under those particular conditions, the electronic states that are formed for Case (4) are true “interface states,” in the sense that they have significant amplitude only in the ISR and decay in both directions away from the interface, as the example of Fig. 30(b) shows.¹⁷³ Analogous to true “surface states” that reside only at the surface region of a solid and are sensitive probes of the atomic structure of the surface,¹⁷¹ these interface states are also sensitive to the atomic structure of the MS interface. Being uncoupled to the bulk states, the interface states are

normalized in the usual fashion, i.e., the absolute square of the wave function, integrated over all z and over the area of the 2D PBC, is 1. Therefore, a complete and filled 2D band of interface states leads to one electron per 2D unit cell.

The spatial distributions of the electronic density associated with the four types of electronic states described above are schematically shown in Fig. 32. Energetic distribution of the electronic states that are allowed at MS interfaces is illustrated in the example of Fig. 29(c) for a specific structure of the CoSi₂/Si(100) interface.⁷⁶ The formation of the SBH is decided by the total charge distribution, due to all four types of occupied electronic states, with energies below the Fermi level, and in particular due to the charge distribution inside the ISR. The exact forms of the wave function in the ISR depends on the bulk band structures of the metal and the semiconductor, as well as the arrangement of atoms in the ISR, as explicitly shown in Eq. (45). There are several quantum-mechanical perspectives on the formation of the interface dipole that should be pointed out, as these are at odds with common perceptions and discussions of SBH formation found in the literature. First of all, the interaction between the metal and semiconductor leads to modifications of the bulk wave functions throughout the valence/conduction bands of both materials. It is in the modifications of these bulk bands, within the process generically associated with bond formation, that the charge rearrangement inside the ISR is accommodated. Therefore, the charge transfer between the two materials, if such a terminology is used, takes place over a very wide range on the energy scale, in sharp contrast to some opinions in the literature that the charge transfer is between electrons near the FL of the metal and the MIGS of the semiconductor. In fact, the formation of interface dipole is not a phenomenon dominated by electrons near the Fermi level. Second, it has often been assumed in the literature that since the metal has mobile carriers it will be able to screen out any disturbance associated with interface formation over a very short, Thomas-Fermi-like, distance on the metal side. This would leave the physical location of the “interface dipole” to be highly asymmetric,

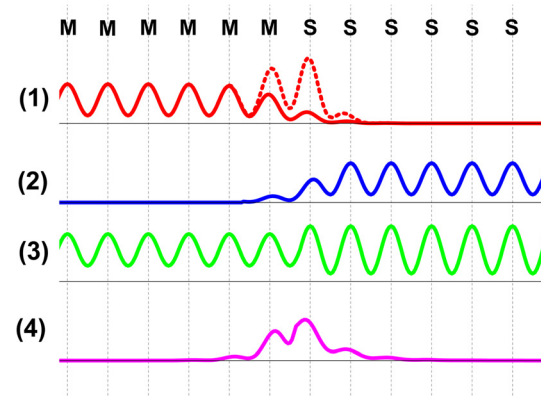


FIG. 32. Schematic drawing of the density of four classes of electronic states found at epitaxial MS interfaces. Layer positions of metal (M) and semiconductor (S) are indicated. The four different types of interface states are (1) metal bulk states, (2) semiconductor bulk states, (3) coupled bulk states, and (4) true interface states. In (1), a possible interface resonance is also drawn as dotted line.

residing mainly inside the semiconductor and affecting only a shallow portion of the metal. There is nothing in the above quantum-mechanical treatment of interface electronic states that supports this scenario of lopsided formation of interface dipole. As just demonstrated, the formation of interface dipole is essentially a manifestation of bond formation that puts the metal and the semiconductor on equal footing. Screening by mobile carriers is irrelevant in this regard because of orthogonality among states belonging to the same quantum system. As already discussed, *ab initio* calculations of the electronic structure at MS interfaces frequently find that the charge rearrangement extends even deeper into the metal than the semiconductor, i.e., the spatial extent of the interface dipole often falls more on the metal side of the interface, as shown in Figs. 13 and 15. The quantum view of interface state formation is complicated and intertwined enough that SBH would be difficult to predict quantitatively. There are also no known laws of quantum mechanics to suggest that simple rules on the interface dipole can be derived without knowledge of the interface structure. As a matter of fact, just the opposite is true: subtle changes in the atomic structure at epitaxial MS interfaces are known to lead to very different SBHs. From the perspective of quantum physics, nothing short of an actual numerical calculation of the entire electronic structure of the ISR seems capable of reliable SBH predictions. In Secs. III C and III D, we will forgo the rigor of physics for the intuitiveness and empiricism of chemical concepts that are friendlier to the modeling of charge distribution.

C. Charge transfer in molecules

The interface dipole resulting from the formation of electronic states in the ISR, discussed above, determines the magnitude of the SBH and, therefore, must be responsible for both the sharp variations of the SBH observed at epitaxial interfaces and the dull “Fermi level pinning” phenomenon observed at inhomogeneous MS interfaces. The reason that, from the same SBH mechanism, such two contrasting behaviors have been put on display has to do with the very different circumstances for these two types of MS interfaces. Therefore, the theoretical treatments of the SBH need to take into account the different circumstances. For an epitaxial MS interface, the measured SBH reflects the interface band alignment condition associated with a specific interface atomic structure. The aim of theoretical investigations is then to accurately compute the SBH for epitaxial MS interfaces. Fortunately, the number of epitaxial MS interfaces that can be produced experimentally is relatively small and the uniqueness in the atomic structure minimizes the size of such calculations. So, detailed numerical computation for the analysis of SBH of a few carefully prepared epitaxial interfaces is manageable.^{39,60,76} For an inhomogeneous MS interface, on the other hand, the measured SBH is an average of a wide range of SBHs arising from different interface structures. Even though the basic process of SBH formation is the same for any kind of atomic structure, homogeneous or inhomogeneous, and calculable in principle, we are today still far from numerical computation capabilities that can handle

real-scale inhomogeneous MS interfaces with unspecified interface structure. High numerical accuracy is unnecessary for inhomogeneous MS interfaces, in any event, because of the uncertainty in the structure. Rather, the main feature of non-epitaxial SBHs has always been the apparent Fermi level pinning phenomenon, which needs to be properly explained. The systematics displayed in Figs. 4 and 6, and Eq. (7) have provided valuable guidance to the empirical engineering of SBH. However, as pointed out, the MIGS model that generated Eq. (7) is unjustifiable. The weakened dependence of the experimental (average) SBH on the metal work function should have a natural explanation within the spirit of bond formation. In this section, we examine general concepts on the charge transfer associated with bond formation, which is a topic usually treated in molecular chemistry. These concepts are expected to shed light on the SBH mechanism because, obviously, there are bonds at MS interfaces.

In a molecule, the electronic states are, strictly speaking, properties of the molecule only. However, the facts that the molecular orbitals derive their characteristics from the core potentials of the ions and that the ions in the molecule settle into configurations favorable in energy are akin to the scenario at MS interfaces. Since the ionic core potentials relevant for molecular orbitals would have rendered atomic orbitals in isolation, chemistry looks for simple ways to rationalize the distribution of molecular charge in terms of the properties of the atoms in the molecule. To be manageable, the chemical roles played by the atoms in a molecule are represented by a small number of parameters and the electron density of the molecule is envisioned to be partitioned into ones centered about the ionic positions. Once that’s done, the net charges associated with the ions in the molecule can be approximated as “point charges” and used to simulate the electrostatic potential of the molecule. If applied to an MS interface, this procedure would obviously generate the sought-after dipole moment for the interface. It is advantageous to bring molecular chemistry into discussions of the SBH mechanism, as this puts the atomistic nature of the interface dipole formation front-and-center, in keeping with the dependence of the SBH on interface structure. The formation of the interface dipole no longer needs to be viewed vaguely as an interaction between the “metal crystal” and the “semiconductor crystal” or, worse yet, between the FL of the metal and the MIGS of the semiconductor.

When an atom becomes part of a molecule, a significant rearrangement of charge usually takes place, resulting in a molecular electron density different from a simple sum of the individual, isolated, atomic densities. Of primary importance in the description of molecular dipoles is the amount of charge transfer among atoms. A parameter called “electronegativity,” which has been loosely defined as “the power of an atom in a molecule to attract electrons to itself,”¹⁷⁶ was proposed to model the transfer of charge. After decades of discussions and the considerations of many different proposals,^{176–183} the community seems to have largely converged on the notion that the electronegativity of an atom, X , is the negative of its electronic chemical potential,^{184–186} which is the derivative of

the energy of an atom, E_a , with respect to the number of its valence electrons, N ,

$$-X = \mu = \frac{\partial E_a}{\partial N}. \quad (62)$$

Although, one cautions that the identity of the electronegativity is not an open and shut case, as new proposals for electronegativity scales continued to emerge in the literature.^{187–192} There is an obvious differentiability problem with the definition given in Eq. (62), because the number of electrons can strictly only assume integer values for any finite electronic system such as an isolated atom. Using an alkali atom as an example, the ground state energies (shown as discrete squares in Fig. 33) for different charge states are known as

$$E_a = \begin{cases} E_{core}, & \Delta N = -1 \\ E_{core} - I, & \Delta N = 0 \\ E_{core} - I - A, & \Delta N = +1 \end{cases}, \quad (63)$$

where I and A are the first ionization potential and the electron affinity, respectively, $\Delta N (= N - 1)$ is the number of excess electrons on the atom, and E_{core} is the ground state energy of the ion core of the alkali atom. We have assumed that the core is “frozen” and does not respond to changes in the outer orbits, in which case the Hamiltonian can be individually written for the two parts and the total energy is a simple sum, as shown in Eq. (63). To make the energy in Eq. (62) differentiable, it is necessary to project or assign a scenario to an atom with a fractional number of electrons. One strategy that accomplishes this is to use a grand canonical ensemble formulation of the density functional theory (DFT),^{193,194} which shows that the energy for a fractionally charged atom amounts to a linear interpolation between neighboring integer values, namely,

$$E_a = \begin{cases} E_{core} - I - I \Delta N, & -1 \leq \Delta N \leq 0 \\ E_{core} - I - A \Delta N, & 0 \leq \Delta N \leq +1 \end{cases}. \quad (64)$$

As represented by straight line segments in Fig. 33, the ground state energy of an isolated atom is piecewise linear, yielding a step-wise electronic chemical potential of $-I$ and $-A$, respectively, for $-1 \leq \Delta N < 0$ and $0 < \Delta N \leq 1$.

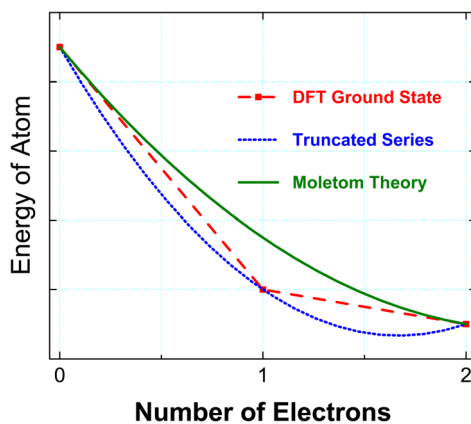


FIG. 33. Energy of an alkali atom as a function of the number of electrons.

Another approach that circumvents the differentiability issue of Eq. (62) is to consider that the atom is in thermal equilibrium with an external system, such as the rest of a molecule of which the atom is a part. In this scenario, the number of electrons of an “atom” can deviate from an integer. There are many proposals on how to identify or partition a molecule into “regions” that represent individual atoms,^{164–168} although inconsistencies among these definitions are known to exist.¹⁶⁹ In addition, a demonstration that the chemical characteristics of “atoms” defined in this fashion have global relevance, i.e., with transferability between dissimilar molecules, is generally lacking. These issues notwithstanding, one proceeds by assuming that the total number of electrons can indeed be assigned fractionally to each atom and that the power to further attract electrons to an atom, the electronegativity, varies with the net charge of the atom. Since electrons tend to flow from atoms with a smaller electronegativity to those with a larger electronegativity, there is the expectation that this flow only stops when their electronegativities become equal.¹⁷⁸ Based on this concept, the electronegativity equalization method (EEM),^{195–197} which is also known as charge equilibration,^{198–200} chemical potential equalization,^{201–205} and electrochemical potential equalization (EECP),²⁰⁶ allows the distribution of charge in a molecule to be modeled as atomically centered point charges, once the energy of the atom as a function of ΔN is known. These simulations typically assume that the energy of a fractionally charged atom can be expanded in a Taylor series in the number of excess electrons. By truncating the polynomial series after the quadratic term^{184,186,198} and fitting to the three known values of the isolated atom, Eq. (63), one gets

$$E_a = E_{core} - I - \frac{I+A}{2} \Delta N + \frac{I-A}{2} (\Delta N)^2 \quad (65)$$

and

$$\frac{\partial E_a}{\partial N} = -\frac{I+A}{2} + (I-A)\Delta N. \quad (66)$$

Interestingly, and perhaps fortuitously, the electronic chemical potential for the neutral atom ($\Delta N = 0$) is predicted to be $-(I+A)/2$, in agreement with Mulliken’s “absolute electronegativity.”¹⁷⁷ Scientifically speaking, the adoption of Eq. (65) to represent the energy of an atom in a molecular environment has little basis. Equation (65) is apparently based on the isolated atom because it arises from a fit to the ground state energies of an isolated atom.¹⁹⁸ The ground-state energy of the isolated atom, on the other hand, is known to be exactly piecewise linear,^{193,194,207,208} i.e., Eq. (64), the form of which, if expanded in a power series, would require many higher order terms. Expression (65), therefore, should be intrinsically less accurate than the DFT result, Eq. (64).²⁰⁹ However, this truncated, approximate form of E_a has found some success in the estimation of molecular charges through EEM, whereas the exact, piecewise-linear, result failed miserably.

The exact total energy of Eq. (64), as it turns out, is actually irrelevant for the electronegativity concept, because the atom described by this equation is understood to be in

isolation, whereas the E_a in Eq. (62) should be that for an atom in a “molecular environment.” Ever since the beginning of the electronegativity concept, the importance of the chemical environment to the electronegativity has been stressed repeatedly.^{177,184,186,210,211} Huheey summed up this sentiment most directly in the following way “Electronegativity is not a property of the isolated atom but rather a property of an atom in a molecule, in the environment of and under the influence of surrounding atoms.”²¹² While that much everybody agrees on, the problem, as it always has been, is how to define a “molecular” environment for an atom without actually putting it in a molecule. Recently, it was proposed that the molecular environment can be imposed on a system of identical, non-interacting, atoms by the constraint that the total spin of the electrons vanishes, i.e., in a singlet state.²¹³ For atoms with a single active orbital, such as alkali atoms, the total energy of an atom in a molecular environment, called a “moletom,” within the Hartree-Fock formalism, can be shown to be exactly²¹³

$$E_{MT} = E_{core} - \frac{3I+A}{4} - \frac{I+A}{2}\Delta N + \frac{I-A}{4}(\Delta N)^2, \quad (67)$$

for which the range of ΔN is the same as Eqs. (63) and (64). This form of energy, plotted in Fig. 33, is very intuitive. First of all, it is quadratic in the number of electrons, similar to the truncated form found in previous numerical simulations to reproduce semi-quantitatively the dipole moments of molecules.^{184,186,198} Second, Eq. (67) reproduces the energies of the $\Delta N = \pm 1$ states of the experimental and the DFT result. The chemical potential of an atom in molecular environment is

$$\mu_{MT} = \frac{\partial E_{MT}}{\partial(\Delta N)} = -\frac{I+A}{2} + \frac{I-A}{2}\Delta N \equiv \mu_0 + \eta_0 \Delta N, \quad (68)$$

which again agrees with the DFT results of $-I$ and $-A$, respectively, for the singlet $\Delta N = -1$ and $\Delta N = +1$ states. A chemical potential of $-(I+A)/2$, defined as the canonical chemical potential for the orbital μ_0 , is predicted for the neutral atom, as before.¹⁷⁷ However, the energy for the moletom is consistently above the true DFT ground state, meeting the expectation that the singlet state is not the ground state for the truly isolated atom, except for the two end points. The hardness of the orbital is a constant for the moletom,

$$\eta_{MT} = \frac{\partial^2 E_{MT}}{\partial(\Delta N)^2} = \frac{I-A}{2} \equiv \eta_0, \quad (69)$$

which is defined as the canonical hardness for an atomic orbital. The hardness of Eq. (69) is only one-half of that predicted from the empirical model, Eq. (66).

With the energy of i -th atom (in molecular environment) written as a function of the excess number of electrons on the atom

$$E_i(Q_i) = E_i^o + \mu_i Q_i + \frac{1}{2} \eta_i Q_i^2, \quad (70)$$

the total energy of a molecule comprising N atoms can be written as the sum of the energies of the individual atoms

and the interactions between them.^{198,201,202} Representing the interatomic interaction by the Coulombic interaction between point charges, one writes

$$E_{tot}(Q_1, Q_2, \dots, Q_N) = \sum_i^N (E_i^o + \mu_i Q_i + \frac{1}{2} \eta_i Q_i^2) + \sum_{i \neq j}^N \frac{Q_i Q_j J_{ij}}{2}, \quad (71)$$

where $J_{ij} = e^2 / (4\pi\epsilon_0 d_{ij})$ and d_{ij} is the distance between the i -th and the j -th atoms. One should note that the point-charge approximation here represents a very substantial simplification as it takes over the complicated roles played by the “bond integral” and the “overlap integral” between orbitals on different atoms, in more realistic treatments of molecular orbitals. In thermal equilibrium, the net charge on each atom will be such that the total energy of Eq. (71) is minimized, while the overall neutrality is maintained, i.e.,

$$\sum Q_i = 0. \quad (72)$$

Such a problem is typically solved by Lagrange’s undetermined multipliers method, with the electrochemical potential playing the role of the multiplier. Requiring that the electrochemical potential to be a constant for every atom throughout the molecule, one writes

$$\mu_i + \eta_i Q_i + \sum_{j(\neq i)}^N Q_j J_{ij} = const. \quad \text{for any } i. \quad (73)$$

The $N-1$ independent linear equations provided through Eq. (73), combined with Eq. (72), lead to a set of Q_i values that minimizes the total energy of Eq. (71). This EECP method assumes that the molecular structure is known and uses two parameters for each atom that can be independently calculated. This simple approach, which has been shown to predict the correct trend of the observed electric dipoles in molecules, seems appropriate for MS interfaces, especially for systematic trends that do not require high numerical accuracy, e.g., the Fermi level pinning phenomenon. Before we end the discussion on how charge transfers between “atoms” in a molecule takes place conceptually, we should mention that the concept of electronegativity has been called “simultaneously one of the most important and one of the most difficult problems in chemistry.”²¹² About it, it has been said that “our seeming inability to define it uniquely and the impossibility of directly measuring it in a molecule has caused frustration and disappointment throughout the chemical community”.¹⁸⁸ It is thus prudent to notice the “intuitive” and “approximate” nature of, rather than the rigor in, these chemical theories and ideas.

D. Estimation of interface dipole

To apply the EECP method to the simplest case of an epitaxial interface between an elemental semiconductor and an elemental metal, the MS interface can be assumed to be

atomically abrupt and the same density of atoms, a_{2D}^{-2} , is assumed to reside on each metal and semiconductor plane, as shown in Fig. 23(b). It seems that one can view the entire ISR region as a “giant molecule” and require that the electrochemical potentials of all the “atoms” in this molecule are equalized. However, the problem with such an approach becomes obvious once we equate the electrochemical potentials of the (neutral) metal and semiconductor atoms away from the immediate MS interface. Because then we find that the difference in electrostatic potential energy between the metal and the semiconductor is simply the difference between the chemical potentials of the metal atom and the semiconductor atom, independent of any specifics of the MS interface. The formation of SBH becomes a bulk effect, contrary to what we know to be the correct physics. This hidden pitfall is a result of the approximate nature of the EECP theory. Despite its limited applicability, the EECP method is still the best available conceptual approach to estimate charge transfer. For the SBH problem, one therefore applies the EECP procedure only locally, to estimate the charge transfer across the immediate MS interface.^{206,214} From symmetry, the same excess number of electrons, Q_{SC} , should be found for every semiconductor atom on the interface plane, and the excess number of electrons on every metal atom is Q_M ($= -Q_{SC}$). We write

$$\mu_M - \eta_M Q_{SC} + \frac{\alpha e^2 Q_{SC}}{4\pi\epsilon_M a_{2D}} = \mu_{SC} + \eta_{SC} Q_{SC} - eU_{SC} - \frac{\alpha e^2 Q_{SC}}{4\pi\epsilon_S a_{2D}}, \quad (74)$$

where μ_{SC} , μ_M , η_{SC} , η_M , ϵ_S , and ϵ_M are the chemical potential, the hardness, and the effective dielectric constant, respectively, for the semiconductor and the metal. The left-hand side of Eq. (74) is the electrochemical potential for metal atom at the interface and the right hand side is the electrochemical potential for a semiconductor atom. In this analysis, the “electrostatic potential” (U) that is relevant is that due to “excess” charge, as referenced with respect to charge distributions of neutral atoms. The average of that potential is assumed to vanish on the plane of the metal atoms, i.e., $U_M = 0$, and takes on the value

$$-eU_{SC} = \frac{e^2 Q_{SC} d_{MS}}{\epsilon_{int} a_{2D}^2}, \quad (75)$$

on the semiconductor plane, with d_{MS} being the distance between the planes and ϵ_{int} the effective dielectric constant for the interface. The first two terms on the left of Eq. (74) represent the chemical potential of the metal atom when its number of excess electrons is $-Q_{SC}$, while the third term is the “empty potential” energy for any metal atom on that interface plane. The adjustable geometric factor α is 2 when the atoms are point charges, 1 when the charge of atoms is assumed to be smeared out on the plane, and less than 1 when the excess electrons on an atom are assumed to distribute in other shapes, e.g., spheres or hydrogen orbitals. Similarly, the right hand side of Eq. (74) can be seen as the sum of the chemical potential (first two terms) and the empty

potential energy (last two terms) for a semiconductor with a net charge of $-eQ_{SC}$. Combining Eqs. (74) and (75), one gets

$$Q_{SC} = \frac{\mu_M - \mu_{SC}}{\eta_{SC} + \eta_M + \kappa}, \quad (76)$$

where κ is the sum of the Coulombic terms

$$\kappa = \frac{e^2 d_{MS}}{\epsilon_{int} a_{2D}^2} - \frac{\alpha e^2}{4\pi\epsilon_S a_{2D}} - \frac{\alpha e^2}{4\pi\epsilon_M a_{2D}}. \quad (77)$$

Equation (76) can now be plugged into Eq. (75) to give the potential drop between the two planes at the interface, which, in this localized application of EECP, is the change in the empty potential energies between the metal and the semiconductor bulk crystals. In other words, Eq. (75) is the interface dipolar term $-e(\Delta V)_{ISR}$ of Eq. (25), which now provides an estimation of the SBH for the MS interface. Previously, Eqs. (75) and (76) were used to compare with the apparent Fermi-level pinning strengths experimentally observed on different semiconductors.^{206,214} In that work, the properties associated with the semiconductor and metal atoms, i.e., μ_{SC} , μ_M , η_{SC} , and η_M , were replaced by their respective equivalents for the semiconductor and metal crystals to make easier the comparison with experimental data presented as a function of the metal work function. As a result, SBH took the form

$$\Phi_{B,p}^o = \gamma_B (I_S - \phi_M) + (1 - \gamma_B) \frac{E_g}{2}, \quad (78)$$

where

$$\gamma_B = 1 - \frac{e^2 N_B d_{MS}}{\epsilon_{it}(E_g/2 + \kappa)}. \quad (79)$$

Obviously, Eq. (78) predicts a dependence of the SBH on the metal work function which is similar to that predicted by gap state models, Eq. (12), with $E_g/2$ taking the place of the CNL. The “interface behavior parameter,” γ_B , according to the EECP approach is in reasonable agreement with experimental data as shown in Fig. 34, lending strong support to the attribution of the Fermi level pinning effect to polarized chemical bonds.^{206,214} However, the replacement of atomic quantities in Eq. (76) by their crystal equivalents is not conducive to accurate description of interface electrostatics, as this procedure brings (the unknown) surface dipole contributions into the equation (cf. Eqs. (38) and (39)). For individual MS interfaces, the use of the atomic form of Eq. (76), combined with the Fermi level and the band edges calculated for appropriate model solids, Eqs. (19) and (20), is likely to render more accurate SBH estimates.

The modeling of the interface dipoles for polar surfaces of compound semiconductors follows the same procedures as just described for elemental semiconductors, although the details require more thought. We shall use the interface between an elemental metal and the As-terminated GaAs(100) interface as an example to illustrate the typical strategies and rules for polar interfaces. Again we shall assume that the

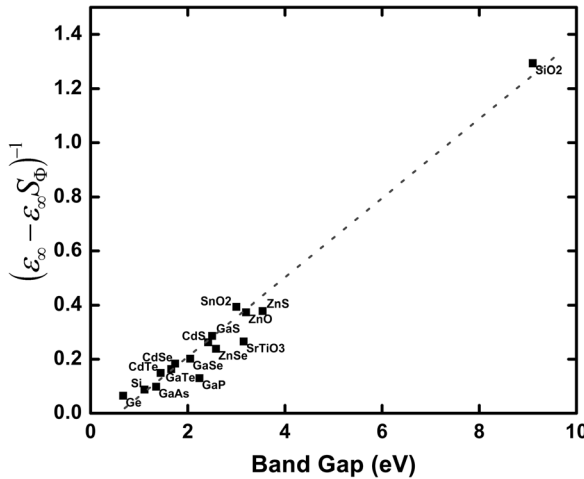


FIG. 34. Experimentally observed interface behavior parameter,¹⁷ plotted as $(\epsilon_0/\epsilon_\infty)/(1 - S_\Phi)$, against the band gap of the semiconductor. Reprinted with permission from R. T. Tung, Phys. Rev. B **64**, 205310 (2001). Copyright 2001 American Physical Society.²⁰⁶

interface is epitaxial and with a lattice parameter of a_{2D} ($= a_{GaAs}/\sqrt{2}$) for the square 2D unit cell for both the metal, e.g., Al, and the GaAs. As before, all metal atoms will be assumed to be neutral except those on the immediate interface plane. Also, we shall assume that all atoms of the semiconductor, except for those As atoms on the immediate interface plane, to have the same net charges they do, respectively, in a bulk GaAs. For neutral bulk GaAs crystal the (positive) net charge on each Ga atom, as a result of EECP, is $-eQ_{Ga}^{(0)}$ ($= eQ_{As}^{(0)}$), where

$$Q_{As}^{(0)} = \frac{\mu_{Ga} - \mu_{As}}{e^2} + \frac{e^2 \alpha}{4\epsilon_{GaAs} a_{GaAs}} - \frac{e^2 \alpha}{\sqrt{2}\pi\epsilon_{GaAs} a_{GaAs}}. \quad (80)$$

From the discussions of Sec. IIIA, we know that the present interface should be analyzed by representing the semiconductor crystal with a model solid constructed with CCMSC. This places one-half of the (non-neutral) bulk charge density of As atoms on the interface plane, and leaves only one-half of the As atoms on the interface free to interact with the metal, as shown in Fig. 27(b). This is a result that also emerges naturally from the EECP analysis. Let the excess number of electrons on the metal and As atoms at the interface be $Q_M^{(int)}$ and $Q_{As}^{(int)}$, respectively. In order for the interface to be electrically neutral, i.e., without long range electric field in the semiconductor, it is required that $Q_M^{(int)} + Q_{As}^{(int)} = Q_{As}^{(0)}/2$. Rewriting, one has

$$Q_M^{(int)} = -(Q_{As}^{(int)} - Q_{As}^{(0)}/2) = -Q_{As}^{(mf)}, \quad (81)$$

where the part of excess charge on interface As atom, due to its interaction with the metal is defined as $Q_{As}^{(mf)}$ (mf: metal-facing). The electrochemical potential can now be equated for the metal and the As atoms at the interface. Assuming the average electrostatic potential to vanish for the metal, one writes

$$\begin{aligned} \mu_M + \eta_M Q_M - \frac{\alpha e^2 Q_M}{2\sqrt{2}\pi\epsilon_M a_{GaAs}} &= \mu_{As} + \eta_{As} Q_{As}^{(int)} - \frac{e^2 Q_M d_{MS}}{\epsilon_{int} a_{GaAs}^2 / 2} \\ &\quad - \frac{\alpha e^2 Q_{As}^{(int)}}{2\sqrt{2}\pi\epsilon_{GaAs} a_{GaAs}}. \end{aligned} \quad (82)$$

Before proceeding further, one notices that an As atom that has already acquired $Q_{As}^{(0)}/2$ number of excess electrons has a chemical potential (pf: partially filled)

$$\mu_{As-pf} = \mu_{As} + \eta_{As} \frac{Q_{As}^{(0)}}{2} - \frac{\alpha e^2}{2\sqrt{2}\pi\epsilon_{GaAs} a_{GaAs}} \frac{Q_{As}^{(0)}}{2}. \quad (83)$$

When Eqs. (81) and (83) are plugged into Eq. (82), one gets

$$\frac{Q_{As}^{(mf)}}{\eta_{As} + \eta_M + \frac{2e^2 d_{MS}}{\epsilon_{int} a_{GaAs}^2} - \frac{\alpha e^2 (\epsilon_M^{-1} + \epsilon_{GaAs}^{-1})}{2\sqrt{2}\pi a_{GaAs}}} = \frac{\mu_M - \mu_{As-pf}}{2e^2 d_{MS}}, \quad (84)$$

which can be seen to be identical in form to Eq. (76). This result shows that, according to the EECP theory, the net charge for atoms on a crystal plane is additive, being the sum of the charge transfer with atomic plane on one side and that with atomic plane on the other side. For the second charge transfer, however, the chemical potential for the atom is shifted from its value while neutral, because the charge state of the atom has already changed due to its first (prior) interaction. The potential difference generated by the charge transfer between metal and As,

$$-eU_{GaAs} = \frac{2e^2 d_{MS}}{\epsilon_{int} a_{GaAs}^2} Q_{As}^{(mf)}, \quad (85)$$

can now be taken as the difference in the empty potentials for model solids of the GaAs and metal to estimate the SBH through Eq. (25).

The EECP theory to estimate the SBH described above can be broken down in two steps, as schematically illustrated in Fig. 27. In the starting or un-equalized configuration, the two model solids, each terminated on one-half monolayer of atoms, are placed next to each other. One-half monolayer each of metal and semiconductor neutral atoms are also placed on the interface planes to complete the chemical composition of the interface, as shown in Fig. 27(b). Because of symmetry, no potential drop can be induced from two layers of neutral atoms. As the result, the empty potential for either the semiconductor model solid or the metal model solid vanishes in the starting configuration, for which we know that Eq. (31) holds at this stage. In the second step, Fig. 27(c), the electrochemical potentials on the free atoms are equalized, leading to charge transfers and potential drops of the form of Eq. (75). Since we have one half monolayer of free atoms on each interface plane to begin with, a question to ask at this point is perhaps “why is the interface dipole simulated as that between a full monolayer of metal-semiconductor pairs (Eq. (85)), rather than one-half of a monolayer (Fig. 27(c))?” The answer has to do with the assumption of “point charges” for atoms in a molecule, which is a basis for all the “equalization” theories.^{195,198,201,206} The spirit of the EECP,

as most clearly suggested by the polar interface example and the forms of Eqs. (84) and (85), seems to be the additivity of the excess charge of an atom from its individual interactions with its neighbors. For example, of the $Q_{As}^{(0)}$ excess electron on each As atom in a bulk GaAs lattice, one half ($Q_{As}^{(0)}/2$) is from its interaction with (two) Ga atoms on its right and one half is from its neighbors on the left. This is the reason the As atoms on the interface start with $Q_{As}^{(0)}/2$ excess electron and the entire monolayer of As atoms now interact with the metal in step two. To make the chemical picture a little more transparent, one can imagine dissecting each atom into two halves. The reason for the $Q_{As}^{(0)}/2$ excess electron in the starting configuration is then because only the right halves of the As atoms are included in the model solid. The left halves of one full monolayer of As atoms are actually the one-half monolayer of neutral atoms added to the interface in step #1, and they naturally still interact as a full monolayer with the metal on their left. In the spirit of chemistry, one would expect the two halves of the As atoms at the actual interface to be uneven. However, when the spatial extent of each atom is condensed into a point charge in the EECP analysis, this directional/dipolar aspect of each atom is lost, which is a price paid for the point-charge simplification. A possible remedy seems to be the use of model solids that terminate on the half-atoms, e.g., constructed from Ga-centered Wigner-Seitz cells for GaAs, and constructed from atom-centered (or hollow-centered) WS cells that terminate on half-atoms for the metal, as shown in Fig. 35(a). However, this would leave the subsequent analyses of charge transfer and interface dipole from a point-charge based EECP theory different from its usual practices. To still make use of the EECP method, one first “caps” the model solids on all surfaces with “halves” of the charge distribution of neutral atoms, as shown in Fig. 35(b). The capping restores full atoms throughout the entire model solid, although the average electrostatic potential inside the WSC-based model solid is rigidly shifted by the added surface dipole layer. The EECP analysis can now be applied to the two monolayers of atoms as before, with the chemical potential for the interface atoms

pre-adjusted in the fashion of Eq. (83) if they already have a net charge, e.g., for compound semiconductors and metallic compounds.

The more straightforward and natural application of the EECP theory involves the use of model solids based on atoms, e.g., proximity-cells or Bader atoms as in Fig. 27, which has the drawback of not handling well the possible dipole moment within the interface “atoms.” The more geometrical application of the EECP, through capping of half-atom terminated model solids, has the drawback of having discontinuity in the density of electrons. Offhand, it is hard to judge which method should work better for the prediction of SBH for MS interfaces. The author’s hunch is that the geometrical approach might be preferred because the absence of dipole moment in the atoms, i.e., the point charge approximation, seems a much more serious deficiency than a discontinuity in electronic density. The latter may be handled in a fashion similar to a successful empirical theory on alloys.^{182,215} Finally, we note that the effect of screening in these analyses has been handled by the use of several dielectric constants, of which the ϵ_{int} parameter is the least understood and yet the most important for the estimation of interface dipoles.²⁰⁶ *Ab initio* calculations suggested that the effective dielectric constant varied rapidly with position near the interface.¹⁰² The uncertainty in the appropriate choice of this parameter should be noted for EECP type analyses. On the other hand, with a little more computation, we may have a cut-and-stitch technique that avoids the uncertainty with interface screening altogether. Starting with the two uncapped model solids shown in Fig. 35(a), one notices that the gap between the two model solids should really be filled by an electron density distribution representative of the chemical interaction between a plane of metal atoms and a plane of semiconductor atoms in a “solid environment.” Such a distribution of electron density can be calculated by putting the two elements, metal and the interface semiconductor elements, in a binary crystal with an appropriate lattice structure to mimic the interface geometry. A bulk calculation involving such a small (two-atom) unit cell

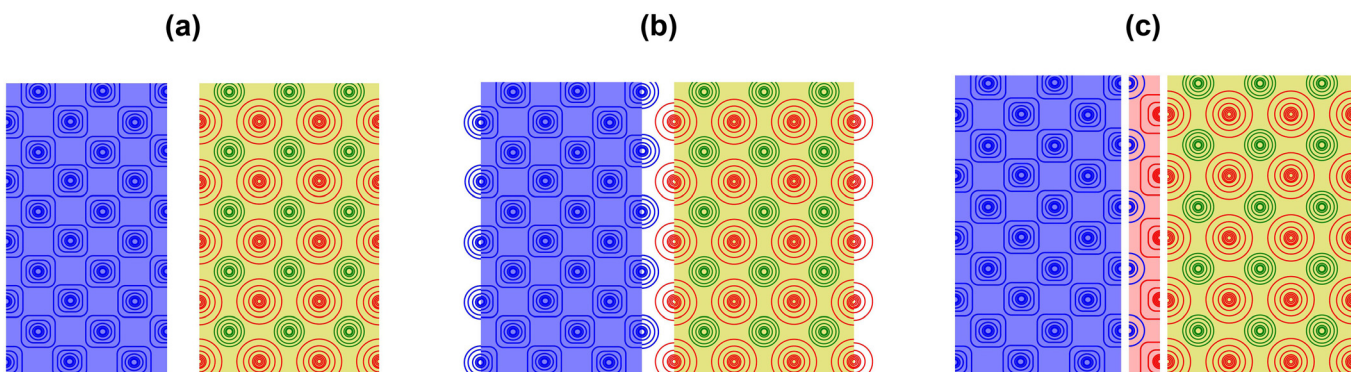


FIG. 35. Alternative method to analyze or estimate the SBH of polar MS interfaces with metal-anion bonds. (a) Model solids built from Wigner-Seitz cells centered about the metal atom and the cation, respectively, are placed close to each other to represent the metal and the semiconductor. The boundaries of the model solids, here drawn as flat for clarity, expose atom halves, but in general may contain facets and are not necessarily flat. (b) The model solids can be capped with a monolayer of halves of neutral atoms. The difference in the empty potentials of the two solids in (b) is the dipole due to the two layers of half atoms. The electrochemical potentials of the half atoms in (b) can be equalized, using Eq. (84), the result of which can be sketched as (c). A more direct “cut-and-stitch” method is to cut a sliver of charge density from a bulk calculation of the metal-anion binary compound and stitch it at the interface to form a configuration also represented by (c).

should be rather routine.¹⁶³ Even though such a binary compound may not always exist in nature, the charge distribution of this crystal captures the entire chemistry between the two elements, including the effect of full screening and the roles played by the “bond” and “overlap” integrals that are omitted in the point-charge approach. The dipole across such a layer from the bulk calculation can be “cut-and-stitched” between the two uncapped model solids to estimate the SBH, as shown in Fig. 35(c), although this entire scheme already approaches in complexity to a full supercell calculation of the MS interface.

E. Non-uniform MS interfaces and defects

A single-crystal epitaxial MS interface is only possible between metal and semiconductor crystals with nearly perfect match in their 2D lattice dimensions. Even with good lattice matching conditions, it requires special equipment, tight process control, and technological know-how to fabricate epitaxial MS interfaces in reality. Ordinary Schottky barriers are fabricated by depositing a layer of metal on a semiconductor crystal substrate without special considerations for lattice matching, and typically under less-than-ideal vacuum and surface cleaning conditions. The overall crystalline quality of the metallic layer, including contamination, grain size, defect density, stoichiometry, partial epitaxy, and axial orientation, is expected to be sensitively dependent on the conditions of deposition and any post-deposition processes the MS contacts receive. Furthermore, surface treatments prior to metal deposition, such as sputtering, plasma etching, ion implantation, etc., or an energetic deposition process itself, such as (bias-) sputtering, could have left considerable damage and disorder in the semiconductor and the MS interface region. Therefore, the atomic structure at ordinary MS interfaces is usually very different from that at homogeneous (and abrupt) interfaces assumed in earlier discussions. To begin a discussion on how structural inhomogeneity may affect the nominal SBH at the interface or the transport phenomenon across the MS interface, we first loosely distinguish several types of “structures” at MS interfaces which may require different types of analysis. As always, the actual behavior of the MS interface is very specific to the details of the particular structure and disorder, and does not have one-size-fit-all type of explanations. Our discussions here serve merely as an examination of possible strategies to delve further into these issues. Typically, the more is known about the specifics of an interface, the clearer the choice is on how to analyze its characteristics.

(a) *There is an identifiable compound phase(s) at the interface, with a structure/composition neither that of the metal nor that of the semiconductor.* This phase could be a uniform layer separating the metal and the semiconductor, such as a thin insulating layer or organic molecular layer deliberately inserted at the interface, or it could be in the form of isolated intermetallic precipitates or incomplete layer. Discretion should be exercised to decide whether such a phase is better considered as a separate material, i.e., a

“third phase,” forming interfaces with both the metal and the semiconductor, or is it better considered as part of the ISR structure. If the size of such a material is substantial, e.g., $>1\text{ nm}$, then it is more reasonable to be treated as a separate material. The simplest approach to analyze such a “stacked interface” would be to consider separately the effects of the two interfaces and then combine them. If the thick phase is metallic, such as metal silicides, germanides, etc., often formed between metals and Si or Ge, it will be the SBH of these metallic compounds that controls electronic transport. If this interface phase turns out to be a thin insulator layer, the transport across such a junction would be dominated by tunneling, which is however a subject already well studied. In the event that such a third-phase layer is incomplete, e.g., a self-assembled monolayer of molecules with incomplete coverage, the nonuniformity in the interface electronic structure can be handled classically by placing sided-by-side patches of different stacks found at the interface and considering the combined effect this has on the junction transport properties. If the thickness of the third phase at the interface is small, $<1\text{ nm}$, such that the ISR for the interphase-metal interface overlaps with the ISR for the interphase-semiconductor interface, the entire third phase is better considered as part of the structure of the ISR for the MS interface.^{216,217} The quantum mechanical approach to the electronic states at such interfaces is not any different than that expressed in Eq. (45), although the potentials in the ISR now also reflect the presence of the thin interphase material.

(b) *There are extended defects or point defects in the semiconductor near the MS interface.* Note that these defects are not inside the ISR, and therefore can retain some of their identifiable characteristics in the bulk semiconductor. (The energy level for a defect in bulk semiconductor is no longer meaningful if the defect is moved inside the ISR. Any structural or chemical irregularities inside the ISR are just part of the (inhomogeneous) atomic structure of the ISR, for which the formation of electronic states depends not only on the immediate structure of the defect but on the structure of its surroundings in the ISR.) Defects near the MS interface and how they may influence the SBH have been a subject extensively studied experimentally and theoretically. In particular, prior investigations have focused on the Fermi-level pinning phenomenon and the possible connection between the apparent pinning level of the SBH and the energy level of structural defects.^{18,218–221} There have been widespread opinions, largely on the basis of analysis model shown in Fig. 5, that when a high density of deep levels, $\sim 10^{14}\text{ cm}^{-2}\text{ eV}^{-1}$, is present near the MS interface, the Fermi level will be pinned close to the characteristic energy of the defects. For deep levels, the density of gap states is assumed to be strongly peaked at a characteristic energy leading to a “flattened” region in the SBH vs. work function plot.¹³ As the discussion of the quantum formation of interface states suggests, analysis models and band diagrams like those shown in Fig. 5 have little connection with reality. With or without defects in the semiconductor, bonds are formed between the metal and the semiconductor inside the ISR that leads to interface dipole. The contribution of additional structural defects to

the band diagram at the MS interface can be included semi-classically. Deep levels are localized and can affect the transport of carriers in their surroundings. However, they cannot have long range effects on the static band bending unless they are charged. Even if charged, point defects such as dopants and deep levels do not yet have a known mechanism by which to change the interface SBH, unless they are specifically modeled to generate the interface dipole as in Fig. 5. The reason for this is that the metal has traditionally been regarded as a conductor that can perfectly screen out external electric fields. The most vivid demonstration of this point of view is in the way the image-force effect is modeled classically for carriers near the MS interface. When a carrier in the semiconductor of charge q is at a distance (x, y, z) from a planar MS interface assumed to be at $z=0$, an image charge with a charge $-q/\epsilon_s$ is assumed to be present at position $(x, y, -z)$, leading to a Coulomb energy for the carrier

$$E_{\text{Coulomb}} = \frac{-q^2}{8\pi\epsilon_s z} \quad (86)$$

that can be added to the band bending. This widely accepted practice implicitly relies on the notion that the interface dipole is non-polarizable, making the interface SBH value unaffected by charges in the semiconductor.

Results from *ab initio* calculations, e.g., Figs. 11, 13, and 14, show that the formation of interface bonds, which is not an effect limited to states near the Fermi level, penetrates a distance into the metal at least as large as that into the semiconductor. There is thus little justification to the assumption that the interface dipole

across the ISR cannot dielectrically respond to external field. From the definition of the SBH (see Fig. 1), the relevant band edge position is that at the semiconductor-ISR interface. Therefore, a change in the local interface dipole in response to the electric field in the semiconductor can have an effect on the SBH. Inside the ISR, the electronic states vary from metallic, i.e., with a finite density of states near the Fermi level, on the metal side to insulating, i.e., with vanishing density of states, at the semiconductor-ISR interface. The effective dielectric constant is also expected to vary with position.¹⁰² To capture the essence of the physics without elaborate procedures, the dielectric response at MS interfaces has often been handled by assuming that the ISR has a uniform dielectric constant twice that of the semiconductor, $2\epsilon_s$.²¹⁴ With that assumption, the band diagram due to a charged defect positioned near an MS interface, with an ISR thickness of $2a$, can be modeled by solving the boundary value problem with the following spatial arrangement: the metal is assumed to occupy the space $z \leq -a$, the semiconductor ($\epsilon = \epsilon_s$) the space $z \geq +a$, and ISR ($\epsilon_{\text{ISR}} = 2\epsilon_s$) the region $-a \leq z \leq +a$. This is a problem that has already been worked out in detail,²²² with solutions expressible as integrals of Bessel functions. A schematic of the band bending around a positive point charge (+e) in a lightly doped ($N_D = 1 \times 10^{17} \text{ cm}^{-3}$, $\epsilon_s = 10$) semiconductor, positioned at $10a_0$ (Bohr radius = 0.053 nm) away from an MS interface ($\Phi_{B,n}^{(0)} = 1.0 \text{ eV}$) is shown in Fig. 36(a). It is seen that the local SBH is reduced due to the presence of the positive charge. The maximum reduction in the SBH (at the center of the valley in Fig. 36(a)) is given by²²²

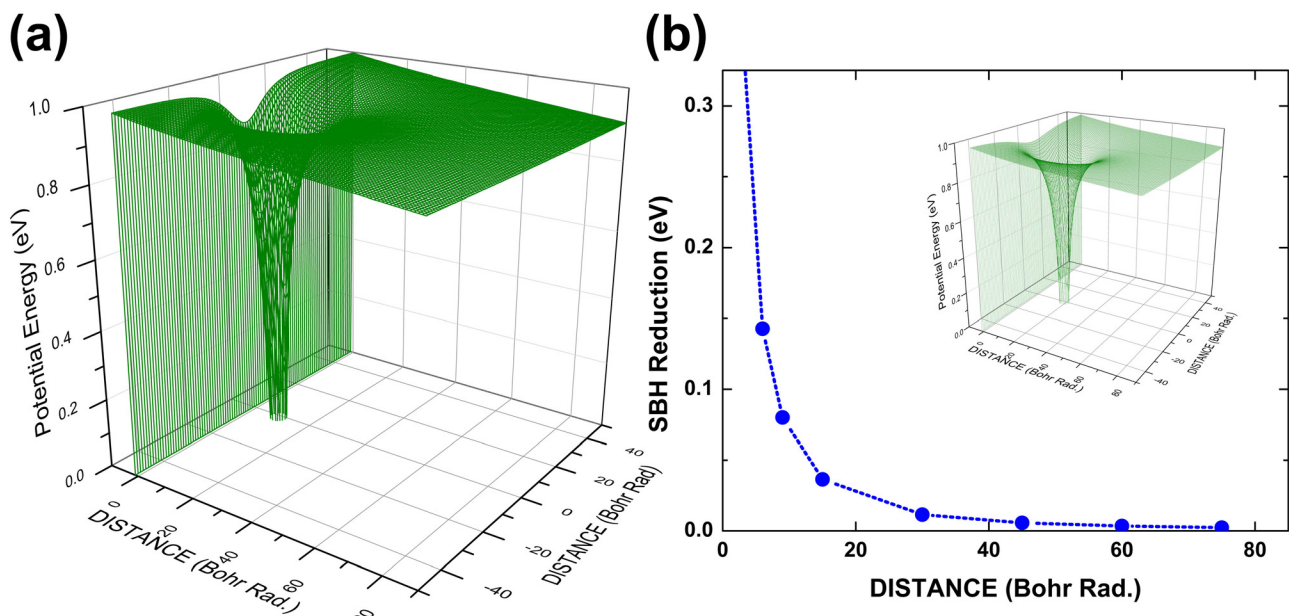


FIG. 36. (a) The potential energy profile for a positive point charge (+e) in a lightly doped ($N_D = 1 \times 10^{17} \text{ cm}^{-3}$, $\epsilon_s = 10$) semiconductor, positioned at $10a_0$ away from the MS interface ($\Phi_{B,n}^{(0)} = 1.0 \text{ eV}$). (b) The maximum reduction in the SBH as a function of distance of the point charge from the MS interface. Inset: same as (a), with the point charge at $20a_0$ from the MS interface.

$$\Delta\Phi_{pt-ch}(z') = \frac{Q}{\pi\epsilon_0\epsilon_s a} \int_0^\infty d\kappa \frac{\sinh(2\kappa)}{3 + e^{-4\kappa}} e^{-(\kappa + \kappa'/a)}, \quad (87)$$

which depends on how far ($z = z'$) the point charge (Q) is away from the MS interface, as shown in Fig. 36(b). The inset of Fig. 36(b) shows that the SBH reduction due to a point charge placed farther ($20a_0$) from the MS interface is smaller than that shown in Fig. 36(a). It should be pointed out that the SBH reduction mechanism described by Eq. (87) is not the image-force lowering mechanism, although there are obvious similarities. For immobile charges, such as impurities and deep levels, both the electronic and the ionic contributions to the dielectric response are included. The band gap narrowing due to image force is a quantum mechanical effect^{223,224} that, when cast in classical models, should involve only the dielectric action due to electrons.

The modification of the local band bending from charges positioned near the MS interface obviously has great implications for a wide range of SBH-related phenomena, the most obvious of which concerns the electronic transport at heavily doped junctions. Because this SBH lowering mechanism only comes to light if the polarizability of the interface dipole is specifically considered, this issue has not been properly addressed previously. It is well known that the I-V SBH measured for a particular MS interface typically decreases with increasing doping level and that low-resistance ohmic contact usually forms when the semiconductor is degenerately doped. Neglecting for the time being the possible change in the interface dipole due to the segregation of dopant impurities inside the ISR, the reduction in the apparent SBH responsible for electronic transport has traditionally been attributed to tunneling. Since the electric field at the MS interface increases with the doping level, tunneling efficiency also increases, thus accounting for the reduction in the effective SBH through either the thermionic field emission (TFE) or the direct-tunneling, field emission (FE), mechanism.^{140,225} In these models for electronic transport at MS junctions, the true SBH (band alignment) at the MS interface has been assumed to be uniform and independent of the doping level. Equations derived from the TFE and FE mechanisms have frequently been used to analyze experimental current-voltage behaviors at doped MS interfaces. While the TFE mechanism could capture the main features observed in some transport experiments, it was apparent that some observed junction characteristics were at odds with the TFE mechanism, e.g., when the doping level is low.²²⁶ The main shortcoming of the TFE model is the neglect of effects on carrier transport through the space charge region due to SBH inhomogeneity, which acts independently of, and in addition to, the transport of carriers across the immediate MS interface, i.e., the ISR. In other words, when the SBH is inhomogeneous, the TFE mechanism is only operative for parts of the MS interface that have higher-than-average local SBH. But these are exactly the portions of the interface whose contributions to the total junction current are insignificant! The simulation presented in Fig. 36 shows that when a low density of isolated, fixed charges is present near the MS interface, as is the case for a lightly doped semiconductor,

the SBH tends to be affected only locally through the discrete nature of the dopants. The effect of small “indentations” in the SBH profile on the overall carrier transport is expected to be small. If, on the other hand, a high density of charges due to exposed dopant ions is present, the discreteness of the charges becomes of minor importance and the SBH lowering effect can be modeled in the same classical one-dimensional model used for band bending analysis. In this exercise, the dielectric response from the interface dipole may be further simplified by assuming the ISR to have the same dielectric constant as the semiconductor, but with the thickness reduced in half, $2a \rightarrow a$. This leads to an approximate analytical expression for a uniform SBH reduction

$$\Delta\Phi_{doping} \approx -a \sqrt{\frac{2e^3 N_D V_{bb}}{\epsilon_s}}, \quad (88)$$

where V_{bb} is the band-bending and N_D is the doping level. Note that because of the dependence of the SBH lowering on V_{bb} , this effect will contribute to the “ideality factor” of the junction I-V characteristics.

With how the interface SBH depends on charges present near the MS interface understood, it is time to return to the earlier question of “how effective can deep levels pin the Fermi level?” It is worthwhile to reiterate that deep levels considered here refer to defects that are outside of the ISR and can maintain some bulk characteristics, e.g., deep energy levels! Only defects with a net charge can have a significant effect on the local band bending, and how a charged deep level influences the SBH is not any different from that of an exposed shallow dopant. Therefore, the scenario presented in Fig. 36 applies to charged deep levels as well. Unlike shallow dopants, which are essentially 100% charged inside the space charge region, the population of deep levels is controlled by its energy in relationship to the Fermi level (technically, the electrochemically potential). A slight complication here is that when a high density of point defects is present near the MS interface, the overlap of electronic wave function could lead to a broadening of the defect energy level. Ignoring this broadening, the average n-type SBH in the presence of (a sheet of donor-type) deep levels, $\Phi_{B,n}^{w/DL}$, can be expressed approximately as a function of the SBH in the absence of deep levels, $\Phi_{B,n}^{wo/DL}$

$$\Phi_{B,n}^{w/DL} = \Phi_{B,n}^{wo/DL} - \frac{e^2 a \sigma_{DL} (1 - f_{DL})}{\epsilon_0 \epsilon_s}, \quad (89)$$

where σ_{DL} is the areal density of the deep levels and f_{DL} is the population of the deep levels, given by the solution to

$$f_{DL} = \frac{1}{1 + \exp \frac{\Phi_{B,n}^{wo/DL} - e^2 z_{DL} \sigma_{DL} (1 - f_{DL}) / (\epsilon_0 \epsilon_s) - E_{DL}^{donor}}{k_B T}}. \quad (90)$$

In Eq. (90), E_{DL}^{donor} is the energy of the deep level below the CBM of the semiconductor and z_{DL} is the distance the deep levels are from the center of the ISR. Being a “donor-type”

defect, this deep level is assumed to be uncharged when occupied and have $a + e$ net charge when unoccupied. As shown in Fig. 37, the presence of deep levels has almost no effect on the magnitude of the SBH, at an areal density of $\sigma_{DL} < 3 \times 10^{13} \text{ cm}^{-2}$. In order to show a noticeable effect, calculations had to assume unreasonably high densities, $\geq 1 \times 10^{14} \text{ cm}^{-2}$, of deep levels, and even then, deep levels are not able to strongly pin the FL to their characteristic energy level(s) as envisioned in previous work,^{13,18} employing the non-physical fixed separation model shown in Fig. 5. The reason, as already mentioned, is that the dipole arising from the charge on deep levels is always in competition with, and is often overwhelmed by, the dipole due to chemical bonds at the interface.

(c) *Interface atomic structure is inhomogeneous.* As the local atomic structure cannot remain constant for a non-epitaxial interface, the local SBH is expected to vary laterally. There are additional mechanisms, such as that demonstrated in Fig. 37, which could lead to SBH inhomogeneity on a fine length scale. From the perspective of current transport across the MS interface, the length scale with which the local SBH varies/fluctuates is an important factor that helps determine whether the SBH inhomogeneity is experimentally observable. For illustration purposes, we can assume that the local SBH fluctuates with an amplitude of $(\Delta\Phi)_{fluc}$ and a spatial periodicity of λ_{fluc} . To take advantage of the local minima in such a distribution of SBH, the carriers need to be confined to a spatial width of $<\sim \lambda_{fluc}/4$. In the semi-classical theory of conduction, spatial confinement of an electron (or hole) is provided by the construction of wave packets from Bloch electrons in a small region of the Brillouin zone about a specific \vec{k} .¹⁶¹ From the uncertainty principle, the region in the reciprocal space needs to be wider than

$$\Delta k_{||} \geq \frac{\hbar}{2\Delta x} = \frac{2\hbar}{\lambda_{fluc}}, \quad (91)$$

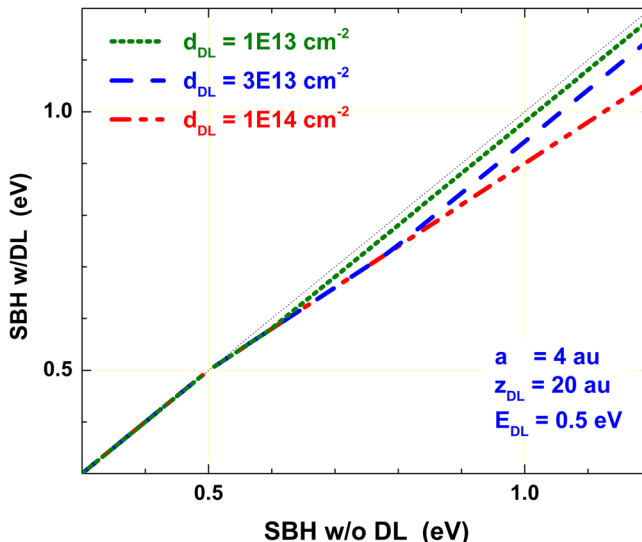


FIG. 37. The effect of deep-levels near the MS interface on the magnitude of the SBH. A density of deep levels, with characteristic energy 0.5 eV below the CBM, is placed at 20 a.u. ($\sim 1.06 \text{ nm}$) from the interface. The dielectric response of the interface dipole is calculated using an ISR width (2a) of $\sim 0.4 \text{ nm}$.

to create a wave packet narrow enough to fit in one of the “valleys” in the SBH profile. Associated with a finite range in \vec{k} -space is a spread in energy, from an assumed band extreme, of

$$\Delta E_{||} = \frac{\hbar^2 (\Delta k_{||})^2}{2m_{||}} = \frac{2\hbar^4}{m_{||} \lambda_{fluc}^2}, \quad (92)$$

where $m_{||}$ is the effective mass of the band along the direction of SBH fluctuations. Therefore, unless the cost in energy to spatially confine the electron is less than the energy gained in the lower SBH, $(\Delta\Phi)_{fluc} > \Delta E_{||}$, it is not worthwhile to take advantage of the troughs in the fluctuating SBH profile. In other words,

$$(\Delta\Phi)_{fluc} < \frac{2\hbar^4}{m_{||} \lambda_{fluc}^2} \quad (93)$$

defines the condition that the SBH is apparently uniform and the fluctuations in SBH are invisible to experimental detection even at very low temperatures. At finite temperatures, there is an additional requirement that the variations in the SBH need to exceed $k_B T$ to have a noticeable effect on the transport phenomenon across the MS interface. As a point of reference, SBH fluctuations on a length scale smaller than $\lambda_{fluc} \sim 2.4 \text{ nm}$ carry an energetic uncertainty greater than the thermal energy at room temperature ($\sim 0.025 \text{ eV}$), for a material with free-electron like ($m_{||} = m$) energy bands. Note, again, that in addition to transport phenomenon through the MS interface governed by quantum mechanics, there is the classical band-bending in the space charge region¹³² that can significantly mask the presence of SBH inhomogeneity in transport experiments.

F. Nanostructures and nano-scale contacts

Nanostructures, such as nanotubes, graphene, nanorods, nanowires, etc., possess novel properties and have already found applications in a wide range of devices. There are immense potentials in nano-materials for possible high-performance and high-functionality future devices. For many applications, it is necessary to make electrical contact to the nanostructures, making the management of the junction characteristics of nano-contacts an important issue.^{227–229} Electronic transport at metallic contacts to carbon nanotubes was recently reviewed and will not be treated in detail here.²³⁰ Instead, we point out some general and surprising results regarding electric dipoles at metal-nanostructure interfaces, purely from the standpoint of electrostatics. When a metal-nanostructure contact is made, bonds naturally form between metal atoms and atoms of the nanostructure, which lead to the formation of local dipoles. However, as pointed out,^{231,232} the potential distribution at contacts to nanotubes and other nanostructures is very different from that encountered at planar MS interfaces. The difference in the “band bending” observed for nanostructure can be attributed to the vast difference in geometry between the planar interface and the nanoscaled interface. Specifically, a uniform density of polarized bonds at planar MS interface generates a rigid

potential shift across the interface, which is more or less uniform laterally.²³³ The approximate translational symmetry within the plane of the interface reduces the analysis of potential distribution at planar MS interfaces to essentially one-dimensional models. If the lateral dimension of a planar contact is reduced to nanoscopic lengths, the potential shift across the MS interface can be significantly reduced from that for the large contacts, even with exactly the same dipole moment per unit area at the interface. Shown in Fig. 38 is the potential shift at the interface (0.5 nm from the assumed interface plane) of circular contacts with radius of a , plotted against r/a , where r is the lateral distance from the center of the disk. The potential shift has been normalized with respect to the magnitude of the shift at semi-infinite planar contact with the same dipole moment per area. The size effect on the potential around a dipole sheet in the shape of a disc, seen in Fig. 38, is relevant for certain nanocontact geometries, such as end-contacts to nanorod/nanowire semiconductors and metallic point-contacts to planar semiconductors. Not only is the potential near the interface of a small disc reduced from the value for large contacts it also falls off more rapidly from the interface than for larger contacts, as shown in Fig. 39. The potential distribution relevant for an end-contact to a nanotube can be modeled with a dipole layer in the shape of a concentric ring. Calculations were conducted¹⁶³ for rings with an outer-radius of a and an inner-radius of $0.9a$. The potential distribution directly on top of the “band” of dipoles, at $0.95a$ from the center of the ring, is also shown in Fig. 39. The ineffectiveness of a ring of dipole layer in inducing a sustained potential shift in the material (nanotubes) on its side, as clearly seen in Fig. 39, is likely responsible for the kind of transport characteristics observed for nanotubes. If a sheet or multiple sheets of graphene were contacted on its side with metal, a line or strip of dipoles is formed due to polarized bonds with metal. For this geometry, the potential at 0.5 nm over the plane of a strip of dipole layer, calculated for different strip thicknesses and shown in Fig. 40,

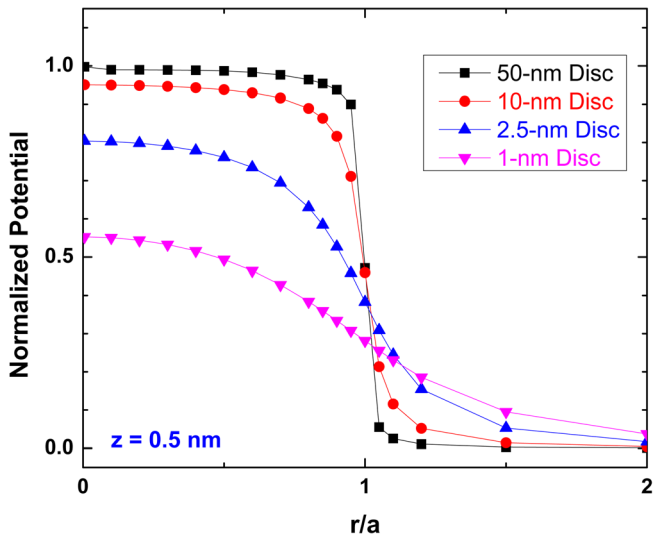


FIG. 38. Potential at the interface of circular contacts with radius of a , plotted against r/a , where r is the lateral distance from the center of the contact. The potential shift has been normalized with respect to the magnitude of the shift at semi-infinite planar contact with the same dipole moment per area.

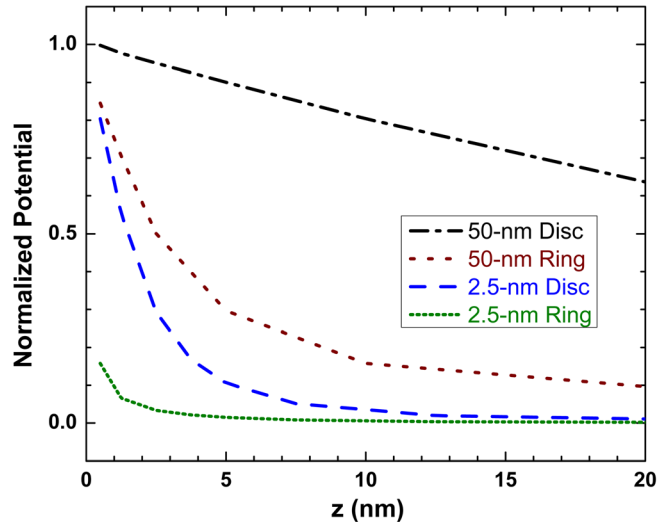


FIG. 39. Potential (normalized) fall-off from the interface of nanoscale contacts in the shape of circular discs and circular rings. For the rings, an outer-radius of a and an inner-radius of $0.9a$ were assumed and the potential plotted is at distance of $0.95a$ from the center of the ring. For the circular discs, the potential along the center of the disc is plotted.

approximately describes the empty potential for end-contacted graphene. Again, the interface “band-bending” for few layers of graphene is much reduced and it also falls off rapidly away from the interface. The basic results here, concerning the distribution of potential around localized or spatially confined dipoles, are fundamentally different from the kind of band-banding usually observed at planar MS interfaces. One notes that because of the more “open” configurations of contacts to nanostructures, the potential in the nanostructures can be manipulated by charges in the general surrounding (e.g., remote gate), which are not on either the metal or the nanostructure. One should also note that the dielectric constant of the nanostructure could make the actual potential distribution near the nanostructure numerically different from those calculated for the free space in Figs. 38–40, although the overall conclusions about how size

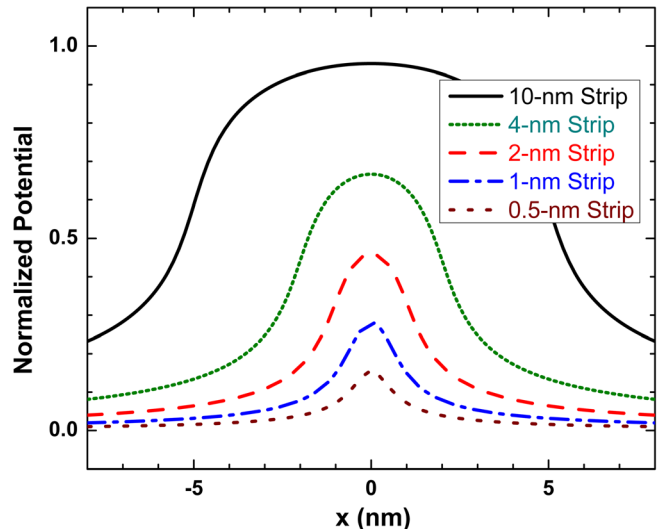


FIG. 40. Normalized potential at the interface of nanoscaled contacts in the shape of semiinfinite strips with different widths.

affects the band bending remains valid. To describe the electronic transport at nano-contacts, it is generally inappropriate to use equations from the thermionic emission theory, which was derived for planar interface. When a nanotube or a graphene sheet is contacted on its end/side by a broad (planar) metal, an electronic state on the nanostructure is necessarily coupled to a broad range of states in the metal because of confinement effect described above. As a result, the coupling between any specific bulk metal state and the nanostructure is expected to be very weak. Such a problem in mesoscopic transport¹⁷⁵ is often modeled with a significant “contact resistance” for the metal and ballistic transport in the nanostructure.²³⁴

IV. MODIFICATION OF SBH

While looking for a particular SBH on a semiconductor, one first has the option of finding a metal/compound that produces the desired SBH. Sometimes, no metals exist with high or low enough work function, or other constraints such as temperature, process, and cost limit the choice of the metal, one is then faced with the task of having to modify or tune the effective SBH without changing the metal used. There were isolated cases where the SBH was discovered to be modified by special processing conditions with no obvious explanation. Most notably, deposition of metal at cryogenic temperatures on compound semiconductors frequently led to an increase in the n-type SBH, when compared with junctions formed at room temperature.^{235–241} Spectacularly, deposition of metal at 77 K was shown to lead to a strong dependence of the SBH with the metal work function at ZnS_xSe_{1-x} interfaces.²³⁸ There was also the discovery of significant modifications in the SBH when electrochemical methods were used to deposit the metal.^{242–245} These discoveries were of great scientific and technological importance. Because the SBH was observed to be modified, it can be concluded from Eq. (25) that the special treatment(s) must have changed the interface dipole and, therefore, the interface structure. How the change in the interface structure was accomplished in these cases was, by and large, unknown. Comprehensibly and systematically, the SBH should be controllable by modifying the interface structure in such a way that will lead to the desired increase or decrease in the interface dipole. However, knowing the need to “change the interface structure” doesn’t narrow down the subject much because the “interface structure” can refer to something as simple as the arrangement of atomic positions on a single crystallographic plane, or the “interface” can actually be quite extended and involve multiple layers of material(s). Experimental efforts to modify the SBH, based on strategies to comprehensively modify the interface structure, can be roughly distinguished into three different groups according to the chemical and compositional profile created at the interface. These strategies include the insertions of (1) organic molecular dipoles, (2) insulating material, and (3) monolayer(s) of inorganic atoms, impurities, or defects at the MS interface. Note however that the distinction between these groups can sometimes be fuzzy. In choosing a strategy for some applications such as the ohmic contact, the current-carrying capability of the MS junction is the only figure of merit. For others,

such as in fabricating gates for field-effect devices or rectifying diodes, both the magnitude of the energy band alignment condition and the uniformity of the interface are important. In addition, the capacitance of the MS interface may be important for high speed applications. Therefore, the constraints and strategies for various applications can be different and should be taken into consideration.

A. SBH modification with molecular dipoles

In searching for strategies that may alter the electrical dipole at an MS interface, the most obvious choice is to insert a material that is itself dipolar. Therefore, the interest in organic molecules is quite natural,²⁴⁶ as the large number of choices in the head/tail groups of the molecules and the wide range in the dipole moment of the molecule seem to offer the ability to tune the surface dipole of a self-assembled monolayer (SAM) almost continuously.²⁴⁷ The use of Langmuir-Blodgett films also offers the option to add a uniform dipole layer to the semiconductor surface.^{248,249} Ideally, the potential drop generated across a uniform layer of dipolar molecules is derivable from the Helmholtz model as²⁵⁰

$$\Delta V = \frac{4\pi}{\epsilon} n P_0 \cos(\varphi), \quad (94)$$

where P_0 is the gas phase dipole of the molecule, n is the areal density of molecules, φ is the molecular tilt angle relative to the surface normal, and ϵ is an *effective* dielectric constant of the monolayer. Studies have shown that this simple classical model, based largely on parallel-plate capacitors,²⁵¹ gives quite accurate description of results from quantum mechanical calculations and experiments.^{252–257} The necessary inclusion of a dielectric constant for the molecular layer in the above equation is due to the polarizability of the molecules. It has been shown that the effect of the depolarization of the molecular dipoles by the presence of other dipoles in the molecular layer can be accounted for by replacing in Eq. (94) the dielectric constant with

$$\epsilon = 1 + \alpha k/a^3, \quad (95)$$

where α is the molecular polarizability, a is the inter-dipole distance along one direction of the periodic array, and k is a constant that depends only on the geometry of the two-dimensional lattice.²⁵⁸ When molecules are bonded onto the surface of a (semiconductor) solid, additional electrical effect, due to the polarized bonds between the anchoring group of the molecule and the substrate, could arise.^{259,260} For such cases, calculations show that, as long as the molecular layer is uniform, the classical model remains valid with the total dipole moment of the molecule understood as the simple sum of the dipole due to the top functional group and that from the molecule-substrate interaction.²⁶¹ The reason for this simple additivity of the dipoles, as well as that for molecular assemblies possessing several “layers” of polar groups,²⁶² is the rapid exponential decay of the potential due to the dipole layer in the direction perpendicular to the layer,²³³ cutting off interactions between the dipole layers.

Surface potential shifts roughly in accordance with Eq. (94) have been experimentally observed for metal surfaces, as monitored by the work function,^{260,263,264} and for semiconductor surfaces,^{265–269} as reflected in its electron affinity or ionization potential. As shown for the GaAs(100) surface in Fig. 41,²⁶⁸ a linear relation generally exists between the observed surface potential shift and the magnitude of the gas phase molecular dipole, such that the semiconductor electron affinity can be either enhanced by negative molecular dipoles (with negative end pointing away from the substrate) or lowered by the use of positive molecular dipoles. However, depolarization effect could lead to a saturation in the range of the surface potential that can be adjusted by molecular dipoles, or even a reversal of effect at large molecular coverages.²⁷⁰

To complete the fabrication of the Schottky junction, a metal layer needs to be applied over a semiconductor surface already covered with a molecular layer. Conventional metal

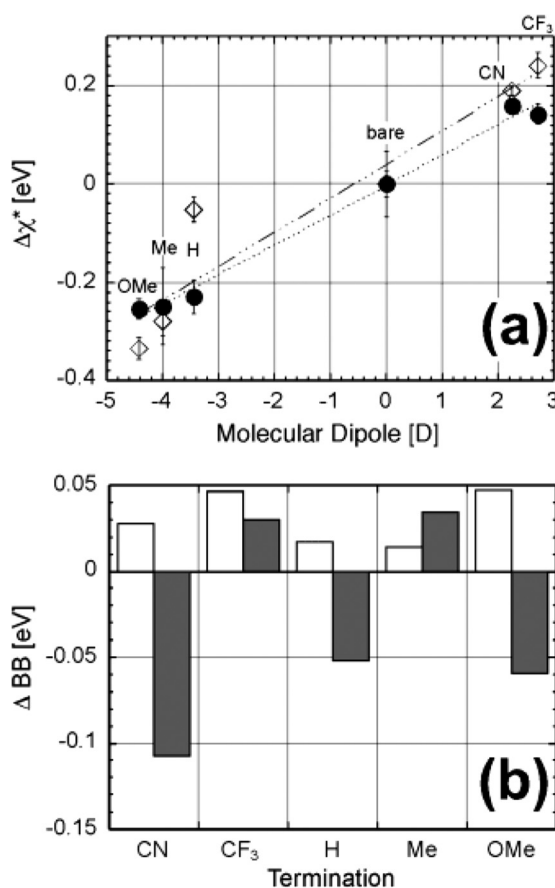


FIG. 41. (a) Molecular film-induced change in surface potential, relative to that of the bare surface, for molecularly modified n-type (closed circles) and p-type (open diamonds) GaAs(100), as measured by a Kelvin probe under illumination (yielding the electron affinity), plotted against the calculated dipole moments of the free molecules. Values are averaged over 5–7 samples with the standard deviation as error bars. (b) Change in band bending of molecularly modified n-GaAs (empty bars) and p-GaAs (filled bars). The error in the band-bending values is in the order of a few tens of millielectronvolts. For the bare surfaces, we measured electron affinities of 0.64 and 0.26 eV below the Au reference (i.e., contact potential difference (CPD) values of 4.36 and 4.74 eV, taking work function of Au to be 5.00 eV) and a lower limit of band bending of 0.23 and 0.16 eV, for n- and p-GaAs, respectively. Reprinted with permission from Vilan *et al.*, J. Phys. Chem. B **107**, 6360–6376 (2003). Copyright 2003 American Chemical Society.²⁶⁸

deposition techniques such as evaporation, sputtering, and chemical vapor deposition bring considerable energy to the surface during the deposition process and are known to damage the surface molecular layer^{271,272} and result in metal-organic interfaces with inconsistent, inhomogeneous, and leaky electrical conducting properties.^{273,274} To minimize the impact of the metallization process, “soft” techniques, such as indirect deposition,^{275–277} nano-particles deposition,^{278–280} electrochemical methods,^{281–283} “lift-off float-on (LOFO),”^{284,285} mercury droplet contacts,^{286,287} micro-contact printing,^{288–291} have been specially designed and implemented to achieve more consistent results. The effect of a molecular layer on the SBH is found to be less consistent and predictable than its effect on the surface potential of the semiconductor or the metal. Generally, systematic shifts of the SBH in the direction consistent with the polarity of the molecules have been frequently observed in experiments,²⁸⁴ even though the magnitudes of such shifts were typically found to be less than those observed for the free surface.^{247,284,292–297} Interaction of the molecules with the metal layer, structural change in the molecules, change in the molecule-semiconductor bond as a result of the metal, and other collective effects could lead to the observed reduction in dipole.^{298–300} Such an expected systematic trend in SBH is shown in Fig. 42 for Au pads deposited by the LOFO method on GaAs surfaces with various SAM.

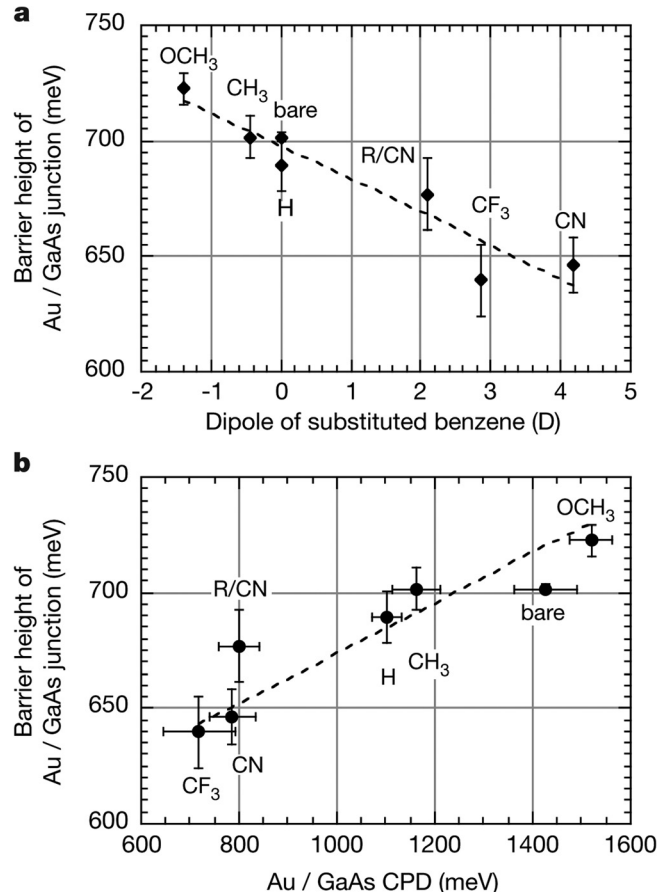


FIG. 42. Dependence of the effective barrier height at the Au/derivatized n-GaAs interface on the following parameters. (a) The dipole moment; (b) the CPD between Au and derivatized n-GaAs surfaces. Reprinted with permission from Vilan *et al.*, Nature **404**, 166. Copyright 2000 Macmillan Publishers Ltd.²⁸⁴

Occasionally, shifts in SBH in the direction opposite to that expected from the polarity of the molecular dipole have also been reported, as shown by the example for Pd “indirectly deposited” on GaAs(100) in Fig. 43.²⁹⁶ It is speculated that in this particular case, the interaction between the deposited Pd and the SAM molecules at these junctions actually led to a reversal of the molecular bond with the GaAs substrate to the metal. The sharp contrast in the behavior of two different metals with the same group of molecules highlights the important role played by energetics in deciding the configuration and the stability in the employment of SAM dipoles. Chemical stability is not only important for the method of SBH modification through molecular dipoles but for all strategies to modify the interface structure.

Detailed investigations of the electrical characteristics of Schottky junctions fabricated with an interfacial SAM layer suggested that the SBH was often inhomogeneous. Spatially resolved imaging of selected Au/n-GaAs contacts by BEEM showed that the SBH was highly non-uniform when a layer of molecules was attached to the GaAs surface through a dicarboxylic acid “anchor.” In fact, BEEM imaging in Fig. 44 revealed that the junction current nearly entirely originated from isolated small, <10 nm, patches that had a local SBH ~ 0.4 eV lower than the background.³⁰¹ Since the molecular dipole in this case, with a CH_3 functional group, was negative and was expected to increase the n-type SBH, the low-SBH patches were likely regions devoid of molecular dipoles, i.e., pinhole regions in the original molecular layer. This example illustrates a common issue for molecule layers: incomplete layer coverage. The main purpose for the use of molecular dipoles in SBH experiments has often been to reduce the effective SBH for low-resistance contacts. However, the addition of an (insulating) molecular layer at the interface reduces

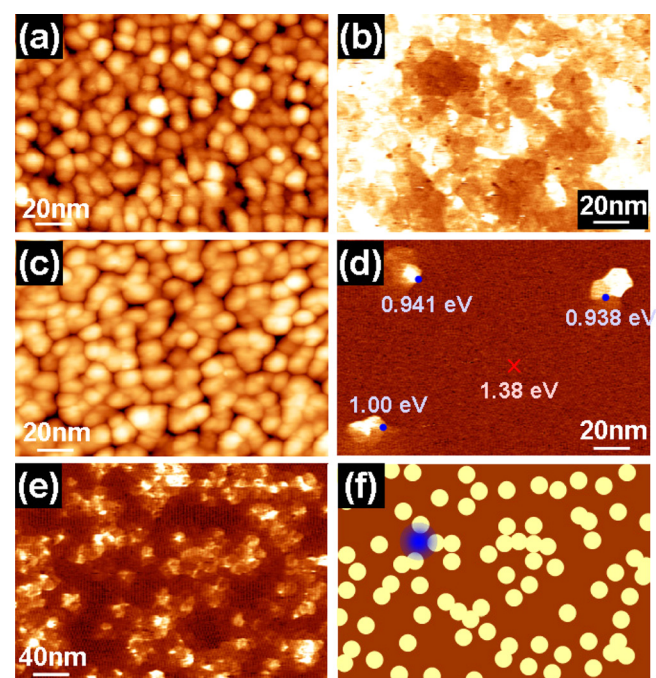


FIG. 44. (a) STM image of top Au film on bare Au/GaAs sample and (b) simultaneous BEEM image of same area, measured with $V_T = 1.2$ V. Color scales are 3.4 nm and 3 pA. (c) STM and (d) simultaneous BEEM image of Au/dC-CH₃/GaAs sample with $V_T = 1.4$ V, revealing pinholes in the dC-CH₃ film. Color scales are 3.6 nm and 1 pA. (e) BEEM image of Au/dC-OCH₃/GaAs sample with $V_T = 1.4$ V. Color scale is 1 pA. (f) Illustration of possible origin of contrast variations in (d) (see text). All images measured with $I_T = 20$ nA. Reprinted with permission from Haick *et al.*, Phys. Status Solidi A **203**, 3438 (2006). Copyright 2006 John Wiley and Sons.³⁰¹

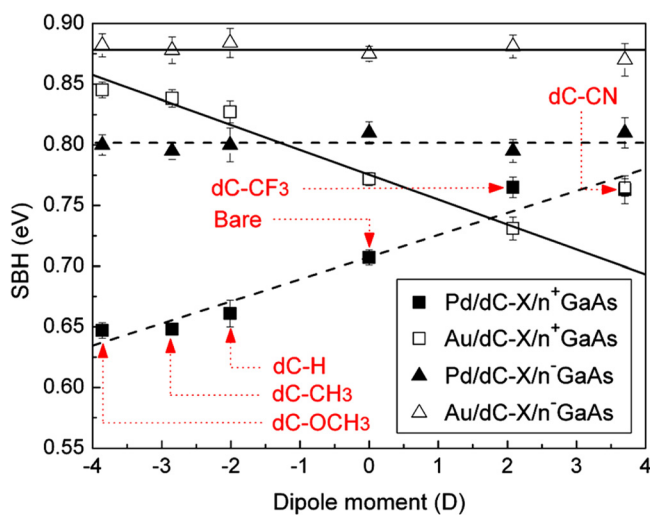


FIG. 43. Dependence of effective SBH of metal/dC-X/n⁻/GaAs or metal/dC-X/n⁺/GaAs junctions, derived from the experimental I-V curves at RT, using the thermionic emission model in the 0.1–0.4 V bias region (with a theoretical Richardson constant of $8.6 \text{ A} \cdot \text{cm}^{-2} \cdot \text{K}^{-2}$ for n-GaAs), on the molecular dipoles of dicarboxylic acid derivatives. Dashed lines (---) are fits to values for Pd-contacted junctions. Solid lines (—) are fits to values for Au-contacted junctions. All results are for junctions made by indirect evaporation of the metal contacts. Reprinted with permission from Haick *et al.*, J. Am. Chem. Soc., **128**, 6854–6869 (2006). Copyright 2006 American Chemical Society.²⁹⁶

the direct coupling between the metal and the semiconductor and may actually lead to a reduction in the current flow at the junction, even for molecular dipoles that reduce the actual band offset between the metal and the semiconductor majority band. This has to do with the tunneling efficiency, which drops exponentially with the thickness of the molecular layer. For common organic molecules, tunneling probability drops by an order of magnitude for every ~ 0.2 – 0.4 nm in molecular length. Therefore, for organic molecules to increase the nominal current carrying capability, they need to be effective in reducing the SBH by ~ 0.1 eV for every 0.3 – 0.5 nm in length, at room temperature. Depolarization and the metal-molecule interaction noted above would seem to make the choices for organic molecule that provide enhanced and uniform current transport very limited. Advantage has actually been taken of the incompleteness in the molecular coverage to avert the problem with diminished current transport over uniform molecular layers.³⁰¹ Enhanced electronic transport was observed with the use of partial molecular layers. The reason for the increased current flow was originally speculated to be due to an increase in the electric field near edges of the pinholes in the molecular layer.^{296,301} However, the potential distribution of nano-contacts, shown in Figs. 38 and 39, offers a more consistent and natural explanation of the observed adjustability of the intimate MS SBH in the pinholes, due to peripheral molecular dipoles. As shown by simulations,²³³ the effect of an absence (pinhole) in an otherwise uniform dipole layer on the potential is the simple addition/superposition of the potential

from a dipole layer patch of the same size and shape as the pinhole, but of opposite polarity. Within a pinhole of the molecular dipole layer, the intimate MS interface region is characterized by a different strength (or even polarity) in the interface dipole. Therefore, the potential for the intimate MS interface is similar to that shown in Fig. 38, after the dielectric constant of the semiconductor is included. The relevant full potential for such an analysis, i.e., 1 in these plots, is the DIFFERENCE in the interface dipoles with and without the molecular layer. For small pinholes, the difference in interface potentials is diminished, as shown in Figs. 38–40, and the SBH for the intimate junction is naturally “pulled” toward the effective SBH for the broader region with the molecular layer. Therefore, the SBH of nano-scale, intimate MS contacts embedded in a partial molecular layer can be adjusted, in either direction, by the magnitude and polarity of the molecular dipoles. SBH reduction with perforated molecular layer can therefore lead to enhanced conduction without suffering limitations from tunneling. The size of the pinholes can be optimized for maximized transport from the perspective of SBH-reduction and contact area. It should also be noted that additional constraint on the size of pinholes useful for conduction is present because of quantum confinement, e.g., Eq. (93).

B. SBH modification with thin layer of insulating material

Investigations into the changes in the SBH characteristics with the insertion of a thin layer of insulating material between the metal and the semiconductor have had a long history. In fact, the use of SAM molecular dipoles just described may be viewed as a special example of such metal-insulator-semiconductor (MIS) structures. In order to distinguish, we limit our discussions in this section to insulating interlayers that are thick enough ($\sim 2 \text{ nm}$) such that the potential distribution and the electron transport across the entire “stack” of the metal-interlayer-semiconductor can be treated as that of a metal-interlayer (M-I) interface and an interlayer-semiconductor (I-S) interface connected in series, without need for explicit coupling between the two interfaces. Inorganic insulating materials, such as oxides and wide-gap semiconductors,^{302–316} organic material, such as polymer or evaporated molecules,^{317–319} and semiconducting material with different band gap,^{320–323} have been employed as the insulating interlayer between metals and semiconductors and have been shown to effectively modify the “overall” SBH. Because of recent interest in Ge and its alloys, e.g., strained GeSn, for high performance semiconductor devices, much research also focused on the well-known “contact problem” with Ge. Strong pinning near the bottom of the band gap usually leads to ohmic contact for the p-type Ge without special care, but leaves n-type Ge with a sizable SBH ($>0.5 \text{ eV}$) to deal with.³²⁴ As shown in Fig. 45, the insertion of a thin GeO_x layer between Ge and common metals led to substantial increases in the n-type junction current and reductions in the p-type junction current (inset). This decrease (increase) in the n-type (p-type) SBH for Ge has also been observed for different metals and for a variety of insulating materials inserted as the interlayer, including amorphous and crystalline Ge_3N_4 ,^{326,327} Si_3N_4 ,³¹¹ AlO_x ,^{312,325} MgO ,³²⁸

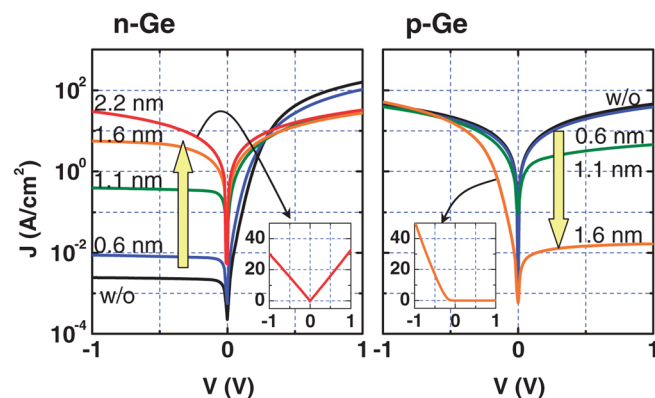


FIG. 45. J-V characteristic of $\text{Al}/\text{GeO}_x/\text{Ge}$ diodes. Reverse biased current increases on n-Ge and decreases on p-Ge as indicated by arrows. Ohmic characteristics are obtained on $\text{Al}/2.2\text{-nm-thick GeO}_x/\text{n-Ge}$. Reprinted with permission from Nishimura *et al.*, Appl. Phys. Express **1**, 051406 (2008). Copyright 2008 The Japan Society of Applied Physics.³²⁵

TaN ,³¹⁴ and organic molecules.²⁹⁷ The nominal SBH obtained from MIS stack typically showed a much stronger dependence on the metal work function than without the insulating interlayer, as shown in Fig. 46.³²⁶

Because of the similarity between the band diagram of an MIS stack used for SBH adjustment and that of the gate stack used in metal-oxide-semiconductor field-effect-transistor (MOSFET) devices, the issues and the physics for the two research fields are obviously similar, despite the differences in these applications. This is especially true of the more recent ULSI technology nodes employing high-K gate dielectrics, where metals and metallic compounds have replaced heavily doped Si as the gate conductor. To analyze the SBH for an MIS stack, we can begin by drawing a canonical “flat-band” band diagram for an (undoped) semiconductor as in Fig. 47(a), without any spurious charge. Note that the “SBH” for the M-I interface should not be assumed to follow the Schottky-Mott Rule because of interface bonds, and the band offset for the I-S interface needs not follow the Anderson Rule for the same reason.³²⁹ Depending on the ionicity of the semiconductor and the insulator, the dipoles at the M-I and I-S interfaces may actually be adjusted with termination in actual experiment, as discussed before. The canonical n-type SBH for the uncharged stack is

$$\Phi_{n,MIS}^{(\text{canon.})} = \Phi_n^{(M-I)} - \Phi_{CBM}^{(I-S)}, \quad (96)$$

where $\Phi_n^{(M-I)}$ is the n-type SBH for the M-I interface and $\Phi_{CBM}^{(I-S)}$ is the conduction band offset at the S-I interface. When the semiconductor is uniformly doped with a concentration of N_D , the zero-bias SBH is only slightly changed if the thickness of the insulating interlayer, t_H , is much smaller than the depletion width

$$\Phi_{n,MIS} = \Phi_n^{(M-I)} - \Phi_{CBM}^{(I-S)} - \frac{et_H}{\varepsilon_H} \sqrt{2e\varepsilon_S N_D V_{bb}} \\ (\text{w/o fixed charge}), \quad (97)$$

where ε_S and ε_H are the dielectric constants of the semiconductor and the interlayer, respectively. The V_{bb} in the above

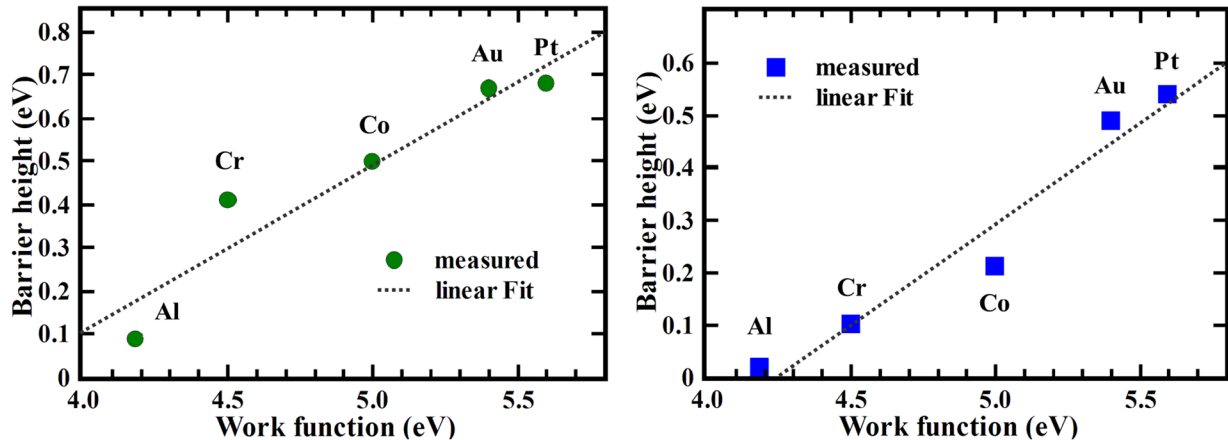


FIG. 46. Schottky barrier height of metal contacts on n-type Ge with a few monolayers of (a) amorphous Ge_3N_4 (b) crystalline Ge_3N_4 , determined by low temperature C-V measurements. Metals with increasing work function were used: Al, Cr, Co, Au, and Pt. Reprinted with permission from Lieten *et al.*, *J. Electrochem. Soc.* **158**, H358–H362 (2011). Copyright 2011 The Electrochemical Society.³²⁶

equation is the band-bending ($\approx \Phi_{n,MIS}^{(\text{canon.})} - eV_N$), as schematically shown in Fig. 47(b). Using the band diagram of Fig. 47(b), one can imagine doing a C-V experiment and convince oneself that the flat-band voltage is independent of the interlayer thickness ($= \Phi_{n,MIS}^{(\text{canon.})} - eV_N$). In the vast literature on the characterization of gate stacks, it has been customary to use the term “fixed charge” to describe immobile charge, likely due to ions, located in the insulating layer. In the presence of fixed charges, a plot of the flat-band voltage against the insulator thickness could exhibit a straight line,

in which case the slope gives the density of the fixed charge residing at the insulator-semiconductor interface, or the plot could exhibit a curve, in which case the slope extrapolated to zero thickness would give the amount of interface fixed charge and the curvature indicates the density of charge residing inside the insulator. For the present discussion involving very thin interlayers, the distinction between the two types of fixed charge is unnecessary and one can simply assume an areal density of (positive) fixed charge, en_{fxch} , to reside at the I-S interface,^{330,331} from which the following zero-bias n-type SBH for the MIS stack can be derived

$$\Phi_{n,MIS}^{(fxch)} \approx \Phi_n^{(M-I)} - \Phi_{CBM}^{(I-S)} - \frac{et_{II}}{\varepsilon_{II}} (\sqrt{2e\varepsilon_S N_D V_{bb}} + en_{fxch}) \quad (\text{with fixed charge}), \quad (98)$$

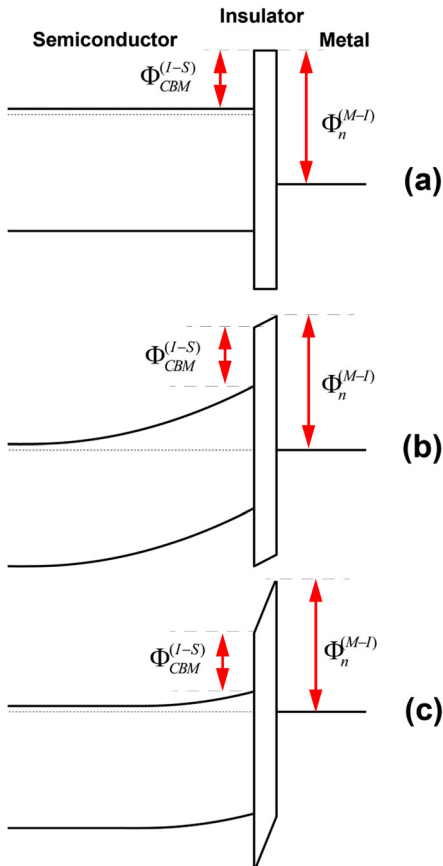


FIG. 47. Band diagram of a metal-insulator-semiconductor structure. (a) Flat band. (b) Zero-bias. (c) With fixed interface charge.

as shown in Fig. 47(c). One can now estimate the dependence of the MIS SBH on the metal work function by noticing that, on the right hand side of Eq. (98), only the quantities $\Phi_n^{(M-I)}$ and V_{bb} depend on the metal. Of the two, the metal dependence is much weaker for the term containing V_{bb} , while the dependence of the SBH for the M-I interface has been shown experimentally to follow roughly Eq. (78). We have, therefore,

$$\frac{\partial}{\partial \phi_M} \Phi_{n,MIS}^{(fxch)} \approx \frac{\partial}{\partial \phi_M} \Phi_n^{(M-I)} = \gamma_{B,M-I}, \quad (99)$$

where $\gamma_{B,M-I}$ is the expected interface behavior factor due to dipole at the M-I interface, given in Eq. (79). The much more pronounced dependence of the SBH of the MIS stack on the metal work function than the SBH at intimate MS interface is consistent with the larger band gap of the insulator than the semiconductor. The actual magnitude of the SBH of an MIS stack depends on two band-offsets, and also on the fixed-charge, as Eq. (98) reveals. One notes that the band diagrams with which to analyze (long) dipolar molecules at MS interfaces of last section are the same as those drawn in Fig. 47 for MIS interfaces. The effect of the dipole of the SAM can actually be introduced into Eq. (98) through an assumed fixed charge! Along the same vein, if the quantities $\Phi_n^{(M-I)}$ and

$\Phi_{CBM}^{(I-S)}$ in Eq. (98) were assumed indiscriminately to take on the values predicted by the Schottky-Mott and Anderson Rules rather than experimental values, the “fixed-charge” deduced from that equation would have little to do with real charge within the insulating layer. One also cautions that the analysis of charge distribution leading to Eq. (98) is valid only when the semiconductor is not in accumulation or strong inversion.

Transport phenomenon across a SBH stack consisting of an insulating layer is considerably more complex than at a single MS junction. Indiscriminate use of equations intended for intimate SBH to analyze electrical data obtained from these stacks could lead to erroneous conclusion about the semiconductor band edge position relative to the metal. In particular, the difficulty with the conduction via the bands of the insulating material could severely limit the current flow across the stack. With a thin enough insulator layer, tunneling may be a more efficient means for current transport, in which case the effective Richardson constant for the analysis of the current-voltage (I-V) characteristics across the stack needs to be significantly reduced by a factor exponentially dependent on the insulator thickness, to deduce physically meaningful results. For example, a thin layer of deposited PO_x layer was shown to increase the Au SBH on n-type InP from typically $\sim 0.4\text{ eV}$ to as high as 0.88 eV , according to I-V determination at a fixed temperature.³⁰⁵ However, activation energy study of the forward-bias current yielded a SBH of 0.41 eV , almost identical to that found without the oxide layer. Similar effects have been seen for other MIS systems.^{332–335}

The insertion of a thin layer of a (different kind of) semiconducting material between a metal and a semiconductor substrate have also been employed to change the SBH for semiconductors.^{320–323,336} The thickness of the interface semiconductor layer, sometimes referred as the interface control layer (ICL), could be as thin as one or two monolayers, in which case the entire ICL is inside the ISR and its effect is better considered quantum mechanically,¹⁰⁶ as discussed in Sec. IV C. Here, we consider semiconducting interlayers (still designated “I” for clarity) that are tens or hundreds of angstroms in thickness such that the MIS stack can be treated as a heterojunction (I-S) and a Schottky barrier (M-I) in series. The use of a narrow-gap ICL layer is a well-known and effective way to lower the overall SBH and reduce contact resistance for wide bandgap semiconductors. The reduction in the effective barrier height through such structures is accomplished largely through the breakdown of one large (Schottky) barrier height into two smaller ones. In addition, the band bending within the ICL due to exposed dopants may become important in rendering the effective barrier height.^{337–341} When the semiconductor interlayer is not in accumulation or strong inversion, the band diagrams for the entire MIS stack are the same as those depicted in Figs. 47(a)–47(c), with the understanding that the band gap for the ICL may be larger or smaller than that of the semiconductor and that the fixed charge assumed for the I-S interface is likely negligible. The effect of charged dopants in the semiconductor interlayer can be included as a density of volume fixed charge for uniformly doped interlayer and as a sheet of charge for delta-doped interlayer.^{342,343} The easiest way to consider how a heavily doped layer at the interface

can affect the SBH is to use the same material for the interlayer as for the semiconductor, as proposed decades ago.³⁴⁴ Heavy doping of the semiconductor interlayer with dopants of the opposite type (e.g., p+ on n-) increases the SBH, because of the expected “hump” shape of the band-bending near the interface,^{343–346} as shown in Fig. 48. Interface doping with the same type as the substrate (e.g., n⁺ on n⁻) is known to lower the effective SBH, which has generally been discussed in terms of increased magnitude of image-force lowering and enhanced tunneling contribution, both associated with increased electric field at the MS interface. However, as shown in Figs. 17 and 36, atomistic effect due to point charges very close to the MS interfaces may be quite significant. Concerning the distribution of dopant atoms, one should be aware of the possibility of interface segregation, especially since it has been shown that the proximity of certain dopants to some MS interfaces could significantly alter their energy level from the normal position for bulk semiconductor and dramatically increase the solid solubility limit of charged dopants or point defects at the interface.^{347–349}

C. SBH modification with atomic monolayer(s)

The dependence of the interface dipole on the atomic structure of the MS interface suggests that any method that leads to a different structure for the interface could potentially change the SBH between the same metal-semiconductor pair. Direct adjustment of the interface structure, if possible, would be much more preferred for device applications than techniques involving interface layer of organic or inorganic materials, just described, as the interface would still remain “intimate” and enjoys efficient, uniform carrier transport and high junction capacitance. Using different surface treatments and processing conditions during the synthesis of the MS

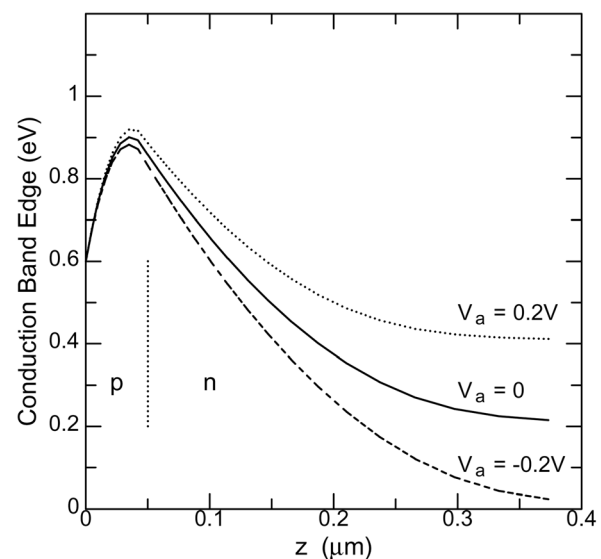


FIG. 48. The effect of surface doping layer on the Schottky-barrier height. Numerically calculated band diagram, under different bias conditions, of a nominally 0.6 eV Schottky barrier formed on $1 \times 10^{16}\text{ cm}^{-3}$ doped n-type Si, but with a thin (50 nm), $3 \times 10^{17}\text{ cm}^{-3}$ p-type doped, layer at the interface. The effective SBH is increased to $\sim 0.9\text{ eV}$ and varies slightly with the applied bias. Reprinted with permission from R. T. Tung, Mater. Sci. Eng. R: Rep. 35, 1–138 (2001). Copyright 2001 Elsevier.⁴

junction may be able to accomplish this. Procedures such as special surface cleaning techniques,^{350–354} exposure to plasma of various gases,^{332,355–359} ion implantation,^{344,360–363} ion etching,^{364–368} and vacuum annealing,³⁶⁹ have all been experimentally found to change the SBH. Changing the method^{242–245} and condition^{235–241} for the metal deposition step was also found to lead to significant modifications in the SBH. How the structure and hence the SBH were modified by these surface treatments and deposition procedures was unclear. On the other hand, bringing in some atoms that are not indigenous to an MS interface necessarily change the composition, structure, and likely the SBH of the original interface. Hydrogen, to which samples are commonly exposed in standard semiconductor processing, is known to induce a variety of effects in metals and semiconductors. It is also known to lead to changes in the SBH of some MS interfaces.^{370–374} The ability of hydrogen to passivate the electrical activity of many dopants is well documented, and this effect alone has led to changes in apparent SBH.^{375–377} Among atomic impurities that have been applied to semiconductor surfaces to change the SBH, chalcogen elements (S, Se, Te,) have had the longest history and have shown significant effects.^{144,307,378–390} However, the net effect of interfacial chalcogen varied, as both significant increases³⁰⁷ and decreases³⁸⁶ in the n-type SBH were observed. To introduce impurities such as metals,^{391–395} dopants,^{348,389,390,396–404} semiconducting,^{405,406} and insulating⁴⁰⁷ elements to the MS interface, various other methods have also been used, including deposition, ion implantation, segregation, etc. As shown in Fig. 49, the effective SBH measured by the activation-energy method of NiGe diodes on n-type Ge(100) was systematically reduced by the method of arsenic implantation and annealing. At epitaxial MS interfaces, the preferred site(s) for impurities and the thermodynamic driving force (formation energy) for interface segregation can both be theoretically computed.^{347,348} How the inclusion of impurity atoms or point defects, such as oxygen vacancies for oxide

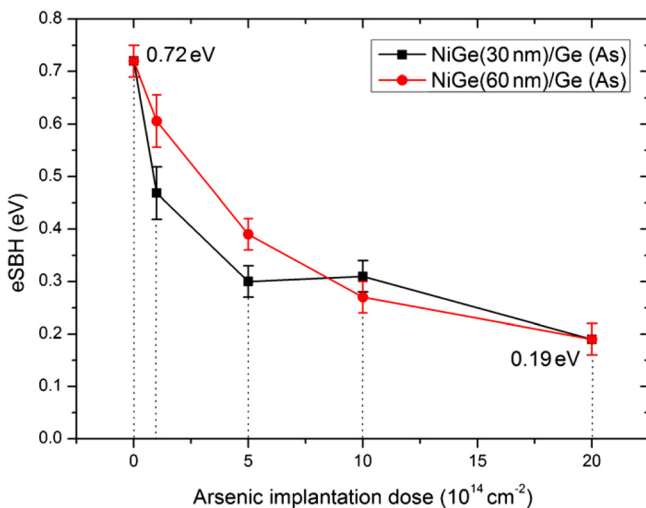


FIG. 49. Extracted effective SBHs from the Arrhenius plots as a function of the implantation dose for the NiGe(30 nm)/Ge(100) and the NiGe(60 nm)/Ge(100) contact with As segregation. Reprinted with permission from Mueller *et al.*, Mater. Sci. Eng., B **154–155**, 168–171 (2008). Copyright 2008 Elsevier.³⁹⁶

semiconductors, affects the magnitude of the local SBH can thus be predicted and understood. Note that the presence at the MS interface of an element that ordinarily is a dopant for the semiconductor directly affects the magnitude of the SBH by modifying the dipole of the ISR, which is a SBH-modification mechanism quite different from the conventional view of dopant effect exerted through modification of the electric field and band-bending in the space charge region, e.g., Fig. 48. In Fig. 50, the reduction in the formation energy of an oxygen vacancy in TiO_2 is shown as a function of the distance of the vacancy from the MS interface.³⁴⁷ As oxygen vacancies are common for oxide insulators and semiconductors, the management of oxygen concentration of oxide material is an important part of the control of its junction characteristics.^{408–410} The use of a thin layer of epitaxial elemental semiconductor for the modification of compound semiconductor SBH^{216,320,322,323,335,405,411–414} was found to already exert its full effect with only $\sim 2\text{ML}$ in ICL thickness. This demonstrated adjustability in the SBH was originally discussed in terms of the properties of separate M-I and I-S interfaces and the band bending across the ICL layer^{411,415} but was shown by *ab initio* calculations to be in quantitative agreement with the charge distribution resulted from interface bonds,^{104,106,217} i.e., the ICL should be included inside the ISR.

Impurity atoms incorporated at an MS interface should ordinarily find their way to preferred sites, in equilibrium. However, thermodynamic equilibrium is not guaranteed for MS interfaces routinely fabricated and the interface atomic structure may depend on the kinetics of interface fabrication. A good example of the non-uniqueness of interface structure is the well-known dependence of the SBH on semiconductor surface termination. The insertion of a (sub-) monolayer of foreign element to an MS interface may therefore affect the overall SBH differently, depending on the local arrangement.^{104,106} From the perspective of modifying the overall interface dipole, the most relevant property of an atomic “interlayer” is the electronegativity of its atomic species. Without specific reference to the valence number, crystal structure, or the bond lengths in the interface region, how the overall interface dipole should vary with the electronegativity of the interlayer is not always predictable from simple chemistry. For example, a layer of large-electronegative (low-electronegativity) element inserted between the metal and the semiconductor is expected to draw electrons from

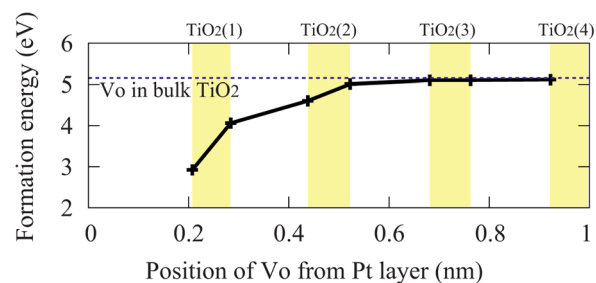


FIG. 50. Formation energies of an oxygen vacancy in TiO_2 as a function of the distance from Pt layer. The formation energy in the bulk anatase is also shown. Reprinted with permission from Tamura *et al.*, Phys. Rev. B **80**, 195302 (2009). Copyright 2009 American Physical Society.³⁴⁷

(donate electrons to) both sides, making the change in the overall dipole from such a layer unclear, although one generally expects charge transfers farther from the metal side to be less screened. When breakage in chemical bonds results in neutral “sub-systems” un-bonded to each other, the total dipole of the entire system becomes predictable as then it is dominated by charge-transfers within “sub-systems.”⁴⁰⁰ Based on this notion, a systematic attempt to fabricate “partisan interlayer,” which is a foreign atomic layer at the MS interface more strongly bonded to the semiconductor side (I-S) than the metal-interlayer (M-I) side of the interface, was undertaken.^{400,416–418} Elements from each of the columns of the Periodic Table (except IV and VIII), selected for the variety in their electronegativities, were deposited on clean Si surfaces in UHV (with the exception of Cl) and processed to form stable adsorbate-terminated semiconductor (ATS) surface structures. On top of ordered and well-characterized ATS surfaces, which included Si(111) 3×1 -K,⁴¹⁹ Si(100) 2×1 -Mg,^{420–423} Si(111) $\sqrt{3} \times \sqrt{3}$ -Ga R30°, Si(111)6.3 \times 6.3-Ga,^{424–427} Si(111) 1 \times 1-As,^{428–430} Si(100) 1 \times 1-S,^{431,432} and Si(111) 1 \times 1-Cl,^{433,434} fabricated *in situ*, different metals were deposited at cryogenic temperatures and occasionally in an inert gas environment. Since the ATS surfaces were known to be stable to various degrees and the metals were deposited “softly,” the expectation was that the surface dipole on the ATS might survive the metal deposition and be available for SBH adjustment. As shown in Figs. 51 and 52, atomic interlayers with electronegativity larger than that of Si indeed led to decreases (increases) in the n-type (p-type) SBH. These SBH shifts were in keeping with the increases (or decreases) in the electron affinity experimentally observed for the ATS surfaces, prior to the metal deposition, for Group V through VII adsorbates (or Group I through III elements), and in good agreement with the expected transfer of electrons from Si to Group V-VII elements (or from the Group I-III elements to Si). Detailed analysis of the junction characteristics of SBH obtained on ATS surfaces generally found significant degree of SBH inhomogeneity, suggesting that the ATS surfaces were not stable enough to completely avoid interaction with

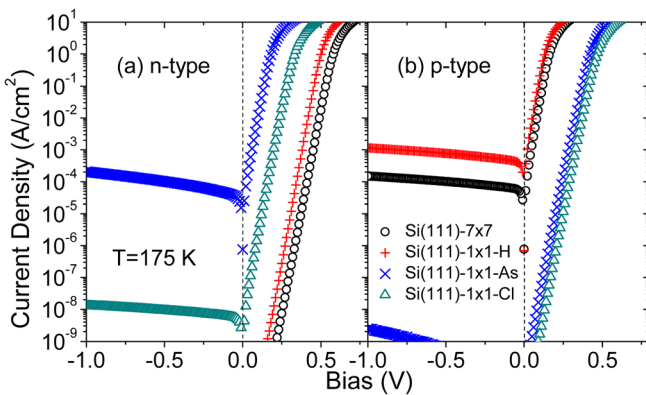


FIG. 51. Experimental I-V curves, obtained at 175 K, for Schottky diodes fabricated on clean, H-, As- and Cl-terminated Si(111) surfaces; (a) n-type, (b) p-type. Reprinted with permission from Li *et al.*, Solid State Commun. **151**, 1641–1644 (2011). Copyright 2011 Elsevier.⁴⁰⁰

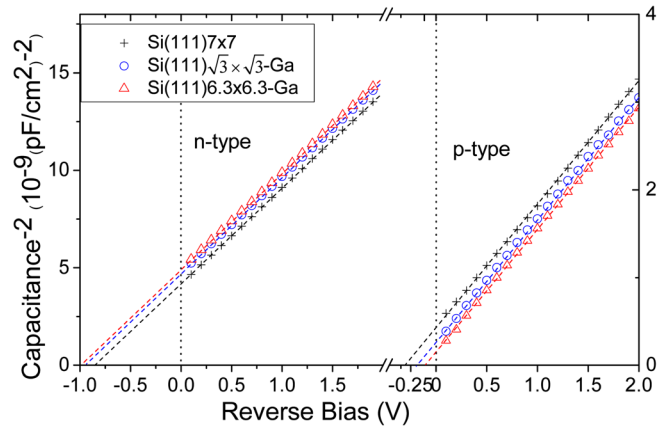


FIG. 52. C-V plots of Ag SBH measured on various Ga-terminated Si(111) surfaces at 77 K and 400 kHz. Reprinted with permission from Long *et al.*, Surf. Sci. **610**, 48 (2013). Copyright 2013 Elsevier.⁴¹⁷

the metal. The observed shifts in the SBH measured by C-V technique for three different metals, due to the use of ATS surface, are summarized in Table II.⁴¹⁸ Because of SBH inhomogeneity at these interfaces, the SBHs measured by current transport techniques were usually lower.^{416,418} As a matter of fact, the Au SBH on n-type Si(100)1 \times 1-S was found to be ohmic, although the semi-quantitative information about the SBH could still be extracted from these diodes through variable temperature analyses.¹⁴⁴ The magnitudes of measured SBH shift in Table II were typically less than the shifts in the electron affinity experimentally observed for the ATS surfaces, which may be viewed as an indication that the interaction between the metal and the ATS was significant. Although, one notes that the reduced SBH shifts are consistent with the rapid increase in the effective dielectric constant in close proximity to the metal,¹⁰² which is expected to significantly reduce the magnitude of any dipole on the free semiconductor surface. The clear conclusion that can be drawn from Table II is that the SBH of an MS interface can indeed be modified in the expected direction by inserting a layer of foreign atoms with polarized bonds to the semiconductor. Quantitative analyses of the SBH shifts suggested that of the ATS surfaces employed in the study, the Si(111) 1 \times 1-As surface appeared to have the best chemical stability to exert dipolar effect at metal-Si interfaces.

TABLE II. The change in measured SBH on adsorbate-terminated Si surfaces from that on the clean Si(111)7 \times 7 or Si(100)2 \times 1. Capacitance-voltage method was used. The value for Au on n-type Si(100)1 \times 1-S was deduced from I-V measurement. Adapted from Ref. 418.

Shift in SBH (eV)	Ag		Au		In	
	n-type	p-type	n-type	p-type	n-type	p-type
Si(111)1 \times 1-Cl	−0.22	+0.37	−0.49	+0.60	−0.50	+0.05
Si(100)1 \times 1-S	−0.19	+0.23	−0.56*	+0.19	−0.12	+0.14
Si(111)1 \times 1-As	−0.40	+0.27	−0.09	+0.48	−0.48	+0.20
Si(111) $\sqrt{3} \times \sqrt{3}$ -Ga	+0.15	−0.11	+0.11	−0.08	+0.15	−0.08
Si(111)6.3 \times 6.3-Ga	+0.17	−0.17	+0.12	−0.08	+0.14	−0.05
Si(100)1 \times 1-Mg	+0.25	−0.07	+0.16	−0.12	+0.16	−0.12
Si(111)3 \times 1-K	+0.14	−0.09	+0.09	−0.07	+0.11	−0.09

V. CONCLUSIONS

Basic physics and chemistry concepts that are essential for the construction of a complete and sound view of the formation mechanism of the SBH are discussed in detail. To start off, a comprehensive analysis of the electrostatics of the MS interface relies on a consistent and simple method to establish the baseline condition for the band alignment. This is shown to be possible with the use of model solids, for the construction of which various methods to handle elemental solids as well as ionic compounds are suggested. A review of the quantum mechanics governing the formation of electronic states at solid interfaces suggests that such problems are complicated and critically dependent on the atomic structure of the interface. Four types of interface states can be distinguished based on the availability of metal and semiconductor bulk states at the specific energy and k_{\parallel} . The formation of these states is associated with chemical bonds at the interface and is dependent on the details of the atomic structure at the interface. The spatial distributions of all the occupied electronic states at the MS interface, which cover a wide range in energy, together are responsible for the magnitude of the interface dipole. There are no general rules on the SBH at MS interfaces that can be established, especially without knowledge of the interface specifics. Existing simple models based on the concept of charge neutrality level and metal induced gap states are not consistent with the general phenomenon of charge transfer calculated at MS interfaces, which take place over wide energy range and are associated with bond formation. In particular, the fixed-separation model widely used in analyses has unrealistic assumptions that are in conflict with results from *ab initio* calculations. To estimate the interface dipole, the concepts of electronegativity and electronegativity equalization (or electrochemical potential equalization) may be employed, although some limitations in these concepts and methods are pointed out. Dipole associated with the formation of polarized bonds at MS interface is shown to successfully account for both the Fermi-pinning phenomenon observed for polycrystalline MS interface and the sharp dependence of the SBH on the interface atomic structure. A strategy to conduct more accurate estimates of the SBH from known interface structures, beyond the point-charge approximation, is suggested. Various issues concerning the potential distribution and the current transport at inhomogeneous SBH are discussed, from both classical and quantum mechanical points of view. Important ramifications of the polarizability of the dipole at MS interfaces are also considered. The significant differences in the potential distributions for wide-area planar interface and that at nanoscale contacts are discussed and shown to have wide implications, as well as possible applications. Different proposals and demonstrated strategies to modify the SBH are discussed and analyzed. Recent results from own laboratory on the use of adsorbate-terminated surfaces for bi-directional adjustment of silicon SBH are also introduced.

In summary, the formation of electronic states at MS interface, as a whole, exhibits the same chemistry and follows the same rules as any other quantum systems. Methods

and insights from molecular chemistry are useful and needed for the construction of an intuitive view of the interface electronics. On the other hand, the formation of individual interface states follows strict rules of solid state physics. In addition, the understanding of various phenomena related to inhomogeneity, interface polarization, carrier confinement, size effects, etc. requires hardcore physics. This review discusses a wide spectrum of topics in physics and chemistry to identify the important roles in SBH formation played by principles from various disciplines. Further progress in SBH research will undoubtedly continue to require insights from both physics and chemistry.

ACKNOWLEDGMENTS

The author would like to thank Dr. Yang Li and Dr. Wei Long for conducting the actual SBH experiments in his laboratory, and the National Science Foundation (DMR) for financial support. He thanks Dr. L. Kronik, Dr. H. Haick, Dr. D. Cahen, Dr. J. Werner, and Dr. S. Oda for exciting collaborations in recent years. He has also benefited greatly from his early collaborations with Dr. J. M. Gibson, Dr. A. F. J. Levi, Dr. J. P. Sullivan, Dr. J. M. Poate, Dr. L. C. Feldman, Dr. W. L. Brown, Dr. K. K. Ng, Dr. H. Fujitani, and Dr. H. Ishiwara on various issues related to the fabrication, characterization, and theoretical understanding of the Schottky barriers.

- ¹S. M. Sze and K. K. Ng, *Physics of Semiconductor Devices*, 3rd ed. (John Wiley and Sons, Hoboken, NJ, 2007).
- ²L. J. Brillson, *Surfaces and Interfaces of Electronic Materials* (Wiley-VCH, 2010).
- ³E. H. Rhoderick and R. H. Williams, *Metal-Semiconductor Contacts*, 2nd ed. (Clarendon Press, Oxford, 1988).
- ⁴R. T. Tung, *Mater. Sci. Eng. Rep.* **35**, 1–138 (2001).
- ⁵W. Schottky, *Z. Phys.* **113**, 367 (1939).
- ⁶N. F. Mott, *Proc. R. Soc. (London) A* **171**, 27 (1939).
- ⁷W. F. Egelhoff, Jr., *Surf. Sci. Rep.* **6**, 253–415 (1987).
- ⁸R. L. Anderson, *Solid-State Electron.* **5**, 341 (1962).
- ⁹H. L. Skriver and N. M. Rosengaard, *Phys. Rev. B* **46**, 7157–7168 (1992).
- ¹⁰M. Weinert and R. E. Watson, *Phys. Rev. B* **29**, 3001–3008 (1984).
- ¹¹A. Franciosi and C. G. Van de Walle, *Surf. Sci. Rep.* **25**, 1–40 (1996).
- ¹²J. R. Waldrop, *Appl. Phys. Lett.* **44**, 1002–1004 (1984).
- ¹³P. E. Schmid, *Helv. Phys. Acta* **58**, 371 (1985).
- ¹⁴W. Mönch, *Surf. Sci.* **21**, 443–446 (1970).
- ¹⁵R. T. Tung, *J. Vac. Sci. Technol. B* **11**, 1546–1552 (1993).
- ¹⁶S. Kurtin, T. C. McGill, and C. A. Mead, *Phys. Rev. Lett.* **22**, 1433 (1969).
- ¹⁷M. Schluter, *Phys. Rev. B* **17**, 5044–5047 (1978).
- ¹⁸W. Monch, *Phys. Rev. Lett.* **58**, 1260 (1987).
- ¹⁹J. P. Sullivan, R. T. Tung, M. R. Pinto, and W. R. Graham, *J. Appl. Phys.* **70**, 7403–7424 (1991).
- ²⁰R. T. Tung, *Phys. Rev. B* **45**, 13509–13523 (1992).
- ²¹J. E. Inglesfield, *Rep. Prog. Phys.* **45**, 223–284 (1982).
- ²²C. B. Duke, A. Paton, W. K. Ford, A. Kahn, and J. Carelli, *Phys. Rev. B* **24**, 562–573 (1981).
- ²³C. A. Swarts, T. C. McGill, and W. A. Goddard III, *Surf. Sci.* **110**, 400–414 (1981).
- ²⁴D. E. Eastman, T. C. Chiang, P. Heimann, and F. J. Himpsel, *Phys. Rev. Lett.* **45**, 656–659 (1980).
- ²⁵J. Bardeen, *Phys. Rev.* **71**, 717 (1947).
- ²⁶A. M. Cowley and S. M. Sze, *J. Appl. Phys.* **36**, 3212 (1965).
- ²⁷J. Tersoff, *Phys. Rev. B* **32**, 6968–6971 (1985).
- ²⁸V. Heine, *Phys. Rev.* **138**, A1689 (1965).
- ²⁹C. Tejedor, F. Flores, and E. Louis, *J. Phys. C* **10**, 2163–2177 (1977).
- ³⁰J. Tersoff, *Phys. Rev. Lett.* **52**, 465–468 (1984).
- ³¹F. Flores and C. Tejedor, *J. Phys. C* **12**, 731–749 (1979).
- ³²J. Tersoff, *Phys. Rev. B* **30**, 4874–4877 (1984).

- ³³M. Cardona and N. E. Christensen, *Phys. Rev. B* **35**, 6182–6194 (1987).
- ³⁴W. A. Harrison and J. Tersoff, *J. Vac. Sci. Technol. B* **4**, 1068–1073 (1986).
- ³⁵A. D. Katnani and G. Margaritondo, *J. Appl. Phys.* **54**, 2522–2525 (1983).
- ³⁶G. H. Parker, T. C. McGill, C. A. Mead, and D. Hoffmann, *Solid-State Electron.* **11**, 201 (1968).
- ³⁷J. M. Andrews and M. P. Lepselter, *Solid-State Electron.* **13**, 1011–1023 (1970).
- ³⁸C. R. Crowell, *J. Vac. Sci. Technol.* **11**, 951–957 (1974).
- ³⁹R. G. Dandrea and C. B. Duke, *J. Vac. Sci. Technol. B* **11**, 1553–1558 (1993).
- ⁴⁰R. T. Tung, J. M. Gibson, and J. M. Poate, *Phys. Rev. Lett.* **50**, 429–432 (1983).
- ⁴¹R. T. Tung, J. M. Gibson, and J. M. Poate, *Appl. Phys. Lett.* **42**, 888–890 (1983).
- ⁴²D. Cherns, G. R. Anstis, J. L. Hutchison, and J. C. H. Spence, *Phil. Mag. A* **46**, 849–862 (1982).
- ⁴³J. M. Gibson, R. T. Tung, and J. M. Poate, in *Defects in Semiconductors, II* (Mater. Res. Soc. Symp. Proc., 1983), Vol. 14, pp. 395–409.
- ⁴⁴H. Foll, *Phys. Status Solidi A* **69**, 779–788 (1982).
- ⁴⁵E. Vlieg, A. E. M. J. Fischer, J. F. Van Der Veen, B. N. Dev, and G. Materlik, *Surf. Sci.* **178**, 36–46 (1986).
- ⁴⁶I. K. Robinson, R. T. Tung, and R. Feidenhans'l, *Phys. Rev. B* **38**, 3632–3635 (1988).
- ⁴⁷R. T. Tung, *Phys. Rev. Lett.* **52**, 461–464 (1984).
- ⁴⁸M. Liehr, P. E. Schmid, F. K. LeGoues, and P. S. Ho, *Phys. Rev. Lett.* **54**, 2139–2142 (1985).
- ⁴⁹R. J. Hauenstein, T. E. Schlesinger, T. C. McGill, B. D. Hunt, and L. J. Schowalter, *Appl. Phys. Lett.* **47**, 853–855 (1985).
- ⁵⁰R. T. Tung, K. K. Ng, J. M. Gibson, and A. F. J. Levi, *Phys. Rev. B* **33**, 7077–7090 (1986).
- ⁵¹M. Ospeleit, J. Henz, L. Flepp, and H. von Kanel, *Appl. Phys. Lett.* **52**, 227–229 (1988).
- ⁵²J. Vrijmoeth, J. F. van der Veen, D. R. Heslinga, and T. M. Klapwijk, *Phys. Rev. B* **42**, 9598–9608 (1990).
- ⁵³J. P. Sullivan, R. T. Tung, and F. Schrey, *J. Appl. Phys.* **72**, 478 (1992).
- ⁵⁴R. T. Tung, F. Schrey, and S. M. Yalisove, *Appl. Phys. Lett.* **55**, 2005 (1989).
- ⁵⁵D. Cherns, C. J. D. Hetherington, and C. J. Humphreys, *Phil. Mag. A* **49**, 165–177 (1984).
- ⁵⁶R. T. Tung, A. F. J. Levi, J. P. Sullivan, and F. Schrey, *Phys. Rev. Lett.* **66**, 72–75 (1991).
- ⁵⁷G. Ottaviani, K. N. Tu, and J. W. Mayer, *Phys. Rev. B* **24**, 3354–3359 (1981).
- ⁵⁸P. E. Schmid, P. S. Ho, H. Föll, and T. Y. Tan, *Phys. Rev. B* **28**, 4593–4601 (1983).
- ⁵⁹G. P. Das, P. Blochl, O. K. Andersen, N. E. Christensen, and O. Gunnarsson, *Phys. Rev. Lett.* **63**, 1168–1171 (1989).
- ⁶⁰H. Fujitani and S. Asano, *Phys. Rev. B* **42**, 1696–1704 (1990).
- ⁶¹H. Fujitani and S. Asano, *J. Phys. Soc. Jpn.* **60**, 2526–2529 (1991).
- ⁶²J. C. Hensel, A. F. J. Levi, R. T. Tung, and J. M. Gibson, *Appl. Phys. Lett.* **47**, 151 (1985).
- ⁶³R. T. Tung, A. F. J. Levi, and J. M. Gibson, *Appl. Phys. Lett.* **48**, 635 (1986).
- ⁶⁴J. M. Gibson, J. C. Bean, J. M. Poate, and R. T. Tung, *Appl. Phys. Lett.* **41**, 818 (1982).
- ⁶⁵R. T. Tung, J. C. Bean, J. M. Gibson, J. M. Poate, and D. C. Jacobson, *Appl. Phys. Lett.* **40**, 684 (1982).
- ⁶⁶F. Hellman and R. T. Tung, *Phys. Rev. B* **37**, 10786 (1988).
- ⁶⁷J. P. Sullivan, R. T. Tung, D. J. Eaglesham, F. Schrey, and W. R. Graham, *J. Vac. Sci. Technol. B* **11**, 1564–1570 (1993).
- ⁶⁸S. Y. Zhu, R. L. Van Meirhaeghe, C. Detavernier, F. Cardon, G. P. Ru, X. P. Qu, and B. Z. Li, *Solid-State Electron.* **44**, 663–671 (2000).
- ⁶⁹D. Loretto, J. M. Gibson, and S. M. Yalisove, *Phys. Rev. Lett.* **63**, 298–301 (1989).
- ⁷⁰C. W. T. Bulle-Lieuwma, A. F. De Jong, and D. E. W. Vandenhoudt, *Phil. Mag. A* **64**, 255–280 (1991).
- ⁷¹S. A. Chambers, Y. Liang, Z. Yu, R. Droopad, and J. Ramdani, *J. Vac. Sci. Technol. A* **19**, 934–939 (2001).
- ⁷²P. Werner, W. Jager, and A. Schuppen, *J. Appl. Phys.* **74**, 3846–3854 (1993).
- ⁷³P. Werner, W. Jager, and A. Schuppen, Mater. Res. Soc. Symp. Proc. **320**, 227–232 (1994).
- ⁷⁴N. V. Rees and C. C. Matthai, *J. Phys. C* **21**, L981 (1988).
- ⁷⁵H. Fujitani and S. Asano, *Appl. Surf. Sci.* **41–42**, 164–168 (1989).
- ⁷⁶R. Stadler and R. Podloucky, *Phys. Rev. B* **62**, 2209–2219 (2000).
- ⁷⁷A. Y. Cho and P. D. Dernier, *J. Appl. Phys.* **49**, 3328–3332 (1978).
- ⁷⁸R. Ludeke, L. L. Chang, and L. Esaki, *Appl. Phys. Lett.* **23**, 201–203 (1973).
- ⁷⁹T. Sands, *Appl. Phys. Lett.* **52**, 197–199 (1988).
- ⁸⁰J. P. Harbison, T. Sands, N. Tabatabaie, W. K. Chan, L. T. Florez, and V. G. Keramidas, *Appl. Phys. Lett.* **53**, 1717–1719 (1988).
- ⁸¹C. J. Palmstrom, B. O. Fimland, T. Sands, K. C. Garrison, and R. A. Bartynski, *J. Appl. Phys.* **65**, 4753–4758 (1989).
- ⁸²W. C. Marra, P. Eisenberger, and A. Y. Cho, *J. Appl. Phys.* **50**, 6927–6933 (1979).
- ⁸³D. J. Eaglesham, C. J. Kiely, D. Cherns, and M. Missous, *Phil. Mag. A* **60**, 161–175 (1989).
- ⁸⁴J. Mizuki, K. Akimoto, I. Horosawa, K. Hirose, T. Mizutani, and J. Matsui, *J. Vac. Sci. Technol. B* **6**, 31–33 (1988).
- ⁸⁵W. I. Wang, *J. Vac. Sci. Technol. B* **1**, 574–580 (1983).
- ⁸⁶K. Hirose, K. Akimoto, I. Horosawa, J. Mizuki, T. Mizutani, and J. Matsui, *Phys. Rev. B* **43**, 4538–4540 (1991).
- ⁸⁷M. Lazzarino, G. Scarel, S. Rubini, G. Bratina, L. Sorba, A. Franciosi, C. Berthod, N. Binggeli, and A. Baldereschi, *Phys. Rev. B* **57**, R9431–R9434 (1998).
- ⁸⁸C. Barret and J. Massies, *J. Vac. Sci. Technol. B* **1**, 819–824 (1983).
- ⁸⁹M. Missous, E. H. Rhoderick, and K. E. Singer, *J. Appl. Phys.* **60**, 2439–2444 (1986).
- ⁹⁰W. Chen, A. Kahn, P. Soukiasian, P. S. Mangat, J. Gaines, C. Ponzoni, and D. Olego, *Phys. Rev. B* **51**, 14265–14270 (1995).
- ⁹¹R. J. Needs, J. P. A. Charlesworth, and R. W. Godby, *Europhys. Lett.* **25**, 31–36 (1994).
- ⁹²J. Bardi, N. Binggeli, and A. Baldereschi, *Phys. Rev. B* **59**, 8054–8064 (1999).
- ⁹³N. Tabatabaie, T. Sands, J. P. Harbison, H. L. Gilchrist, and V. G. Keramidas, *Appl. Phys. Lett.* **53**, 2528–2530 (1988).
- ⁹⁴J. G. Zhu, C. B. Carter, C. J. Palmstrom, and K. C. Garrison, *Appl. Phys. Lett.* **55**, 39–41 (1989).
- ⁹⁵T. L. Cheeks, T. Sands, R. E. Nahory, J. Harbison, N. Tabatabaie, H. L. Gilchrist, B. J. Wilkens, and V. G. Keramidas, *Appl. Phys. Lett.* **56**, 1043–1045 (1990).
- ⁹⁶T. Sands, C. J. Palmstrom, J. P. Harbison, V. G. Keramidas, N. Tabatabaie, T. L. Cheeks, R. Ramesh, and Y. Silberberg, *Mater. Sci. Rep.* **5**, 99–170 (1990).
- ⁹⁷C. J. Palmstrom, S. Mounier, T. G. Finstad, and P. F. Miceli, *Appl. Phys. Lett.* **56**, 382–384 (1990).
- ⁹⁸C. J. Palmstrom, T. L. Cheeks, H. L. Gilchrist, J. G. Zhu, C. B. Carter, B. J. Wilkens, and R. Martin, *J. Vac. Sci. Technol. A* **10**, 1946–1953 (1992).
- ⁹⁹W. R. L. Lambrecht, A. G. Petukhov, and B. T. Hemmelman, *Solid State Commun.* **108**, 361–365 (1998).
- ¹⁰⁰K. T. Delaney, N. A. Spaldin, and C. G. Van De Walle, *Phys. Rev. B* **81**, 165312 (2010).
- ¹⁰¹S. Picozzi, A. Continenza, G. Satta, S. Massidda, and A. J. Freeman, *Phys. Rev. B* **61**, 16736–167342 (2000).
- ¹⁰²C. Berthod, N. Binggeli, and A. Baldereschi, *Phys. Rev. B* **68**, 085323 (2003).
- ¹⁰³C. Berthod, J. Bardi, N. Binggeli, and A. Baldereschi, *J. Vac. Sci. Technol. A* **14**, 3000–3007 (1996).
- ¹⁰⁴C. Berthod, N. Binggeli, and A. Baldereschi, *Europhys. Lett.* **36**, 67–72 (1996).
- ¹⁰⁵M. Peressi, N. Binggeli, and A. Baldereschi, *J. Phys. D* **31**, 1273–1299 (1998).
- ¹⁰⁶C. Berthod, N. Binggeli, and A. Baldereschi, *J. Vac. Sci. Technol. B* **18**, 2114–2118 (2000).
- ¹⁰⁷J. R. Waldrop and R. W. Grant, *Appl. Phys. Lett.* **56**, 557–559 (1990).
- ¹⁰⁸J. R. Waldrop, R. W. Grant, Y. C. Wang, and R. F. Davis, *J. Appl. Phys.* **72**, 4757–4760 (1992).
- ¹⁰⁹J. R. Waldrop, *J. Appl. Phys.* **75**, 4548–4550 (1994).
- ¹¹⁰A. Itoh and H. Matsunami, *Phys. Status Solidi A* **162**, 389–408 (1997).
- ¹¹¹S. Hara, T. Teraji, H. Okushi, and K. Kajimura, *Appl. Surf. Sci.* **117–118**, 394–399 (1997).
- ¹¹²M. O. Aboelfotoh, C. Fröjd, and C. S. Petersson, *Phys. Rev. B* **67**, 075312 (2003).
- ¹¹³M. Kohyama and J. Hoekstra, *Phys. Rev. B* **61**, 2672–2679 (2000).
- ¹¹⁴G. Profeta, A. Blasetti, S. Picozzi, A. Continenza, and A. J. Freeman, *Phys. Rev. B* **64**, 235312 (2001).

- ¹¹⁵S. Tanaka, T. Tamura, K. Okazaki, S. Ishibashi, and M. Kohyama, *Phys. Status Solidi C* **4**, 2972–2976 (2007).
- ¹¹⁶R. A. McKee, F. J. Walker, and M. F. Chisholm, *Phys. Rev. Lett.* **81**, 3014–3017 (1998).
- ¹¹⁷K. Ueno, I. H. Inoue, H. Akoh, M. Kawasaki, Y. Tokura, and H. Takagi, *Appl. Phys. Lett.* **83**, 1755–1757 (2003).
- ¹¹⁸Y. Hikita, M. Nishikawa, T. Yajima, and H. Y. Hwang, *Phys. Rev. B* **79**, 073101 (2009).
- ¹¹⁹M. Mrovec, J. M. Albina, B. Meyer, and C. Elsasser, *Phys. Rev. B* **79**, 245121 (2009).
- ¹²⁰R. Schafranek, S. Payan, M. Maglione, and A. Klein, *Phys. Rev. B* **77**, 195310 (2008).
- ¹²¹M. Nunez and M. B. Nardelli, *Phys. Rev. B* **73**, 235422 (2006).
- ¹²²M. Nunez and M. B. Nardelli, *Phys. Status Solidi B* **243**, 2081–2084 (2006).
- ¹²³R. A. McKee, F. J. Walker, M. B. Nardelli, W. A. Shelton, and G. M. Stocks, *Science* **300**, 1726–1730 (2003).
- ¹²⁴T. Okumura and K. N. Tu, *J. Appl. Phys.* **54**, 922–927 (1983).
- ¹²⁵O. Engstrom, H. Pettersson, and B. Sernelius, *Phys. Status Solidi A* **95**, 691–701 (1986).
- ¹²⁶A. Tanabe, K. Konuma, N. Teranishi, S. Tohyama, and K. Masubuchi, *J. Appl. Phys.* **69**, 850–853 (1991).
- ¹²⁷L. D. Bell and W. J. Kaiser, *Phys. Rev. Lett.* **61**, 2368–2371 (1988).
- ¹²⁸M. H. Hecht, L. D. Bell, W. J. Kaiser, and F. J. Grunthaner, *Appl. Phys. Lett.* **55**, 780–782 (1989).
- ¹²⁹A. E. Fowell, R. H. Williams, B. E. Richardson, A. A. Cafolla, D. I. Westwood, and D. A. Woolf, *J. Vac. Sci. Technol. B* **9**, 581–584 (1991).
- ¹³⁰H. Palm, M. Arbes, and M. Schulz, *Phys. Rev. Lett.* **71**, 2224–2227 (1993).
- ¹³¹L. J. Schowalter and E. Y. Lee, *Phys. Rev. B* **43**, 9308–9311 (1991).
- ¹³²R. T. Tung, *Appl. Phys. Lett.* **58**, 2821–2823 (1991).
- ¹³³A. Olbrich, J. Vancea, F. Kreupl, and H. Hoffmann, *Appl. Phys. Lett.* **70**, 2559–2561 (1997).
- ¹³⁴A. Olbrich, J. Vancea, F. Kreupl, and H. Hoffmann, *J. Appl. Phys.* **83**, 358–365 (1998).
- ¹³⁵S. Yae, R. Tsuda, T. Kai, K. Kukuchi, M. Uetsuji, T. Fujii, M. Fujitani, and Y. Nakato, *J. Electrochem. Soc.* **141**, 3090–3095 (1994).
- ¹³⁶R. C. Rossi, M. X. Tan, and N. S. Lewis, *Appl. Phys. Lett.* **77**, 2698–2700 (2000).
- ¹³⁷S. M. Sze, C. R. Crowell, and D. Kahng, *J. Appl. Phys.* **35**, 2534 (1964).
- ¹³⁸C. R. Crowell and G. I. Roberts, *J. Appl. Phys.* **40**, 3726–3730 (1969).
- ¹³⁹H. C. Card and E. H. Rhoderick, *J. Phys. D* **4**, 1589–1601 (1971).
- ¹⁴⁰F. A. Padovali and R. Stratton, *Solid-State Electron.* **9**, 695 (1966).
- ¹⁴¹V. L. Rideout and C. R. Crowell, *Solid-State Electron.* **13**, 993 (1970).
- ¹⁴²R. H. Cox and H. Strack, *Solid-State Electron.* **10**, 1213 (1967).
- ¹⁴³Y. Li, Ph.D. thesis, Graduate Center, CUNY, 2012.
- ¹⁴⁴Y. Li, W. Long, and R. T. Tung, *Appl. Phys. Lett.* **101**, 051604 (2012).
- ¹⁴⁵A. Thamailakis and A. Rasul, *J. Phys. C* **9**, 337–343 (1976).
- ¹⁴⁶N. Newman, M. van Schilfgaarde, T. Kendelvitz, M. D. Williams, and W. E. Spicer, *Phys. Rev. B* **33**, 1146–1159 (1986).
- ¹⁴⁷A. B. McLean and R. H. Williams, *J. Phys. C* **21**, 783–806 (1988).
- ¹⁴⁸I. Ohdomari and K. N. Tu, *J. Appl. Phys.* **51**, 3735–3739 (1980).
- ¹⁴⁹J. L. Freeouf, T. N. Jackson, S. E. Laux, and J. M. Woodall, *Appl. Phys. Lett.* **40**, 634–636 (1982).
- ¹⁵⁰H. H. Guttler and J. H. Werner, *Appl. Phys. Lett.* **56**, 1113–1115 (1990).
- ¹⁵¹J. Werner, A. F. J. Levi, R. T. Tung, M. Anzlowar, and M. Pinto, *Phys. Rev. Lett.* **60**, 53–56 (1988).
- ¹⁵²B. Bati, C. Nuhoglu, M. Saglam, E. Ayyildiz, and A. Turut, *Phys. Scr.* **61**, 209–212 (2000).
- ¹⁵³G. L. Hall, *Phys. Rev. B* **19**, 3921 (1979).
- ¹⁵⁴F. W. de Wette, *Phys. Rev. B* **21**, 3751 (1980).
- ¹⁵⁵J. Ihm and M. L. Cohen, *Phys. Rev. B* **21**, 3754 (1980).
- ¹⁵⁶L. Kleinman, *Phys. Rev. B* **24**, 7412 (1981).
- ¹⁵⁷P. Bagno, L. F. D. Rose, and F. Toigo, *Adv. Phys.* **40**, 685–718 (1991).
- ¹⁵⁸L. F. Mattheiss, *Phys. Rev.* **133**, A1399–A1403 (1964).
- ¹⁵⁹C. G. Van de Walle and R. M. Martin, *Phys. Rev. B* **35**, 8154–8165 (1987).
- ¹⁶⁰A. Baldereschi, S. Baroni, and R. Resta, *Phys. Rev. Lett.* **61**, 734–737 (1988).
- ¹⁶¹N. W. Ashcroft and N. D. Mermin, *Solid State Physics* (Holt, Rinehart and Winston, New York, 1976).
- ¹⁶²C. Pisani, R. Dovesi, and C. Roetti, *Hartree-Fock Ab Initio Treatment of Crystalline Systems*, Lecture Notes in Chemistry, Vol. 48 (Springer-Verlag, Berlin, 1988).
- ¹⁶³R. T. Tung and L. Kronik, “Cut-and-stitch analysis of potential distribution at metal-semiconductor interfaces” (unpublished).
- ¹⁶⁴R. S. Mulliken, *J. Chem. Phys.* **23**, 1833–1840 (1955).
- ¹⁶⁵R. F. W. Bader, *Acc. Chem. Res.* **18**, 9–15 (1985).
- ¹⁶⁶A. D. Becke and K. E. Edgecombe, *J. Chem. Phys.* **92**, 5397–5403 (1990).
- ¹⁶⁷M. H. Cohen, A. Wasserman, and K. Burke, *J. Phys. Chem. A* **111**, 12447–12453 (2007).
- ¹⁶⁸F. L. Hirshfeld, *Theor. Chim. Acta* **44**, 129–138 (1977).
- ¹⁶⁹K. B. Wiberg and P. R. Rablen, *J. Comp. Chem.* **14**, 1504–1518 (1993).
- ¹⁷⁰W. A. Harrison, E. A. Kraut, J. R. Waldrop, and R. W. Grant, *Phys. Rev. B* **18**, 4402–4410 (1978).
- ¹⁷¹N. Memmel, *Surf. Sci. Rep.* **32**, 91–163 (1998).
- ¹⁷²M. Di Ventra, C. Berthod, and N. Binggeli, *Phys. Rev. B* **62**, R10622–R10625 (2000).
- ¹⁷³M. K. Nirajan, L. Kleinman, and A. A. Demkov, *Phys. Rev. B* **77**, 155316 (2008).
- ¹⁷⁴M. Buttiker, *IBM J. Res. Dev.* **32**, 317–334 (1988).
- ¹⁷⁵S. Datta, *Electronic Transport in Mesoscopic Systems* (Cambridge University Press, Cambridge, 1995).
- ¹⁷⁶L. Pauling, *J. Am. Chem. Soc.* **54**, 3570–3582 (1932).
- ¹⁷⁷R. S. Mulliken, *J. Chem. Phys.* **2**, 782–793 (1934).
- ¹⁷⁸R. T. Sanderson, *Science* **114**, 670–672 (1951).
- ¹⁷⁹W. Gordy and W. J. Orville-Thomas, *J. Chem. Phys.* **24**, 439 (1956).
- ¹⁸⁰A. L. Allred and E. G. Rochow, *J. Inorg. Nucl. Chem.* **5**, 264–268 (1958).
- ¹⁸¹J. St. John and A. N. Bloch, *Phys. Rev. Lett.* **33**, 1095–1098 (1974).
- ¹⁸²A. R. Miedema, P. F. de Chatel, and F. R. de Boer, *Physica B & C* **100**, 1–28 (1980).
- ¹⁸³R. J. Boyd and G. E. Markus, *J. Chem. Phys.* **75**, 5385 (1981).
- ¹⁸⁴R. P. Iczkowski and J. L. Margrave, *J. Am. Chem. Soc.* **83**, 3547 (1961).
- ¹⁸⁵R. G. Parr, R. A. Donnelly, M. Levy, and W. E. Palke, *J. Chem. Phys.* **68**, 3801–3807 (1978).
- ¹⁸⁶J. Hinze, M. A. Whitehead, and H. H. Jaffé, *J. Am. Chem. Soc.* **85**, 148–154 (1963).
- ¹⁸⁷J. K. Nagle, *J. Am. Chem. Soc.* **112**, 4741–4747 (1990).
- ¹⁸⁸L. C. Allen and E. T. Knight, *J. Mol. Struc. THEOCHEM* **261**, 313–330 (1992).
- ¹⁸⁹Y. R. Luo and S. W. Benson, *Acc. Chem. Res.* **25**, 375–381 (1992).
- ¹⁹⁰J. L. Reed, *J. Phys. Chem. A* **106**, 3148–3152 (2002).
- ¹⁹¹C. H. Suresh and N. Koga, *J. Am. Chem. Soc.* **124**, 1790–1797 (2002).
- ¹⁹²A. Cherkasov, *J. Chem. Inf. Comput. Sci.* **43**, 2039–2047 (2003).
- ¹⁹³J. P. Perdew, R. G. Parr, M. Levy, and J. L. Balduz, Jr., *Phys. Rev. Lett.* **49**, 1691–1694 (1982).
- ¹⁹⁴W. Yang, Y. Zhang, and P. W. Ayers, *Phys. Rev. Lett.* **84**, 5172–5175 (2000).
- ¹⁹⁵W. J. Mortier, K. Van Geuchten, and J. Gasteiger, *J. Am. Chem. Soc.* **107**, 829–835 (1985).
- ¹⁹⁶R. F. Nalewajski, *J. Phys. Chem.* **89**, 2831–2837 (1985).
- ¹⁹⁷P. Bultinck, W. Langenaeker, P. Lahorte, F. De Proft, P. Geerlings, M. Waroquier, and J. P. Tollenaere, *J. Phys. Chem. A* **106**, 7887–7894 (2002).
- ¹⁹⁸A. K. Rappe and W. A. Goddard III, *J. Phys. Chem.* **95**, 3358–3363 (1991).
- ¹⁹⁹T. Ogawa, N. Kurita, H. Sekino, O. Kitao, and S. Tanaka, *Chem. Phys. Lett.* **397**, 382–387 (2004).
- ²⁰⁰R. A. Nistor, J. G. Polihrone, M. H. Muser, and N. J. Mosey, *J. Chem. Phys.* **125**, 094108 (2006).
- ²⁰¹D. M. York and W. Yang, *J. Chem. Phys.* **104**, 159–172 (1996).
- ²⁰²P. Itskowitz and M. L. Berkowitz, *J. Phys. Chem. A* **102**, 4808–4812 (1998).
- ²⁰³C. Bret, M. J. Field, and L. Hemmingsen, *Mol. Phys.* **98**, 751–763 (2000).
- ²⁰⁴J. Morales and T. J. Martinez, *J. Phys. Chem. A* **105**, 2842–2850 (2001).
- ²⁰⁵A. Wadehra and S. K. Ghosh, *J. Chem. Sci.* **117**, 401–409 (2005).
- ²⁰⁶R. T. Tung, *Phys. Rev. B* **64**, 205310 (2001).
- ²⁰⁷S. M. Valone and S. R. Atlas, *Phys. Rev. Lett.* **97**, 256402 (2006).
- ²⁰⁸J. P. Perdew, A. Ruzsinszky, G. I. Csonka, O. A. Vydrov, G. E. Scuseria, V. N. Staroverov, and J. Tao, *Phys. Rev. A* **76**, 040501 (2007).
- ²⁰⁹J. Ciosowski and B. B. Stefanov, *J. Chem. Phys.* **99**, 5151–5162 (1993).
- ²¹⁰H. O. Pritchard and H. A. Skinner, *Chem. Rev.* **55**, 745–786 (1955).
- ²¹¹A. L. Companion and F. O. Ellison, *J. Chem. Phys.* **28**, 1–8 (1958).
- ²¹²J. E. Huheey, *Inorganic Chemistry: Principles of Structure and Reactivity* (Harper & Row, New York, 1978).
- ²¹³R. T. Tung, “Spin-singlet atoms in molecules: Electrochemical potential equalization” (unpublished).
- ²¹⁴R. T. Tung, *Phys. Rev. Lett.* **84**, 6078–6081 (2000).

- ²¹⁵F. R. de Boer, R. Boom, W. C. M. Mattens, A. R. Miedema, and A. K. Niessen, *Cohesion in Metals: Transition Metal Alloys* (North-Holland, Amsterdam, 1988), p. 711.
- ²¹⁶M. Akazawa, H. Ishii, and H. Hasegawa, *Jpn. J. Appl. Phys., Part 1* **30**, 3744–3749 (1991).
- ²¹⁷C. Berthod, N. Binggeli, and A. Baldereschi, *Phys. Rev. B* **57**, 9757–9762 (1998).
- ²¹⁸W. E. Spicer, P. W. Chye, P. R. Skeath, C. Y. Su, and I. Lindau, *J. Vac. Sci. Technol.* **16**, 1422–1433 (1979).
- ²¹⁹M. S. Daw and D. L. Smith, *Solid State Commun.* **37**, 205 (1981).
- ²²⁰R. E. Allen, T. J. Humphreys, J. D. Dow, and O. F. Sankey, *J. Vac. Sci. Technol. B* **2**, 449–452 (1984).
- ²²¹W. Walukiewicz, *J. Vac. Sci. Technol. B* **5**, 1062–1067 (1987).
- ²²²R. G. Barrera, O. Guzman, and B. Balaguer, *Am. J. Phys.* **46**, 1172–1179 (1978).
- ²²³J. P. A. Charlesworth, R. W. Godby, and R. J. Needs, *Phys. Rev. Lett.* **70**, 1685–1688 (1993).
- ²²⁴J. P. A. Charlesworth, R. W. Godby, R. J. Needs, and L. J. Sham, *Mater. Sci. Eng., B* **14**, 262–265 (1992).
- ²²⁵C. R. Crowell and V. L. Rideout, *Solid State Electron.* **12**, 89–105 (1969).
- ²²⁶V. B. Bikbaev, S. C. Karpinskas, and J. J. Vaitkus, *Phys. Status Solidi A* **75**, 583–590 (1983).
- ²²⁷B. Shan and K. Cho, *Phys. Rev. B* **70**, 233405 (2004).
- ²²⁸F. Léonard and A. A. Talin, *Phys. Rev. Lett.* **97**, 026804 (2006).
- ²²⁹V. Vitale, A. Curioni, and W. Andreoni, *J. Am. Chem. Soc.* **130**, 5848–5849 (2008).
- ²³⁰J. Svensson and E. E. B. Campbell, *J. Appl. Phys.* **110**, 111101 (2011).
- ²³¹F. Leonard and J. Tersoff, *Phys. Rev. Lett.* **84**, 4693–4696 (2000).
- ²³²J. Guo, J. Wang, E. Polizzi, S. Datta, and M. Lundstrom, *IEEE Trans. Nanotechnol.* **2**, 329–334 (2003).
- ²³³A. Natan, L. Kroni, H. Haick, and R. T. Tung, *Adv. Mater.* **19**, 4103–4117 (2007).
- ²³⁴Y. Matsuda, W. Q. Deng, and W. A. Goddard, *J. Phys. Chem. C* **114**, 17845–17850 (2010).
- ²³⁵Z. Q. Shi and W. A. Anderson, *Solid-State Electron.* **35**, 1427–1432 (1992).
- ²³⁶Z. Q. Shi and W. A. Anderson, *J. Appl. Phys.* **72**, 3803–3807 (1992).
- ²³⁷H. J. Lee, W. A. Anderson, H. Hardtdegen, and H. Luth, *Appl. Phys. Lett.* **63**, 1939–1941 (1993).
- ²³⁸A. Wang and W. A. Anderson, *J. Electron. Mater.* **25**, 201–205 (1996).
- ²³⁹S. A. Clark, S. P. Wilks, A. Kestle, D. I. Westwood, and M. Elliott, *Surf. Sci.* **352–354**, 850–854 (1996).
- ²⁴⁰H.-T. Wang, B. S. Kang, F. Ren, A. Herrero, A. M. Gerger, B. P. Gila, S. J. Pearton, H. Shen, J. R. LaRoche, and K. V. Smith, *J. Electrochem. Soc.* **153**, G787–G790 (2006).
- ²⁴¹A. M. Herrero, A. M. Gerger, B. P. Gila, S. J. Pearton, H.-T. Wang, S. Jang, T. Anderson, J. J. Chen, B. S. Kang, and F. Ren, *Appl. Surf. Sci.* **253**, 3298 (2007).
- ²⁴²H. Hasegawa, *Jpn. J. Appl. Phys., Part 1* **38**, 1098–1102 (1999).
- ²⁴³H. Hasegawa, T. Sato, and T. Hashizume, *J. Vac. Sci. Technol. B* **15**, 1227–1235 (1997).
- ²⁴⁴T. Hashizume, G. Schweeger, N. J. Wu, and H. Hasegawa, *J. Vac. Sci. Technol. B* **12**, 2660–2666 (1994).
- ²⁴⁵S. Uno, T. Hashizume, S. Kasai, N. J. Wu, and H. Hasegawa, *Jpn. J. Appl. Phys., Part 1* **35**, 1258–1263 (1996).
- ²⁴⁶J. R. Heath and M. A. Ratner, *Phys. Today* **56**(5), 43–49 (2003).
- ²⁴⁷I. H. Campbell, S. Rubin, T. A. Zawodzinski, J. D. Kress, R. L. Martin, D. L. Smith, N. N. Baraskov, and J. P. Ferraris, *Phys. Rev. B* **54**, R14321–R14324 (1996).
- ²⁴⁸J. E. Pattison, M. F. Daniel, D. A. Anderson, P. R. Tapster, N. Apsley, and M. J. Slater, in *External Abstract of European Solid-State DEvice Research Conference (ESSDERC)* (1981), pp. 64–65.
- ²⁴⁹R. H. Tredgold and Z. I. El-Badawy, *J. Phys. D* **18**, 103–109 (1985).
- ²⁵⁰L. Kronik and Y. Shapira, *Surf. Sci. Rep.* **37**(5), 206 (1999).
- ²⁵¹J. Ross Macdonald and C. A. Barlow, Jr., *J. Chem. Phys.* **39**, 412–422 (1963).
- ²⁵²A. Natan, Y. Zidon, Y. Shapira, and L. Kronik, *Phys. Rev. B* **73**, 193310–193314 (2006).
- ²⁵³H. Fukagawa, H. Yamane, S. Kera, K. K. Okudaira, and N. Ueno, *Phys. Rev. B* **73**, 041302 (2006).
- ²⁵⁴D. Cornil, Y. Olivier, V. Geskin, and J. Cornil, *Adv. Funct. Mater.* **17**, 1143–1148 (2007).
- ²⁵⁵V. De Renzi, *Surf. Sci.* **603**, 1518–1525 (2009).
- ²⁵⁶G. Heimel, L. Romaner, E. Zojer, and J. L. Bredas, *Nano Lett.* **7**, 932–940 (2007).
- ²⁵⁷M. L. Sushko and A. L. Shluger, *Adv. Funct. Mater.* **18**, 2228–2236 (2008).
- ²⁵⁸J. Topping, *Proc. Royal Soc. London, Ser. A* **114**, 67 (1927).
- ²⁵⁹T. Aqua, H. Cohen, O. Sinai, V. Frydman, T. Bendikov, D. Krepel, O. Hod, L. Kronik, and R. Naaman, *J. Phys. Chem. C* **115**, 24888–24892 (2011).
- ²⁶⁰L. Wang, G. M. Rangger, L. Romaner, G. Heimel, T. Bučko, M. Zhongyun, Q. Li, Z. Shuai, and E. Zojer, *Adv. Funct. Mater.* **19**, 3766–3775 (2009).
- ²⁶¹P. C. Rusu and G. Brocks, *Phys. Rev. B* **74**, 073414 (2006).
- ²⁶²D. M. Taylor and G. F. Bayes, *Phys. Rev. E* **49**, 1439–1449 (1994).
- ²⁶³B. De Boer, A. Hadipour, M. M. Mandoc, T. Van Woudenberg, and P. W. M. Blom, *Adv. Mater.* **17**, 621–625 (2005).
- ²⁶⁴R. Rousseau, V. De Renzi, R. Mazzarello, D. Marchetto, R. Biagi, S. Scandolo, and U. Del Pennino, *J. Phys. Chem. B* **110**, 10862–10872 (2006).
- ²⁶⁵S. Bastide, R. Butruille, D. Cahen, A. Dutta, J. Libman, A. Shanzer, L. M. Sun, and A. Vilan, *J. Phys. Chem. B* **101**, 2678–2684 (1997).
- ²⁶⁶M. Bruening, E. Moons, D. Cahen, and A. Shanzer, *J. Phys. Chem.* **99**, 8368–8373 (1995).
- ²⁶⁷R. Cohen, N. Zenou, D. Cahen, and S. Yitzchaik, *Chem. Phys. Lett.* **279**, 270–274 (1997).
- ²⁶⁸A. Vilan, J. Ghabboun, and D. Cahen, *J. Phys. Chem. B* **107**, 6360–6376 (2003).
- ²⁶⁹C. H. Kuo, C. P. Liu, S. H. Lee, H. Y. Chang, W. C. Lin, Y. W. You, H. Y. Liao, and J. J. Shyue, *Phys. Chem. Chem. Phys.* **13**, 15122–15126 (2011).
- ²⁷⁰S. R. Puniredd, I. Platzman, R. T. Tung, and H. Haick, *J. Phys. Chem. C* **114**, 18674–18678 (2010).
- ²⁷¹G. C. Herdt, D. R. Jung, and A. W. Czanderna, *Prog. Surf. Sci.* **50**, 103–129 (1995).
- ²⁷²B. de Boer, M. M. Frank, Y. J. Chabal, W. Jiang, E. Garfunkel, and Z. Bao, *Langmuir* **20**, 1539–1542 (2004).
- ²⁷³W. R. Salaneck, M. Logdlund, J. Birgersson, P. Barta, R. Lazzaroni, and J. L. Bredas, *Synth Met* **85**, 1219–1220 (1997).
- ²⁷⁴A. V. Walker, T. B. Tighe, B. C. Haynie, S. Uppili, N. Winograd, and D. L. Allara, *J. Phys. Chem. B* **109**, 11263–11272 (2005).
- ²⁷⁵J. Chen, M. A. Reed, A. M. Rawlett, and J. M. Tour, *Science* **286**, 1550–1552 (1999).
- ²⁷⁶E. A. Speets, B. J. Ravoo, F. J. G. Roesthuis, F. Vroegindeweij, D. H. A. Blank, and D. N. Reinhoudt, *Nano Lett.* **4**, 841 (2004).
- ²⁷⁷H. Haick, M. Ambrico, J. Ghabboun, T. Ligonzo, and D. Cahen, *Phys. Chem. Chem. Phys.* **6**, 4538–4541 (2004).
- ²⁷⁸M. Dorogi, J. Gomez, R. Osipchin, R. P. Andres, and R. Reifenberger, *Phys. Rev. B* **52**, 9071–9077 (1995).
- ²⁷⁹D. I. Gittins, D. Bethell, D. J. Schiffrian, and R. J. Nichols, *Nature* **408**, 67–69 (2000).
- ²⁸⁰I. Amlani, A. M. Rawlett, L. A. Nagahara, and R. K. Tsui, *Appl. Phys. Lett.* **80**, 2761–2763 (2002).
- ²⁸¹H. O. Finkela and D. D. Hanshew, *J. Am. Chem. Soc.* **114**, 3173–3181 (1992).
- ²⁸²J. F. Smalley, S. W. Feldberg, C. E. D. Chidsey, M. R. Linford, M. D. Newton, and Y.-P. Liu, *J. Phys. Chem.* **99**, 13141–13149 (1995).
- ²⁸³H. Hagenström, M. J. Esplandi, and D. M. Kolb, *Langmuir* **17**, 839–848 (2001).
- ²⁸⁴A. Vilan, A. Shanzer, and D. Cahen, *Nature* **404**, 166–168 (2000).
- ²⁸⁵A. Vilan and D. Cahen, *Adv. Funct. Mater.* **12**, 795–807 (2002).
- ²⁸⁶K. Slowinski, R. V. Chamberlain, C. J. Miller, and M. Majda, *J. Am. Chem. Soc.* **119**, 11910–11919 (1997).
- ²⁸⁷M. A. Rampi and G. M. Whitesides, *Chem. Phys.* **281**, 373–391 (2002).
- ²⁸⁸Y. Xia and G. M. Whitesides, *Angew. Chem. Int. Ed.* **37**, 550–575 (1998).
- ²⁸⁹P. M. S. John and H. G. Craighead, *Appl. Phys. Lett.* **68**, 1022–1024 (1996).
- ²⁹⁰Y.-L. Loo, R. L. Willett, K. W. Baldwin, and J. A. Rogers, *Appl. Phys. Lett.* **81**, 562–564 (2002).
- ²⁹¹Y.-L. Loo, D. V. Lang, J. A. Rogers, and J. W. P. Hsu, *Nano Lett.* **3**, 913–917 (2003).
- ²⁹²L. Zuppiroli, L. Si-Ahmed, K. Kamaras, F. Nuesch, M. N. Bussac, D. Ades, A. Siove, E. Moons, and M. Gratzel, *Euro. Phys. J. B* **11**, 505–512 (1999).
- ²⁹³Y. Selzer and D. Cahen, *Adv. Mater.* **13**, 508 (2001).

- ²⁹⁴J. W. P. Hsu, Y. L. Loo, D. V. Lang, and J. A. Rogers, *J. Vac. Sci. Technol. B* **21**, 1928–1935 (2003).
- ²⁹⁵S. Lodha, P. Carpenter, and D. B. Janes, *J. Appl. Phys.* **99**, 024510 (2006).
- ²⁹⁶H. Haick, M. Ambrico, T. Ligonzo, R. T. Tung, and D. Cahen, *J. Am. Chem. Soc.* **128**, 6854–6869 (2006).
- ²⁹⁷W. Wang, J. Wang, M. Zhao, R. Liang, and J. Xu, *J. Semicond.* **33**, 102004 (2012).
- ²⁹⁸V. Perebeinos and M. Newton, *Chem. Phys.* **319**, 159–166 (2005).
- ²⁹⁹L. Segev, A. Salomon, A. Natan, D. Cahen, L. Kronik, F. Amy, C. K. Chan, and A. Kahn, *Phys. Rev. B* **74**, 165323 (2006).
- ³⁰⁰M. L. Sushko and A. L. Shluger, *J. Phys. Chem. B* **111**, 4019–4025 (2007).
- ³⁰¹H. Haick, J. P. Pelz, T. Ligonzo, M. Ambrico, D. Cahen, W. Cai, C. Marginean, C. Tivarus, and R. T. Tung, *Phys. Status Solidi A* **203**, 3438 (2006).
- ³⁰²R. H. Williams, V. Montgomery, R. R. Varma, and A. McKinley, *J. Phys. D* **10**, L253–L256 (1977).
- ³⁰³F. Hasegawa, M. Onomura, C. Mogi, and Y. Nannichi, *Solid-State Electron.* **31**, 223–228 (1988).
- ³⁰⁴M. A. Sobolewski and C. R. Helms, *Appl. Phys. Lett.* **54**, 638–640 (1989).
- ³⁰⁵K. Hattori and Y. Torii, *Solid-State Electron.* **34**, 527–531 (1991).
- ³⁰⁶J. Nakamura, H. Niu, and S. Kishino, *Jpn. J. Appl. Phys., Part 1* **32**, 699–703 (1993).
- ³⁰⁷J. Her, H. Lim, C. H. Kim, I. K. Han, J. I. Lee, and K. N. Kang, *J. Korean Inst. Tel. Elec.* **31A**, 56–63 (1994).
- ³⁰⁸H. Sawatari and O. Oda, *J. Appl. Phys.* **72**, 5004–5006 (1992).
- ³⁰⁹C. J. Huang, *J. Appl. Phys.* **89**, 6501–6505 (2001).
- ³¹⁰M. Biber, C. Termirci, and A. Turut, *J. Vac. Sci. Technol. B* **20**, 10–13 (2002).
- ³¹¹M. Kobayashi, A. Kinoshita, K. Saraswat, H. S. P. Wong, and Y. Nishi, *J. Appl. Phys.* **105**, 023702 (2009).
- ³¹²Y. Zhou, M. Ogawa, X. Han, and K. L. Wang, *Appl. Phys. Lett.* **93**, 202105 (2008).
- ³¹³R. Wang, M. Xu, P. D. Ye, and R. Huang, *J. Vac. Sci. Technol. B* **29**, 041206 (2011).
- ³¹⁴Z. Wu, W. Huang, C. Li, H. Lai, and S. Chen, *IEEE Trans. Electron Devices* **59**, 1328–1331 (2012).
- ³¹⁵D. Connolly, C. Faulkner, P. A. Clifton, and D. E. Grupp, *Appl. Phys. Lett.* **88**, 012105 (2006).
- ³¹⁶B. E. Coss, W. Y. Loh, R. M. Wallace, J. Kim, P. Majhi, and R. Jammy, *Appl. Phys. Lett.* **95**, 222105 (2009).
- ³¹⁷S. Aydogan, M. Saglam, and A. Türüt, *J. Phys. D: Condens. Matter* **18**, 2665–2676 (2006).
- ³¹⁸A. A. Kumar, V. Rajagopal Reddy, V. Janardhanam, H. D. Yang, H. J. Yun, and C. J. Choi, *J. Alloys Compd.* **549**, 18–21 (2013).
- ³¹⁹M. Soylu and F. Yakuphanoglu, *Superlattices Microstruct.* **52**, 470–483 (2012).
- ³²⁰J. R. Waldrop, *Appl. Phys. Lett.* **53**, 1518–1520 (1988).
- ³²¹J. C. Costa, F. Williamson, T. J. Miller, K. Beyzavi, M. I. Nathan, D. S. L. Mui, S. Strite, and H. Morkoc, *Appl. Phys. Lett.* **58**, 382–384 (1991).
- ³²²H. Hasegawa, H. Ishii, and K. Koyanagi, *Appl. Surf. Sci.* **56–58**, 317–324 (1992).
- ³²³M. Cantile, L. Sorba, S. Yildirim, P. Faraci, G. Biasiol, A. Franciosi, T. J. Miller, and M. I. Nathan, *Appl. Phys. Lett.* **64**, 988–990 (1994).
- ³²⁴T. Nishimura, K. Kita, and A. Toriumi, *Appl. Phys. Lett.* **91**, 123123 (2007).
- ³²⁵T. Nishimura, K. Kita, and A. Toriumi, *Appl. Phys. Express* **1**, 051406 (2008).
- ³²⁶R. R. Lieten, V. V. Afanas'ev, N. H. Thoan, S. Degroote, W. Walukiewicz, and G. Borghs, *J. Electrochem. Soc.* **158**, H358–H362 (2011).
- ³²⁷R. R. Lieten, S. Degroote, M. Kuijk, and G. Borghs, *Appl. Phys. Lett.* **92**, 022106 (2008).
- ³²⁸Y. Zhou, W. Han, Y. Wang, F. Xiu, J. Zou, R. K. Kawakami, and K. L. Wang, *Appl. Phys. Lett.* **96**, 102103 (2010).
- ³²⁹W. Mönch, *J. Appl. Phys.* **111**, 073706 (2012).
- ³³⁰J. Hu, A. Nainani, Y. Sun, K. C. Saraswat, and H. S. Philip Wong, *Appl. Phys. Lett.* **99**, 252104 (2011).
- ³³¹A. M. Roy, J. Lin, and K. C. Saraswat, *IEEE Electron Device Lett.* **33**, 761–763 (2012).
- ³³²Y. Sakamoto, T. Sugino, T. Miyazaki, and J. Shirafuji, *Electron. Lett.* **31**, 1104 (1995).
- ³³³D. T. Quan and H. Hbib, *Solid-State Electron.* **36**, 339–344 (1993).
- ³³⁴T. Sugino, Y. Sakamoto, and J. Shirafuji, *Jpn. J. Appl. Phys., Part 2* **32**, L239–L242 (1993).
- ³³⁵S. Kasai and H. Hasegawa, in *IEEE International Conference on Indium Phosphide* (1994), pp. 220–223.
- ³³⁶Y. Gülen, K. Ejderha, Č. Nuholu, and A. Turut, *Microelectron. Eng.* **88**, 179–182 (2011).
- ³³⁷C. Gaonach, S. Cassette, M. A. Di Forte-Poisson, C. Brylinski, M. Champagne, and A. Tardella, *Semicond. Sci. Technol.* **5**, 322–327 (1990).
- ³³⁸P. Kordos, M. Marso, R. Meyer, and H. Luth, *J. Appl. Phys.* **72**, 2347–2355 (1992).
- ³³⁹S. A. Chambers, *J. Vac. Sci. Technol. A* **11**, 860–868 (1993).
- ³⁴⁰Y. Bing, J. C. Chen, and F. S. Choa, *Mater. Res. Soc. Symp. Proc.* **340**, 259–263 (1994).
- ³⁴¹K. Shiojima, K. Nishimura, T. Aoki, and F. Hyuga, *J. Appl. Phys.* **77**, 390–392 (1995).
- ³⁴²H. J. Gossmann and E. F. Schubert, *Crit. Rev. Solid State Mater. Sci.* **18**, 1–67 (1993).
- ³⁴³A. V. Murel, A. V. Novikov, V. I. Shashkin, and D. V. Yurasov, *Semiconductors* **46**, 1358–1361 (2012).
- ³⁴⁴J. M. Shannon, *Solid-State Electron.* **19**, 537–543 (1976).
- ³⁴⁵S. J. Egash, P. Shihong, M. Dang, W. E. Spicer, and D. M. Collins, *Jpn. J. Appl. Phys. Suppl.* **22-1**, 431–435 (1982).
- ³⁴⁶Z. J. Horvath, V. Van Tuyen, S. Franchi, A. Bosacchi, P. Frigeri, E. Gombia, R. Mosca, D. Pal, I. Kalmar, and B. Szentpali, *Mater. Sci. Eng., B-Solid State Mater. Adv. Technol.* **80**, 248–251 (2001).
- ³⁴⁷T. Tamura, S. Ishibashi, K. Terakura, and H. Weng, *Phys. Rev. B* **80**, 195302 (2009).
- ³⁴⁸Y. Nishi, T. Yamauchi, T. Marukame, A. Kinoshita, J. Koga, and K. Kato, *Phys. Rev. B* **84**, 115323 (2011).
- ³⁴⁹J. D. Hwang, Y. L. Lin, and C. Y. Kung, *Nanotechnology* **24**, 115709 (2013).
- ³⁵⁰G. A. Adegboyega, *Phys. Status Solidi A* **111**, K31–K35 (1989).
- ³⁵¹Y. H. Wang, M. P. Houng, P. W. Sze, J. F. Chen, and A. Y. Cho, *J. Appl. Phys.* **71**, 2760–2764 (1992).
- ³⁵²T. Teraji, S. Hara, H. Okushi, and K. Kajimura, *Appl. Phys. Lett.* **71**, 689–691 (1997).
- ³⁵³J.-S. Jang and T.-Y. Seong, *J. Appl. Phys.* **88**, 3064–3066 (2000).
- ³⁵⁴T. Tsuzuku, T. Sugimura, Y. Kasai, T. Inokuma, K. Iiyama, and S. Takamiya, *Jpn. J. Appl. Phys., Part 1* **39**, 5788–5793 (2000).
- ³⁵⁵H. Iwakuro, T. Inoue, and T. Kuroda, *Jpn. J. Appl. Phys., Part 2* **30**, L255–L257 (1991).
- ³⁵⁶H. Iwakuro, M. Tokonami, T. Kuroda, S. Tamaki, and Y. Kitatsujii, *Jpn. J. Appl. Phys., Part 1* **32**, 5487–5495 (1993).
- ³⁵⁷A. Paccagnella and A. Callegari, *Solid-State Electron.* **34**, 1409–1414 (1991).
- ³⁵⁸A. Y. Polyakov, M. Stam, A. G. Milnes, A. E. Bochkarev, and S. J. Pearton, *J. Appl. Phys.* **71**, 4411–4414 (1992).
- ³⁵⁹T. Sugino, Y. Sakamoto, T. Sumiguchi, K. Nomoto, and J. Shirafuji, *Jpn. J. Appl. Phys., Part 2* **32**, L1196–L1199 (1993).
- ³⁶⁰S. Ashok, H. Krautle, and H. Beneking, *Appl. Phys. Lett.* **45**, 431–433 (1984).
- ³⁶¹R. Tyagi, T. P. Chow, J. M. Borrego, and K. A. Pisarczyk, *Appl. Phys. Lett.* **63**, 651–653 (1993).
- ³⁶²P. C. Srivastava, C. Colluza, S. Chandra, and U. P. Singh, *Solid-State Electron.* **37**, 520–522 (1994).
- ³⁶³A. Fricke, G. Stareev, T. Kummetz, D. Sowada, J. Mahnss, W. Kowalsky, and K. J. Ebeling, *Appl. Phys. Lett.* **65**, 755–757 (1994).
- ³⁶⁴E. Grusell, S. Berg, and L. P. Andersson, *J. Electrochem. Soc.* **127**, 1573–1576 (1980).
- ³⁶⁵S. Ashok, T. P. Chow, and B. J. Baliga, *Appl. Phys. Lett.* **42**, 687–689 (1983).
- ³⁶⁶X. C. Mu and S. J. Fonash, *IEEE Electron Device Lett.* **6**, 410–412 (1985).
- ³⁶⁷Y. G. Wang and S. Ashok, *Physica B* **170**, 513–517 (1991).
- ³⁶⁸H. Thomas and J. K. Luo, *Solid-State Electron.* **35**, 1401–1407 (1992).
- ³⁶⁹M. Yamada, C. J. Spindt, K. E. Miyano, P. L. Meissner, A. Herrera-Gomez, T. Kendelewicz, and W. E. Spicer, *J. Appl. Phys.* **71**, 314–317 (1992).
- ³⁷⁰Y. Q. Jia and G. G. Qin, *Appl. Phys. Lett.* **56**, 641–643 (1990).
- ³⁷¹P. P. Sahay, M. Shamsuddin, and R. S. Srivastava, *Solid-State Electron.* **34**, 727–729 (1991).
- ³⁷²E. K. Kim, Y. J. Park, S.-K. Min, J.-G. Lee, and W. C. Choi, *Ungyong Mulli* **8**, 132–137 (1995).

- ³⁷³Z. M. Wang, Y. X. Zhang, K. Wu, M. H. Yuan, W. X. Chen, and G. G. Qin, *Phys. Rev. B* **51**, 7878–7881 (1995).
- ³⁷⁴V. G. Bozhkov, V. A. Kagadei, and N. A. Torkhov, *Izv. Vyssh. Uchebn. Zaved., Fiz.* **40**, 115–121 (1997).
- ³⁷⁵R. L. van Meirhaeghe, W. H. Lafleure, and F. Cardon, *J. Appl. Phys.* **76**, 403–406 (1994).
- ³⁷⁶S. A. Ding and Z. Xu, *Chin. J. Semicond.* **15**, 367–372 (1994).
- ³⁷⁷J. P. Sullivan, W. R. Graham, R. T. Tung, and F. Schrey, *Appl. Phys. Lett.* **62**, 2804 (1993).
- ³⁷⁸J. J. Coleman, *Appl. Phys. Lett.* **31**, 283–285 (1977).
- ³⁷⁹V. Montgomery, R. H. Williams, and G. P. Srivastava, *J. Phys. C* **14**, L191–L194 (1981).
- ³⁸⁰J. R. Waldrop, *Appl. Phys. Lett.* **47**, 1301–1303 (1985).
- ³⁸¹S. Hoheneger, T. U. Kampen, W. Braun, and D. R. T. Zahn, *Surf. Sci.* **433–435**, 347–351 (1999).
- ³⁸²E. K. Kim, M. H. Son, Y. J. Park, J.-G. Lee, and S.-K. Min, *J. Appl. Phys.* **78**, 4276–4278 (1995).
- ³⁸³M. Yamada, A. K. Wahi, T. Kendelewicz, and W. E. Spicer, *Phys. Rev. B* **45**, 3600–3605 (1992).
- ³⁸⁴T. S. Huang and R. S. Fang, *Solid-State Electron.* **37**, 1461–1466 (1994).
- ³⁸⁵H. Nobusawa and H. Ikoma, *Jpn. J. Appl. Phys., Part 1* **32**, 3713–3719 (1993).
- ³⁸⁶S. Meskinis, K. Slapikas, V. Grigaliunas, J. Matukas, and S. Smetona, *Phys. Status Solidi A* **180**, 499–505 (2000).
- ³⁸⁷M. Tao, D. Udeshi, N. Basit, E. Maldonado, and W. P. Kirk, *Appl. Phys. Lett.* **82**, 1559–1561 (2003).
- ³⁸⁸S.-H. Kim, T.-Y. Seong, and H.-K. Kim, *Appl. Phys. Lett.* **86**, 022101 (2005).
- ³⁸⁹Q. T. Zhao, U. Breuer, E. Rije, S. Lenk, and S. Mantl, *Appl. Phys. Lett.* **86**, 062108 (2005).
- ³⁹⁰K. Ikeda, Y. Yamashita, N. Sugiyama, N. Taoka, and S.-i. Takagi, *Appl. Phys. Lett.* **88**, 152115 (2006).
- ³⁹¹H. Mazari, Z. Benamara, O. Bonnaud, and R. Olier, *Mater. Sci. Eng. B—Solid State Mater. Adv. Technol.* **90**, 171–175 (2002).
- ³⁹²J.-O. Song, J. S. Kwak, and T.-Y. Seong, *Semicond. Sci. Technol.* **21**, L7–L10 (2006).
- ³⁹³L. Geng, B. Magyari-Kope, Z. Y. Zhang, and Y. Nishi, *IEEE Electron Device Lett.* **29**, 746–749 (2008).
- ³⁹⁴M. Sinha, E. F. Chor, and Y. C. Yeo, *Appl. Phys. Lett.* **92**, 222114 (2008).
- ³⁹⁵S. M. Koh, X. Wang, T. Thanigaivelan, T. Henry, Y. Erokhin, G. S. Samudra, and Y. C. Yeo, *J. Appl. Phys.* **110**, 073703 (2011).
- ³⁹⁶M. Mueller, Q. T. Zhao, C. Urban, C. Sandow, D. Buca, S. Lenk, S. Estévez, and S. Mantl, *Mater. Sci. Eng., B* **154–155**, 168–171 (2008).
- ³⁹⁷Y. Guo, X. An, R. Huang, C. Fan, and X. Zhang, *Appl. Phys. Lett.* **96**, 143502 (2010).
- ³⁹⁸J. Chan, N. Y. Martinez, J. J. D. Fitzgerald, A. V. Walker, R. A. Chapman, D. Riley, A. Jain, C. L. Hinkle, and E. M. Vogel, *Appl. Phys. Lett.* **99**, 012114 (2011).
- ³⁹⁹N. Reckinger, C. Poleunis, E. Dubois, C. Augustin Duu, X. Tang, A. Delcorte, and J. P. Raskin, *Appl. Phys. Lett.* **99**, 012110 (2011).
- ⁴⁰⁰Y. Li, W. Long, and R. T. Tung, *Solid State Commun.* **151**, 1641–1644 (2011).
- ⁴⁰¹Y. Tong, B. Liu, P. S. Y. Lim, and Y. C. Yeo, *IEEE Electron Device Lett.* **33**, 773–775 (2012).
- ⁴⁰²Z. Li, X. An, M. Li, Q. Yun, M. Lin, M. Li, X. Zhang, and R. Huang, *IEEE Electron Device Lett.* **33**, 1687–1689 (2012).
- ⁴⁰³M. Koike, Y. Kamimuta, and T. Tezuka, *Appl. Phys. Lett.* **102**, 032108 (2013).
- ⁴⁰⁴X. Guo, Y. Tang, Y. L. Jiang, X. P. Qu, G. P. Ru, D. W. Zhang, D. Deduytsche, and C. Detavernier, *Microelectron. Eng.* **106**, 121 (2013).
- ⁴⁰⁵J. Ivancic, H. Kobayashi, J. Almeida, and G. Margaritondo, *J. Appl. Phys.* **87**, 795–800 (2000).
- ⁴⁰⁶C. Marinelli, L. Sorba, M. Lazzarino, D. Kumar, E. Pelucchi, B. H. Muller, D. Orani, S. Rubini, A. Franciosi, S. De Franceschi, and F. Beltran, *J. Vac. Sci. Technol. B* **18**, 2119–2127 (2000).
- ⁴⁰⁷P. Kalra, N. Vora, P. Majhi, P. Y. Hung, H. H. Tseng, R. Jammy, and T. J. K. Liu, *Electrochem. Solid-State Lett.* **12**, H1–H3 (2009).
- ⁴⁰⁸M. W. Allen and S. M. Durbin, *Appl. Phys. Lett.* **92**, 122110 (2008).
- ⁴⁰⁹L. J. Brillson, Y. Dong, D. Doutt, D. C. Look, and Z. Q. Fang, *Physica B* **404**, 4768–4773 (2009).
- ⁴¹⁰L. J. Brillson, Y. Dong, F. Tuomisto, B. G. Svensson, A. Y. Kuznetsov, D. Doutt, H. L. Mosbacher, G. Cantwell, J. Zhang, J. J. Song, Z. Q. Fang, and D. C. Look, *J. Vac. Sci. Technol. B* **30**, 050801 (2012).
- ⁴¹¹J. C. Costa, T. J. Miller, F. Williamson, and M. I. Nathan, *J. Appl. Phys.* **70**, 2173–2184 (1991).
- ⁴¹²L. Sorba, G. Bratina, G. Ceccone, A. Antonini, J. F. Walker, M. Micovic, and A. Franciosi, *Phys. Rev. B* **43**, 2450–2453 (1991).
- ⁴¹³K. Koyanagi, S. Kasai, and H. Hasegawa, *Jpn. J. Appl. Phys. Pt. 1* **32**, 502–510 (1993).
- ⁴¹⁴T. dell’Orto, J. Almeida, A. Terrasi, M. Marsi, C. Coluzza, G. Margaritondo, and P. Perfetti, *Phys. Rev. B* **50**, 18189–18193 (1994).
- ⁴¹⁵Z. Chen, S. N. Mohammad, and H. Morkoç, *Phys. Rev. B* **53**, 3879–3884 (1996).
- ⁴¹⁶Y. Li, W. Long, and R. T. Tung, *Appl. Surf. Sci.* **284**, 720 (2013).
- ⁴¹⁷W. Long, Y. Li, and R. T. Tung, *Surf. Sci.* **610**, 48–52 (2013).
- ⁴¹⁸W. Long, Y. Li, and R. T. Tung, “Schottky barrier height systematics studied by partisan interlayer,” *Thin Solid Films* (in press).
- ⁴¹⁹M. Gurnett, J. B. Gustafsson, L. J. Holleboom, K. O. Magnusson, S. M. Widstrand, L. S. O. Johansson, M. K.-J. Johansson, and S. M. Gray, *Phys. Rev. B* **71**, 195408 (2005).
- ⁴²⁰E. Kaxiras, *Phys. Rev. B* **43**, 6824 (1991).
- ⁴²¹P. Hutchison, M. M. R. Evans, and J. Nogami, *Surf. Sci.* **411**, 99–110 (1998).
- ⁴²²O. Kubo, A. A. Saranin, A. V. Zotov, T. Harada, T. Kobayashi, N. Yamaoka, J.-T. Ryu, M. Katayama, and K. Oura, *Jpn. J. Appl. Phys., Part 1* **39**, 3740 (2000).
- ⁴²³R. Shalafat, E. Mete, and S. Ellialtioglu, *Phys. Rev. B* **69**, 125417 (2004).
- ⁴²⁴J. Zegenhagen, M. S. Hybertsen, P. E. Freeland, and J. R. Patel, *Phys. Rev. B* **38**, 7885–7888 (1988).
- ⁴²⁵A. Kawazu and H. Sakama, *Phys. Rev. B* **37**, 2704–2706 (1988).
- ⁴²⁶M. Y. Lai and Y. L. Wang, *Phys. Rev. B* **60**, 1764–1770 (1999).
- ⁴²⁷P. Kumar, J. Kuyyalil, M. Kumar, and S. M. Shivaprasad, *Solid State Commun.* **151**, 1758–1762 (2011).
- ⁴²⁸M. A. Olmstead, R. D. Bringans, R. I. G. Uhrberg, and R. Z. Bachrach, *Phys. Rev. B* **34**, 6041–6044 (1986).
- ⁴²⁹R. I. G. Uhrberg, R. D. Bringans, M. A. Olmstead, R. Z. Bachrach, and J. E. Northrup, *Phys. Rev. B* **35**, 3945–3951 (1987).
- ⁴³⁰R. L. Headrick and W. R. Graham, *Phys. Rev. B* **37**, 1051–1054 (1988).
- ⁴³¹J. P. Lacharme, N. Benazzi, and C. A. Sebenne, *Surf. Sci.* **433–435**, 415–419 (1999).
- ⁴³²A. Papageorgopoulos, A. Corner, M. Kamaratos, and C. A. Papageorgopoulos, *Phys. Rev. B* **55**, 4435–4441 (1997).
- ⁴³³S. Rivillon, F. Amy, Y. J. Chabal, and M. M. Frank, *Appl. Phys. Lett.* **85**, 2583–2585 (2004).
- ⁴³⁴B. J. Eves and G. P. Lopinski, *Surf. Sci.* **579**, 89 (2005).